Republic of Iraq
Ministry of Higher Education
and Scientific Research
The University of Babylon
College of Science
Department of Physics

Synthesis, Characterization and Sensing applications of ZnO /MWCNTs Thin Films Using Sol-Gel Technique

Thesis
Submitted to the Council of the College of Science
University of Babylon in Partil Fulfilment of the Requirements for the Degree of Doctor of Philosophy in Science / Physics

By

Jumana Kareem Buraihi Mahdi

B.Sc. University of Babylon / 2013

M.Sc. University of Babylon / 2016

Supervised by

Assist. Prof. Dr.

Hikmat Adnan Jawad Banimuslem

2022 A.D. **1444 A.H.**

جمهورية العراق

وزارة التعليم العالي والبحث العلمي

جامعة بابل

كلية العلوم- قسم الفيزياء

تواليف و خصائص و تطبيقات التحسسية لأغشية ZnO/MWCNTs باستخدام تقنية Sol-Gel

اطروحة

مقدمة الى مجلس كلية العلوم- جامعة بابل

وهي جزء من متطلبات نيل درجة الدكتوراه فلسفة في العلوم/ الفيزياء

من قبل

جمانه كريم بريهي محمدي

بكالوريوس جامعة بابل /٢٠١٣

ماجستير جامعة بابل / ٢٠١٦

بإشراف

أ.م.د.

حكمت عدنان جواد بني مسلم

١٤٤٤هـ ٢٠٢٢م

Summary:

The current project investigate the optical, electrical and structural properties of novel hybrid nano materials compromising Zinc oxide and carbon nano tube (CNT) with apply the prepared hybrid as a sensor to detect some contaminant gases.

The first chapter employed to understand the behavior of ZnO/CNT composite by going through full literature review of the related works. Chapter two focuses on theoretical background of the equations and mathmatical relations that is are used for the analysis of the results. Chapter three explains the methodology and materials as well as the work scheme that followed to finish the current work. In chapter four, all the results and the discussions related to the results have been comprehensively investigated.

A composite material of zinc oxide and carbon nanotubes have been synthesized via a sol-gel process using zinc acetate dehydrate and acid modified multiple-wall carbon nanotubes. Colloidal nanoparticles were achieved as color indicated. Thin films were deposited utilizing spray pyrolysis technique onto glass substrate as well as interdigitated electrodes to perform electrical characterization.

Samples were heated at different annealing temperatures (250 and 500) ^{o}C and only samples heated with 500 ^{o}C have shown reasonable results.

The optical energy gap has been investigated using UV-Visible absorption spectroscopy and Tauc calculations. It has been found that the energy gaps were in the range of (2.63-3.28) eV.

Temperature dependence conductivity has been studied using semiconductor characterization system and reviled that, at low annealing temperature (250)^{o}C, zinc

oxide would not be achieved were as at higher temperature (500) ^{o}C films visually looked transparent and shown quite interesting results and the smallest activation energy shown in the samples having CNT.

Sensor has been manufactured in the mean of the detection of some hazardous gases such as (Nitric Oxide, Dimethyl formamide, Ethanol, Chloroform and Acetone**)** gases using resistance based actuator.

The response of the prepared devices were found to be as follows; (8.4% , 2.6%, 0.2% , 0.6% and 4.2%) for (Nitric Oxide, Dimethyl formamide, Ethanol, Chloroform and Acetone**)** gases respectively in case of ZnO. However, It was found that for ZnO/CNT, the response are; (24.7% , 0.24% , 0.05% , 16.98% and 0.25%) for the same gases respectively.

The response time and recovery time were calculated to ZnO/CNT thin film towards NO_2 gas and found to be (10) sec and (151) sec respectively.

الخلاصة:

الدراسة الحالية تتضمن دراسة الخواص البصرية والكهربائية والتركيبية لمتراكب أوكسيد الخارصين والكاربون الانبوبي النانوي لتطبيقه في مجال المتحسسات الغازية للكشف عن بعض الغازات الملوثة.

الفصل الأول من الاطروحة يتضمن عرض جميع الدراسات السابقة المتعلقة بالموضوع لفهم طبيعة و خواص أوكسيد الخارصين وكذلك الكاربون الانبوبي النانوي .

يركز الفصل الثاني على الخلفية النظرية للموضوع لكل المعادلات والعلاقات الرياضية المرتبطة بالبحث والمستخدمة لتحليل النتائج وفهمها.

تم في الفصل الثالث توضيح الجزء العملي من الاطروحة من خلال استعراض الأجهزة والتقنيات المستخدمة وكذلك المواد وطرق تحضيرها من خلال المخططات التوضيحية التي اتبعت في هذه الاطروحة.

في الفصل الرابع، كل النتائج التي تم الحصول عليها وتفسيراتها دُرست بشكل تفصيلي. ويمكن تلخيص اهم الخطوات واهم النتائج المستحصلة بالآتي:

تم تحضير متراكب أوكسيد الخارصين و الكاربون الانبوبي النانوي بطريقة الـ sol-gel المحسنة باستخدام أسيتات الخارصين المهدرجة وانابيب الكاربون النانوية متعددة الجدران. تغيّر اللون في المحلول أكّد استحصال جسيمات نانوية غروية.

تم ترسيب أغشية رقيقة من المواد المحضرة بطريقة الرش الكيميائي على ركائز زجاجية تارة و كذلك أقطاب متداخلة تارة أخرى لدراسة الخواص الكهربائية.

تم تسخين النماذج بواسطة فرن مبرمج لدرجات حرارة (250 و 500) درجة مئوية لدراسة تأثير درجة حرارة التلدين. بيّنت النتائج ان النماذج الملدنة بدرجة حرارة (500) درجة مئوية اعطت نتائج جيدة.

تم دراسة الخواص البصرية وحسابات فجوة الطاقة البصرية ووجد ان فجوة الطاقة تتراوح من (2.63-3.28) الكترون - فولت.

تم في هذه الاطروحة دراسة اعتمادية التوصيلية على زيادة درجة الحرارة باستخدام جهاز فحص اشباه الموصلات. وقد تبين ان أوكسيد الخارصين لا يتحقق عند درجة حرارة تلدين واطئة (250) درجة مئوية كما هو الحال عند درجة حرارة أعلى (500) درجة مئوية ، وتبين ان الأغشية شفافة

بصريًا وأظهرت نتائج مثيرة للاهتمام وأظهرت ايضاً ان أصغر طاقة تنشيط في العينات التي تحتوي على CNT.

تم فحص النماذج باستخدامها لاستشعار بعض الغازات السامة مثل غازات (أكسيد النيتريك، ثنائي ميثيل فورماميد، الإيثانول، الكلوروفورم والأسيتون) باستخدام مشغل يعتمد على المقاومة. ويتبين انها تصلح للكشف عن الملوثات الموجودة في الهواء.

وجد ان استجابة النماذج المحضرة كالتالي ؛ (8.4٪ ، 2.6٪ ، 0.2٪ ، 0.6٪ ، 4.2٪) لكل من غاز (أكسيد النيتريك ، ثنائي ميثيل فورماميد ، الإيثانول ، الكلوروفورم والأسيتون) على التوالي في حالة أكسيد الخارصين. ومع ذلك ، وجد أن في حالة متراكب أوكسيد الخارصين و الكاربون الانبوبي النانوي ، الاستجابة هي ؛ (24.7٪ ، 0.24٪ ، 0.05٪ ، 16.98٪ و 0.25٪) لنفس الغازات على التوالي.

تم حساب زمن الاستجابة و زمن الاسترجاع للغشاء الرقيق لمتراكب أوكسيد الخارصين و الكاربون الانبوبي النانوي (ZnO/CNT) لغاز NO_2 ووجد أنه (10) ثانية و (151) ثانية على التوالي.

Contents

List of Symbols

Symbol	Description
ZnO	Zinc oxide
TCO	Transparent conducting oxide
UV	Ultraviolet
LEDs	Light-Emitting Diodes
LDs	Laser Diodes
V.B.	Valence Band
C.B.	Conduction Band
$h\upsilon$	Photon Energy
h	Plank's Constant
υ	Incident Photon Frequency
E_g	Energy Gap
λ_{max}	Maximum Wavelength
$I_\circ$	Incident Photon Intensity
I_T	Transmitted Photon Intensity
α	Absorption Coefficients
t	Thickness of The Film
A_b	Absorption
r	Constant Which Takes the Values (1/2, 3/2, 2, and 3)
B	Edge Width Parameter
n	Refractive Index
n_c	Complex Refractive Index
ϑ	Velocity of Propagation
c	Light Velocity
R_e	Reflectance

Symbol	Description
T_r	Transmittance
λ	Wavelength
S	Siemens (Conductivity Unit)
I	Current
V	Potential Difference
R	Resistance
ρ_{el}	Resistivity
l	Length
A	Cross Section Area
σ	Conductivity
L	Gap Between Fingers
W	Overlap Distance Between the Electrodes
N_r	Number of Fingers of Interdigitated Electrodes
σ_o	Constant
E_a	Activation Energy
kB	Boltzmann Constant
T	Temperature
XRD	X- Ray Diffraction
FESEM	Field Emission Scanning Electron Microscopy
θ	Bragg Diffraction Angle of The XRD Peak
m	Integer Representing the Order of The Diffraction Peak
$d_{(hkl)}$	Inter-Plane Distance of Atoms or Ions or Molecules
β = FWHM	Full Width at Half Maximum in radians
D_s	Crystallite Size
I-V	Current-Voltage

Symbol	Description
M	Molarity
W_t	Weight of Sample
M_{wt}	Molecular Weight
V	Solvent Volume
TCO	Transparent Conducting Oxide
MOS	Metal Oxide Semiconductor
MOCVD	Metal Organic Chemical Vapor Deposition
MBE	Molecular Beam Epitaxy
PLD	Pulsed Laser Deposition
TEM	Transmission Electron Microscopy
IDEs	Interdigitated Gold Electrodes
HOMO	Higher Occupied Molecular Orbitals
LUMO	Lower Unoccupied Molecular Orbitals
ITO	Indium Tin Oxide
$C_3H_8O_2$	2-methoxyethanol
MEA	Monoethanolamine
MWCNTs	Multi Walled Carbon Nanotubes
SWCNTs	Single Walled Carbon Nanotubes

List of Figures

List of Tables

1.1: Introduction

Zinc oxide (ZnO) is a semiconductor material with a wide band gap (3.37 eV) and a large exciton binding energy (60 MeV) at a room temperature with good optical transparency in the visible range [1].

Zinc oxide (ZnO) thin films have been investigated in recent years as transparent conducting oxide (TCO) because of their good electrical and optical properties in combination with a high electron mobility, high thermal conductivity, good transparency, wide and direct band gap at room temperature, large exciton binding energy and easiness of growing it in the nanostructure form by many different methods making ZnO suitable for a wide range of applications [2]; including light-emitting devices, varistors, solar cells and gas sensors. Moreover, ZnO is a promising material for short-wavelength optoelectronic devices, especially for ultraviolet (UV) Light-Emitting Diodes (LEDs) and Laser Diodes (LDs), due to its large exciton binding energy [3].

ZnO has high chemical and mechanical stability; furthermore, it is nontoxic and widespread in nature [1]. Recently, transparent-conducting oxides on the base of ZnO have been studied well [4]. ZnO is one of the most promising materials for the fabrication of the next generation of optoelectronic devices in the UV region and optical or display devices [5]. As a matter of fact, simultaneous occurrence of both high optical transmittances in the visible range and low resistivity make ZnO an important material for manufacturing of heat mirrors used in gas stoves, conducting coatings in aircraft glasses to avoid surface icing, and thin film electrodes in amorphous silicon solar cells [5]. ZnO belongs to hexagonal wurtzite class; it is a semiconducting, piezoelectric, and optical waveguide material used in sensors, surface acoustic devices, transparent electrodes, and solar cells [6]. Controlling of ZnO physical properties depending on various factors, such as doping and temperature growth, is important for efficient function of devices on the base of ZnO structures. The existence of both (n and p) conduction

types is of fundamental importance for application in light-emitting devices [7]. The nanostructures like nanotubes, nanorods, nanowalls, nanofibers and high-quality undoped and doped ZnO thin films have been grown with plasma-assisted molecular beam epitaxy, vapor transport deposition method, vacuum arc deposition metal organic chemical vapor deposition (MOCVD), sol–gel process, and spray pyrolysis [8, 9]. Such nanotubes, nanowires, nanoribbons, and nanofibers have deserved special attention for their potential applications in applied fields such as field emission displays, optical waveguides, solar cells, ultraviolet photodetectors, optical switches, and gas sensing [4–7]. The chemical bath deposition and sol–gel technique are also well known methods of preparation of ZnO thin films. Among these methods, spray pyrolysis is useful in a wide range of applications [10]. This method is cheaper, simpler and permits to obtain films for optoelectronic applications with required properties. Structural, electrical, and optical properties dependence the on thickness of ZnO films has been investigated. The unique and fascinating properties of nanostructured materials have triggered tremendous motivation among scientists to explore the possibilities of using them in technological applications. In particular, the electronic and optical properties of nanostructured materials have been of great interest because of their potential applications in the fabrication of microelectronic and optoelectronic devices [11].

Apart from the technological significance of ZnO nanostructures, their nano-dimensional structure with diameters in the range of ten to hundreds of nanometers makes them quite interesting from a scientific point of view. In this size range, they are expected to possess promising physical properties and pronounced that are quite different from their bulk counterpart [12].

Various deposition techniques were used for the preparation of ZnO thin films, such as molecular beam epitaxy (MBE), chemical vapor deposition, electrochemical deposition, pulsed laser deposition (PLD), reactive evaporation, magnetron sputtering technique , spray pyrolysis and sol-gel

process [13]. Among these techniques, the sol-gel process has many advantages such as being simple, having low production cost, and large-area coating without any need for high vacuum.

In addition, the preparation of nanoparticles is a complicated process, and a wide variety of different variables may affect the properties of the final product. In the case of ZnO, it is very important to obtain a narrow size distribution of the final species and to be able to control the morphology of ZnO thin films [14].

Carbon nanotubes are allotropes of carbon with a tube-shaped nanostructure.They are generally referred to as CNTs in short. Nanotubes are developed with a length-to-width proportion of up to 132,000,000:1. They have extraordinary properties which offer remarkable opportunities for the development of new materials and devices. The reinforcement of CNTs with the matrix material adds value and makes it as advanced multifunctional material [1]. They have amazing properties that are significant for nanotechnology, hardware, optics, and numerous different fields of materials science and innovation. Because of their phenomenal warm conductivity, mechanical and electrical properties they discover applications as added substances to different auxiliary materials [15].

Nanotubes are the members of the fullerene structural family. Their name is derived from their long, empty structure with the dividers shaped by one-particle thick sheets of carbon, called graphene. These sheets are moved at particular and discrete edges, and the blend of the moving edge and span chooses the nanotube properties. For instance, whether the individual nanotube shell is a metal or a semiconductor [15]. The combination of the complementary properties of ZnO and CNTs creates many exceptional mechanical, electrical and electromechanical properties that cannot be achieved by CNTs and ZnO individually. ZnO/CNT nanocomposite has been widely studied in the last few years due to their remarkable properties and versatile applications. Various preparative methods have been used in order

to enhance the excellent properties of ZnO/CNTs nanocomposite. Methods of preparation of ZnO/CNT nanocomposite and its application as electrochemical sensor have been discussed in this Thesis [1].

1.2: Structure of ZnO

ZnO nanostructures can be divided into four groups, (0-D) (or dimensionless) structures, known as atom clusters, (1-D) structures (with dimensions within the nanometric size range, such as nanorods, nanoneedles, nanotubes and nanowires) [16], (2-D) structures, such as thin films and monolayers structures haveing two dimensions that exceed the nanometric size range, and (3-D) structures, such as a bulk structure (nucleation) [17].

ZnO is an II-VI compound semiconductor whose ionicity resides at the borderline between covalent and ionic semiconductor. The crystal structures shared by ZnO are; wurtzite (hexagonal), zinc-blende (cubic), and rock salt (cubic)[17]. At ambient conditions, the thermodynamically stable phase is wurtzite. The zinc-blende ZnO structure can be stabilized only by growth on cubic substrates, and the rock salt NaCl structure may be obtained at relatively high pressures.

Zinc oxide hexagonal wurtzite-type structure has a polar hexagonal axis, the c-axis, chosen to be parallel to z. The primitive translation vectors a and b lay in the x–y plane, are of equal length, and include an angle of 120°, while c is parallel to the z-axis [18].

The crystal can be described as alternating planes composed of tetrahedrally coordinated $O^{-2}$and Zn^{+2} ions, stacked along the c-axis [19], as shown in Figure (1) [20]. That is one zinc ion is surrounded tetrahedral by four oxygen ions and vice versa. The primitive unit cell contains two formula units of ZnO. The values of the primitive translation vectors are at room temperature (a = b = 0.3249 nm) and (c = 0.5206 nm) [18].

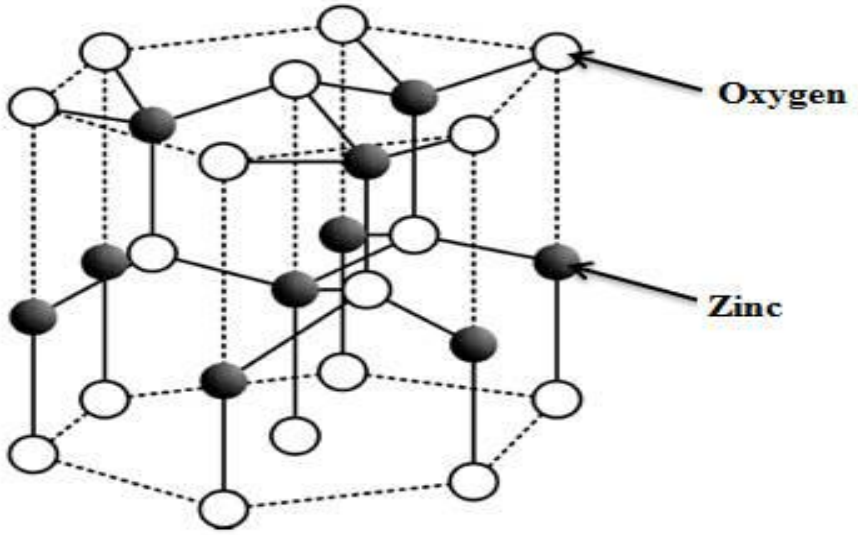

Figure (1.1): The hexagonal wurtzite structure of ZnO [19].

ZnO has a relatively large direct band gap of (~3.37 eV) at room temperature, therefore, pure ZnO is colorless and transparent and most ZnOs has n-type character, even in the absence of intentional doping [21]. Generally, ZnO thin films show n-type conduction due to oxygen deficiencies and interstitial Zn ions which act as donors in the ZnO lattice [22].

ZnO thin films exhibit a good optical transmission (over 70%) in the visible and near infrared wavelength range due to its wide bandgap energy. This transmission value of ZnO thin films depends on its microstructure and roughness [23].

As mentioned previously, ZnO have broad range of applications, is already widely used in our society, and indeed it is a key element in many industrial manufacturing processes including paints, cosmetics, pharmaceuticals, plastics, batteries, electrical equipment, rubber, soap, textiles, floor coverings to name just a few. With improvements in growth technology of ZnO nanostructures, epitaxial layers, single crystals and nanoparticles, we are now moving into an era where ZnO devices will become increasingly functional and exotic. ZnO-based nanostructures

including nanowire arrays hold a host of opportunities for flat screen displays, field emission sources, gas, chemical [24] and biological sensors, and as UV light emitters and switches [25]. Epitaxial layers and single crystals will be important for the development of optoelectronic (blue and ultraviolet light emitters and detectors) , piezoelectric and spintronic devices, and together with GaN may form the light source of the 21st century [26]. Epitaxial ZnO also holds much promise as a semi-conducting transparent thin film, which again will be important for solar cells, gas sensors, displays and wavelength selective applications. Existing technologies are also being revolutionized with ZnO nanoparticles, which have led to the development of improved sunscreens, paints and coatings [27].

The future in which ZnO devices become part of our everyday lives is already approaching reality.

1.3: Electrical Properties of ZnO

Wurtzitic ZnO is a wide-bandgap (3. 37 eV) semiconductor which has many applications, such as piezoelectric transducers, varistors, phosphors, and transparent conducting films. Most of these applications require only polycrystalline material; however, recent successes in producing large-area single crystals have opened up the possibility of producing blue and UV light emitters, high-temperature and high-power transistors. The main advantages of ZnO as a light emitter are its large exciton binding energy, and the existence of well-developed bulk and epitaxial growth processes; for electronic applications, its attractiveness lies in having high breakdown strength and high saturation velocity. ZnO is also much more resistant to radiation damage than are other common semiconductor materials, such as Si, GaAs, CdS, and even GaN; thus, it should be useful for space applications [28].

Zinc white crystallizes mainly in two forms viz cubic zinc blende and hexagonal wurtzite. The most common and stable structure at ambient conditions is wurtzite. Zincblende can be stabilized by growing zinc oxide on substrates

which has a cubic lattice structure. The oxide and zinc centres are tetrahedral [28].

Calamine is a white solid which is insoluble in water and has no smell. Crude zinc oxide appears yellow-grey in colour which exists in a granular solid form with no odour. In its natural form, it is obtained as a mineral zincite which consists of manganese (Mn) and some other impurities which makes it appear yellow-red colour. In its crystalline form, it is thermochromic which on heating in the presence of air changes its colour from white to yellow and on cooling it turns white in colour. It is an amphoteric oxide which is insoluble in water. It dissolves in acids and alkalis [28].

1.4: Optical Properties of ZnO

Optical characterization of thin films gives information about other physical properties, e.g., bandgap energy, band structure, and optically active defects. The effects of thickness and annealing on the optical transmittance and the bandgap (E_g) values of the ZnO films have been studied [29]. The fabricated ZnO films are considered as a material having direct bandgap energy [30].

1.5: Structure of CNTs

The structure of CNTs depends on the different angles and curvatures in which the graphene sheet could be rolled into a tube and is determined by a single vector. This vector is called chiral vector, which discriminate CNTs into three forms; zigzag, armchair and chiral, as shown in Figure (1.2). The electronic properties of CNTs vary according to their structure. Armchair nanotubes are metallic, while zigzag and chiral are either metallic or semiconducting nanotubes. SWCNTs, in general can be a mixture of metallic and semiconducting tubes, depending sensitively on the structure, however, MWCNTs are considered to be metallic material [31].

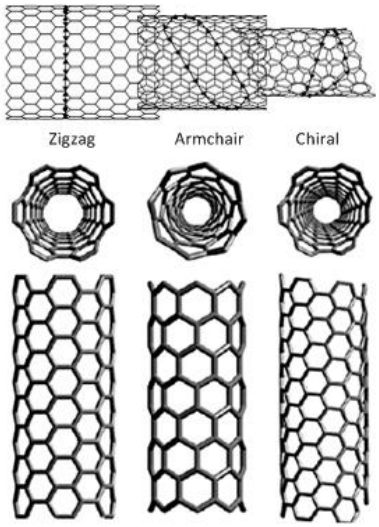

Figure (1.2): Classification of carbon nanotubes according to the chiral vector [32]

1.6: Production of CNTs

In general, CNTs always grow from carbon plasma in the presence of directing agents which are usually transition metal nanoparticals such as Co, Fe, Ni, V, etc [33]. The most important differences between the available methods could be summarised as:

- The method of plasma generation.
- The technique of introducing the catalyst metal.
- CNTs yield.
- The quality of CNTs.
- Commercialization and up-scaling possibilities.

1.7: Electrical Properties of CNT

Unlike graphene, which is a two-dimensional semimetal, carbon nanotubes are either metallic or semiconducting along the tubular axis. For a given (*n*,*m*) nanotube, if $n = m$, the nanotube is metallic; if $n - m$ is a multiple of 3 and $n \neq m$, then the nanotube is quasi-metallic with a very small band

gap, otherwise the nanotube is a moderate semiconductor [34]. Thus, all armchair ($n = m$) nanotubes are metallic, and nanotubes (6,4), (9,1), etc. are semiconducting [35]. Carbon nanotubes are not semimetallic because the degenerate point (the point where the π [bonding] band meets the π* [anti-bonding] band, at which the energy goes to zero) is slightly shifted away from the *K* point in the Brillouin zone because of the curvature of the tube surface, causing hybridization between the σ* and π* anti-bonding bands, modifying the band dispersion [35].

The rule regarding metallic versus semiconductor behavior has exceptions because curvature effects in small-diameter tubes can strongly influence electrical properties. Thus, a (5,0) SWCNT that should be semiconducting in fact is metallic according to the calculations. Likewise, zigzag and chiral SWCNTs with small diameters that should be metallic have a finite gap (armchair nanotubes remain metallic) [35]. In theory, metallic nanotubes can carry an electric current density of 4×10^9 A/cm^2, which is more than 1,000 times greater than those of metals such as copper, [36] where for copper interconnects, current densities are limited by electromigration. Carbon nanotubes are thus being explored as interconnects and conductivity-enhancing components in composite materials, and many groups are attempting to commercialize highly conducting electrical wire assembled from individual carbon nanotubes. There are significant challenges to be overcome however, such as undesired current saturation under voltage [37] and the much more resistive nanotube-to-nanotube junctions and impurities, all of which lower the electrical conductivity of the macroscopic nanotube wires by orders of magnitude, as compared to the conductivity of the individual nanotubes [37].

1.8: Optical properties of CNT

Carbon nanotubes have useful absorption, photoluminescence, and Raman spectroscopy properties. Spectroscopic methods offer the possibility of quick and non-destructive characterization of relatively large amounts of carbon nanotubes. There is a strong demand for such characterization from the industrial point of view: numerous parameters of nanotube synthesis can be changed, intentionally or unintentionally, to alter the nanotube quality. As shown below, optical absorption, photoluminescence, and Raman spectroscopies allow quick and reliable characterization of this "nanotube quality" in terms of non-tubular carbon content, structure (chirality) of the produced nanotubes, and structural defects. These features determine nearly any other properties such as optical, mechanical, and electrical properties [38].

Carbon nanotubes are unique "one-dimensional systems" which can be envisioned as rolled single sheets of graphite (or more precisely graphene). This rolling can be done at different angles and curvatures resulting in different nanotube properties. The diameter typically varies in the range 0.4–40 nm , but the length can vary ~100,000,000,000 times, from 0.14 nm to 55.5 cm [38]. The nanotube aspect ratio, or the length-to-diameter ratio, can be as high as 132,000,000:1,[39] which is unequalled by any other material. Consequently, all the properties of the carbon nanotubes relative to those of typical semiconductors are extremely anisotropic (directionally dependent) and tunable.

Whereas mechanical, electrical, and electrochemical (supercapacitor) properties of the carbon nanotubes are well established and have immediate applications, the practical use of optical properties is yet unclear [39].

1.9: ZnO / CNT Composite

Carbon nanotubes have extraordinary properties that offer remarkable opportunities for the development of new materials and devices. The reinforcement of CNTs with the matrix material adds value and makes it as advanced multifunctional material. Zinc oxide (ZnO) is a semiconducting material with a wide band gap and a large excitation binding energy. The combination of the complementary properties of ZnO and CNTs creates many exceptional mechanical, electrical and electromechanical properties that cannot be achieved by CNTs and ZnO individually. ZnO-CNT nanocomposite has been widely studied in the last few years due to their remarkable properties and versatile applications [40].

Carbon nanotubes (CNTs) have drawn great attention since they were discovered because of their fascinating structural, mechanical, electronic, optical and thermal properties, and excellent chemical stability, leading to potential high-technology applications such as biosensor, supercapacitor, hydrogen storage and field emission devices .It has been reported that CNTs properties can be influenced by surface modification with nanoparticlesand many metal oxide nanostructures. Among functional metal oxide materials, Zinc oxide(ZnO) is especially attractive for their versatile practical applications, ranging from photodetector, transparent electrode, spintronic devices, surface acoustic wave devices, and thin film gas sensors,[41] attributed to their outstanding properties such as wide direct optical bandgap, large exciton binding energy, excellent chemical and thermal stability, and excellent piezoelectric properties [42]. It is believed that novel functionality combined with extra ordinary properties of ZnO and CNT, especially in the form of low-dimensional composite structures, is expected to appear [43].

1.10: Sensing Application of ZnO and CNT

Gas sensors are now playing an important role in detecting traces amounts of hazardous gasses in the atmosphere An effective sensor should have high response and anappreciable selectivity at lower temperature [44]. Most of the sensors used have made from semiconductingmetal oxides,

mixed oxides, conducting polymers and carbon nonmaterials. Metal oxide semiconductors have been explored extensively because of good sensitivity for hazardous gases, faster recovery and response, lower cost, smaller size and facile execution [45]. In past few years ago, sensors based on various metal oxide semiconductors (Fe_2O_3,TiO_2,CuO,WO_3, ZnO etc.) have been widely used forthe detection of hazardous gases. Among these metal oxides, ZnO has been extensively used as a gas sensing material [46], because ZnO nanostructures have a wide range of operating temperature, stability, and flexibility, which make them a good candidate for sensing applications [47]. ZnO is a wide band gap semiconductor and used as gas sensors for detecting hazardous gases [48].

The combination of wurtzite structure of ZnO with high electromechanical property makes ZnO as a good piezoelectric material applicable for the fabrication of piezoelectric sensors and mechanical actuators. ZnO has large band gap which makes it appropriate material for small wave length electronic devices, Light emitting diodes (LED) and laser diodes [48]. ZnO has strong binding energy of 60 meV and as a result it is a strong source of UV rays generation [49].

Piezoelectric tensor of ZnO is highest as compared to other semiconductors and because of this it works as piezoelectric material . Attempts have been made for higher gas sensing response by controlling morphology, using differ-ent composites and by doping. ZnO sensors are generallyused at higher temperatures and as a result consume morepower and may be liable for degradation [50].

On the other hand carbon materials have outstanding sensing capabilities with remarkable transduction properties [51]. In recent years amongst carbon materials, carbon nanotubes (CNTs) have been studied widely dueto their extraordinary chemical, mechanical and electrical properties [52] and applications in the area of nanotechnology [53]. Basically carbon nanotubes are of two types: single walled (SWCNT) and multi walled (MWCNT).

Carbon nanotubes are cylindrical tubes composed of carbon atoms and have diameter in nanometres (nm) with length in micrometres (Mm) and has largest length versus diameter ratio of around 132,000,000:1 as compared to other materials [54] This provides an extraordinary stiffness to carbon nanotubes. Sp^2 hybridized carbon atoms provide remarkable strength to CNT which is far greater than diamond. Previous studies reported that the individual MWCNT has tensile strength of (63 GPa) [55]. Thus, these properties make CNT as a stiffest and stronges material than other materials. CNTs have outstanding gas absorption capabilities due to their higher surface area. However, sensors based on CNTs have some limitations such as humidity weakness, longer recovery duration and detect those gases which have larger charge transfers and binding energies with CNTs. In recent years the hybrid materials made of car-bon nanotubes (CNTs) and metal oxide semiconductor (MOS) have been actively studied due to their numerous applications such as gas sensors, as an electrode for lithium ion batteries and photocatalysis [56]. To enhance CNTs gas sensing capability, conductive polymers or semiconductive metal oxides, catalytic metal nanoparticles were mixed with CNTs for the formation of nanocomposites [56]. ZnO-CNT nanocomposite shows many improved mechanical, electrical and sensing properties that cannot be attained by CNTs and ZnO alone. The nanodevices developed using ZnO-CNT nanocomposite come with improved performance and numerous applications, such as nano resonators, [57] biosensors [58] with high sensitivity and selectivity and super capacitors [59].

Thus the studied nanocomposite opens the door to develop new devices with enhanced properties and thus expanding the applications of ZnO and CNT in the field of nanotechnology. Thus formed nanocomposites have the combination of properties of parent materials and make a new group of material having extraordinary gas sensing properties [60].

1.11: Literature Review

This literature study provides an extensive analysis of the literature as related to the proposed work and gives an overview of the literature study for some authors.

ZnO sol-gel coatings are a promising candidate to be used as optical filters or coatings for solar and eyeglass industry [61]. In this literature, *Moszak and coworkers* reported that ZnO prepared by sol-gel can be deposited on substrate to reduce harmful effect of high energy light as optical filter. The transparency obtained was 95% in the visible light whereas samples exhibited opaque behavior in the UV range. However, 80% transparency has been achieved in the work reported by *Sanjeev et al* [62]. ZnO films was spun on glass substrate and heat treated under the temperature range between 200 and 400 ^{o}C. The absorption of UV light by the ZnO coatings depends on their thickness and temperature of the stabilization. Its efficiency can be control through thickness of coatings and thermal condition of stabilization. The analyzed coatings exhibited good adhesion to glass substrate and the obtained value is high in comparison to the results described in the literature. The results suggest that the obtained materials have proper parameters for UV optical filters [61,62].

The optical energy gap of ZnO thin films was recorded by many literatures [62,63]. The previous works show that optical energy gap value in all ZnO samples decreases as the annealing temperature increases. *Mulmi et al,* reported that the optical energy gap of ZnO thin films prepared by spin coating is 3.22 eV for the samples heated at 300 ^{o}C and becames 3.14 and 3.05 eV at 400 and 500 ^{o}C annealing temperature correspondingly [63]. The films are also transparent from near ultraviolet to infrared region.

The annealing temperature, there is very important factor that play a major role in the performance of final devices. In addition to the above literatures, The hexagonal structure is confirmed by the XRD in the work done by *Ghosh and co-researchers* [64]. The grain size is also increased from 8.65 to 18.39 nm for as-grown sample (at room temperature) to 450 ^{o}C. It is important to note that a specific annealing temperature is sufficient to get the improved properties of ZnO thin films for device grade applications.

The molarity of the precursor during sol-gel process is, furthermore, crucial and studied expansively in the previous literatures. For instance, *Keskenler and co-workers* [65] have studied the influence of the molar concentration of zinc acetate precursor solution on the structural characteristics of ZnO films prepared by sol-gel spin coating method. They have found that, the grown ZnO films exhibit a higher degree of preference along the c-axis perpendicular to the substrate surface, except 1.5 M sample, as determined from XRD measurements. The (002) peak intensity of the films gradually decreases, the crystal structures of the films changed from single to poly crystalline with the increasing molarity from 0.5 M to 1.5 M. The calculated values of grain size and roughness are 36.31 nm, 24 nm; 41.32 nm, 176 nm; and 42.33 nm, 404 nm for samples 0.5 M, 1.0 M and 1.5 M, respectively [65]. However, *Ghazai et al* [66] reported that, for the ZnO thin films deposited on glass substrate using spin coating method using zinc acetate and for both triethanolamine (TEA) with NaOH and menoethanolamine (MEA) as solvents and stabilizer materials, XRD results show that the prepared films have polycrystalline in nature and the referred orientation ZnO is (002) have low grain size to be 9.9 and 5.3 nm for zinc acetate, both triethanolamine (TEA) with NaOH and menoethanolamine (MEA) of concentration ratio of 1:4 which calculated using Debye Scherer's formula [66]. It may be concluded that molarity could affect the grain size, orientation and crystallinity of ZnO and the appropriate molarity (0.5 M) can improve ZnO structural properties in general. In addition, SEM images are

agreement with the XRD results that films with zinc acetate and menoethanolamine (MEA) have smooth surface, make ZnO thin film a promising material to solar cells and optoelectronic devices [64,66].

Ambalagi and co-workers [67] reported the polyaniline-zinc oxide Nanocomposites was successfully synthesized by in-situ polymerization method. The electrical conductivity in these Nanocomposites shows a strong dependence on content of zinc oxide nanoparticles in PANI-ZnO Nanocomposites. The maximum conductivity is observed for 50 wt% of Zinc oxide nanocomposites. Hence these nanocomposites are found to be promising material for potential applications. *Natsume and co-workers* [68] reported the Undoped ZnO films were fabricated by the sol-gel spin-coating method; its D.C. electrical conductivity was investigated. The (160-230 nm) thick films formed on pyrex glass substrate. A minimum D.C. resistivity of 28.2 Ω.cm is obtained by a 10-cycle spin-coating of zinc acetate film followed by annealing in air at a temperature of 525 ºC. From the temperature dependence of D.C. conductivity, the electron conduction was confirmed to be due to transport in the conduction band at temperatures above 250 K, where grain boundary scattering was caused by thermionic emission of electrons over grain boundaries. Nearest neighbor hopping conduction between donors was dominant for temperatures below 250 K.

The first discovery of multi-walled carbon nanotubes (MWCNTs) [69] and single-walled carbon nanotubes (SWCNTs) [70] was made by Iijama in 1991 and 1993 respectively. The diameters are approximately 1-2 nm for SWCNTs and 2-100nm for MWCNTs, which consist of more than one concentrically rolled layer of graphene, and their length are roughly between 1-10μm. Therefore, the aspect ratio (ratio of length to diameter) becomes 1000 or more [71-73].

Based on the unique structure of the parent material (graphene), carbon nanotubes are suggested to have novel properties that make them potentially beneficial in many applications. These include high performance

nanocomposites which are conductive and of natural high strength [74], nanosized semiconductor devices [75], nano-probes [76], energy conversion devices [77], sensors [78,79], field emission displays [80], radiation sources [81] and drug delivery systems [82,83]; however these applications still remain in the "possible" stage. Lack of availability of bulk quantities of high quality and low cost, as well as processing difficulties are the main obstacles in expanding the technological applications of carbon nanotubes.

As a member of the fullerene structural family, the carbon atoms in carbon nanotubes are sp^2-bonded. Due to the extended electron system, the surface electrons are highly polarizable, and so are subject to large attractive inter-tubular van der Waals forces [84].

In addition, carbon nanotubes are smooth-sided compounds with attractive interactions of 0.5 eV per nanometer of tube-to-tube contact. These extreme cohesive forces could account for the bundled structure of SWCNTs. The size of bundles has been shown to be judged by distortions of van der Waals bonds between nanotubes in the surrounding area of a catalytic particle and the degree of nanotube bending in the bundle [85].

The typical bundle size of as-produced SWNTs varies between nanometers to microns. Figure. (1.3b) shows a Transmission Electron Microscopy (TEM) image of a nanotube bundles [86].

Although the chemical reactivity of carbon nanotubes, compared with graphene, is enhanced as a result of the surface curvature, carbon nanotubes tend to aggregate together when exposed to most solvents, aqueous or organic due to their hydrophobic nature [87]. Therefore, the studies and applications of CNTs are hindered by processing and manipulation difficulties owing to their insolubility or poor dispersion in common solvents and polymeric matrices [88].

The combination of the complementary properties of ZnO and CNTs creates many exceptional mechanical, electrical and electromechanical

properties that cannot be achieved by CNTs and ZnO individually. ZnO-CNT nanocomposite has been widely studied in the last few years due to their remarkable properties and versatile applications. Methods of preparation of ZnO-CNT nanocomposite and its application as electrochemical sensor have discussed by *S. Barthwal and N. B. Singhc* [89]. Conductive composites include any composite having significant electrical conductivity. These conductive composites may replace the metals in some applications. The applications of conductive composites include, for example, electromagnetic interference shielding materials, coatings, sensors, batteries, electrodes. This review paper focused on carbon-based materials such as graphene, as a conductive nanofiller, and it provides a review of the properties and synthesis of graphene by *Alemour et al* [90].

Cursaru et al, reported obtain of ZnO-CNT nanocomposites by in situ hydrothermal method in high-pressure conditions. The structure and morphology of ZnO-CNT nanocomposites were analyzed by Fourier transform infrared spectroscopy (FTIR). FTIR spectra suggest possible interactions between CNT and ZnO [91]. The properties of the synthesized ZnO/CNTs nanocomposite structure in comparison with that of ZnO nanoparticles and CNTs were studied by several techniques to prove the generation of nanostructure form of ZnO the complete interaction between ZnO nanoparticles and CNTs in the work done by *Alamro et al* [92]. *Basit et al*, reported that Zinc oxide/carbon nanotube (ZnO/CNTs) nanocomposites are developed on gold (Au)-coated unpolished Si p-type (100) substrates with 2, 4, 6, 8, and 10 nm thicknesses by vapor–liquid–solid method. XRD, FE-SEM, Raman, and photoluminescence spectroscopic characterizations are used to study structural, morphological, and optical properties [93].

In addition, carbon nanotubes are smooth sided compounds with attractive interactions of 0.5 eV per nanometer of tube-to-tube contact. These extreme cohesive forces could account for the bundled structure of SWCNTs. The size of bundles shown to be judged by distortions of van der Waals bonds

between nanotubes in the surrounding area of a catalytic particle and the degree of nanotube bending in the bundle [94].

The typical bundle size of as-produced SWNTs varies between nanometers to microns. Figure (3.1b) shows a Transmission Electron Microscopy (TEM) image of a nanotube bundles [95].

a

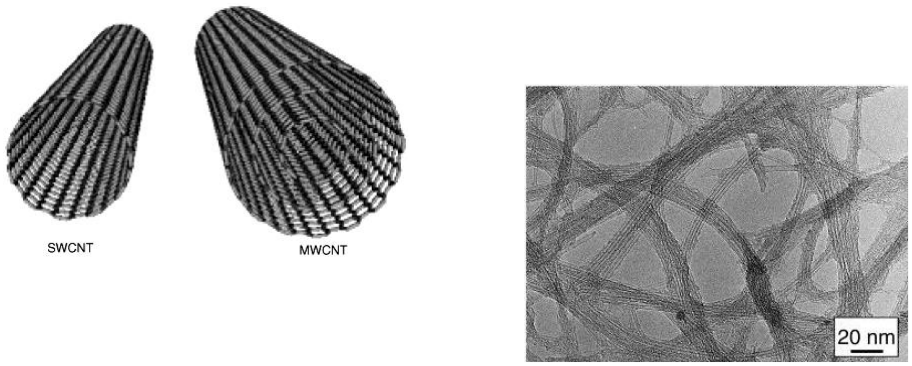

Figure (1.3): (a) Conceptual diagram of SWCNT and MWCNT, (b) TEM image of SWCNTs [95]

Although the chemical reactivity of carbon nanotubes, compared with graphene, is enhanced as a result of the surface curvature, carbon nanotubes tend to aggregate together when exposed to most solvents, aqueous or organic due to their hydrophobic nature [96]. Therefore, the studies and applications of CNTs are hindered by processing and manipulation difficulties owing to their insolubility or poor dispersion in common solvents and polymeric matrices [97].

1.12 :Aims and Objectives

The principle aim of this research is to synthesis of zinc oxide modified carbon nanotubes using obtimized sol-gel technique and to investigate the sensing performance of the prepared devices towards some odorants. Some other objectives can be achieved throughout this work such as;

• Study the optical properties and optical energy gap for the pure zinc and the carbon nanotubes improved samples.

• Investigate the electrical properties including I-V measurements as well as temperature dependence conductivity and the activation energy.

• Study the structural properties through FESEM images, FTIR and X-Ray Diffraction. In addition, Scherrer calculation could be conducted to investigate the crystallite size of the prepared samples.

• Sensing activity towards some gases could be studied using homemade sensing chamber and to investigate the effect of carbon nanotubes on the activity of the sensor devices.

2.1: Introduction

This chapter provides a comprehensive consequent of the theoretical aspects of the structural, morphological, optical, and electrical measurements, as well as a thorough summary of the relationships, scientific explanations, and equations utilised in this thesis.

2.2: Sol - Gel Technology

One of the simplest methods for synthesis metal oxide nanoparticles is the Sol-Gel approach. It is used to make new structures of materials (mostly metal oxides and similar inorganic materials) when an inorganic precursor and an organic solvent are present [98]. This method is used to calculated the molar concentration can be used the following equation (2-1) [99]:

$$\mathbf{M = (W_t/M_{wt}).(1000/V)} \qquad \textbf{(2-1)}$$

Where M represents the molarity, W_t refers to the weight of sample, M_{wt} represents the molecular weight, V represents the water volume.

The sol–gel method was first used to make silica gel in the middle of the 19th century. When coupled with appropriate solvents and reactants, metal alkoxides can create homogeneous solutions, colloidal suspensions (Sol), and integrated networks (Gel) [100]. These gels can then be dried to make xerogels or aerogels.

2.3: Spray Pyrolysis

There are several methods for creating thin films, including spin coating, drop casting, spray coating, and more. Spray coating is the method employed in this study. Spray is a low-cost and straightforward way to make thin films, and it can generate uniformly thick and high-quality coatings across huge areas. Spray technique doesnot require high-quality targets or substrates or vacuum at any phase, which is beneficial for industrial applications. By adjusting spray settings, deposition rate and film thickness may be readily regulated. Simply by adding or modifying the composition of the spray solution during spraying, one may dope films with nearly any ingredient in

any proportion. As long as you can find a spray solution that can be modified while spraying, you can dot films with practically any element in any proportion. Spray coating is advantageous because it may be used to create multilayer and multi-component films with varying thicknesses [101].

The different properties of deposited thin films are essentially a result of the preparation circumstances. The substrate's surface temperature has the greatest influence on the film's roughness, breaking, crystallinity, etc. Aerosol transport, precursor disintegration, and atomization of the precursor solution are essential components of the spray method [102].

2.4: Optical Properties

Intrinsic effect is connected to a semiconductor's optical characteristics. The creation of electron-hole pairs can take place directly or indirectly depending on the inherent placement of the valence band's top and conduction band's bottom in the band structure. A compound semiconductor with a broad straight band gap is ZnO thin film. Depending on the deposition method and thickness, it is very transparent in the visible range [103, 104]. In the molecular scale valence and conduction bands become higher occupied molecular orbital (HOMO) and lower un-occupied molecular orbital (LUMO). Figure (2.1) represents the possible electronic transition.

Many molecules absorb ultraviolet or visible light. The basic absorption, which includes the movement of electrons from the valence to the conduction band and expresses itself by a sharp increase in absorption , is the most significant absorption process and may be used to calculate the semiconductor's energy gap [105].

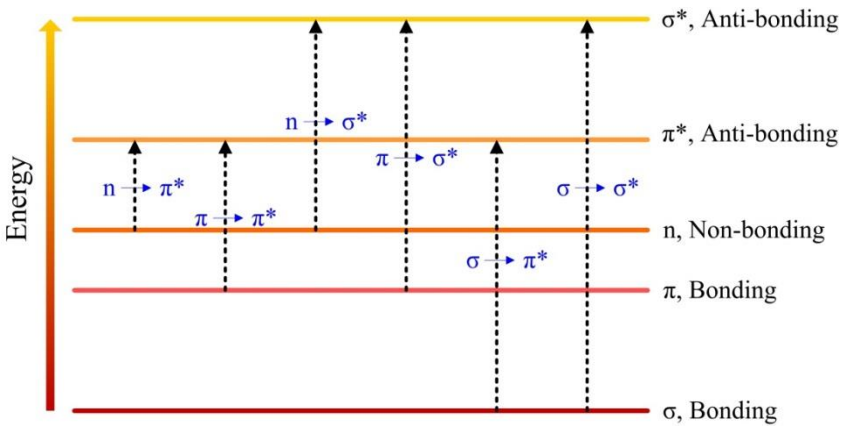

Figure (2.1): Possible electronic transition between intermolecular orbitals[106].

Photons from the incident beam are captuced by the semiconductor. The amount of photons taken in depends on their energy ($h\upsilon$), where (h) represents Plank's constant and (υ) represents the frequency of the incident photons. Begining at the absorption edge, that matches the least energy difference (E_g) between the HOMO minimum and LUMO maximum, absorption is connected to the HOMO-LUMO electronic transition. If the photon energy ($h\upsilon$) is equal to or larger than the energy gap (E_g), it can elevate a valence electron into the LUMO and produce an electron-hole pair [107]. The incoming photon's maximum wavelength (λ_{max}) that forms the electron-hole pair is specified as [108]:

$$\boldsymbol{\lambda_{max} = \frac{hc}{E_g} = \frac{1.24}{E_{g(eV)}}} \qquad \textbf{(2-2)}$$

According to Beer's law, the photon flux intensity drops exponentially with semiconductor distance [109].

$$\boldsymbol{I_t = I_o e^{-\alpha t}} \qquad \textbf{(2-3)}$$

Where:

I_o *and* I_t = represent, the incident and transmitted photon intensities respectively.

α represents the absorption coefficient, that is the proportional quantity of photons absorbed per unit distance of semiconductor, and (T) is the film thickness [110]:

$$\boldsymbol{\alpha = 2.303 \frac{A_b}{T}} \qquad \textbf{(2-4)}$$

Where (A_b) is the absorption.

Radiation absorption results in electronic transitions between the valence and conduction bands in two unique ways: "direct and indirect".The Tauc equation describes these transitions [111]:

$$\boldsymbol{(\alpha h\nu) = B(h\nu - E_g)^r} \qquad \textbf{(2-5)}$$

Where $(h\nu)$ represents the incident photon energy and (r) represents a constant that recieves the values (1/2, 3/2, 2, and 3) basing on the material and the kind of optical transition (direct or indirect), with (r) equal to 1/2, 2, 3/2, or 3 for direct allowed, direct forbidden, and indirect forbidden transitions, correspondingly. In this research of ZnO, (r) of Equation (2-5) was set to 2 and (B) is the edge width parameter [112,113].

Because of they characterise the optical behaviour of the materials, optical constants are critical characteristics. The material's absorption coefficient has a very strong relationship with the energy of the photons and the energy of the band gap. As it is possible to know the nature of electronic transfers from knowing the value of the absorption coefficient, if the value of the absorption coefficient is high (α>10^4), then this means the possibility of a direct electronic transmission [114].

2.5: Electrical Properties

At zero Kelvin temperature, semiconductor materials are insulators, but they can become conductors when the temperature rises to the limit values that convert to an increase in electron density. Therefore, the materials can be classified according to the values of its electrical conductivity into three

types; Conductor (σ 10^{3}-10^{8} S/m), Semiconductor (σ 10^{-3} - 10^{-8} S/m), and Insulator (σ 10^{-8}-10^{-18} S/m) [115].

These parameters are essential for their use in many electronic and optoelectronic applications. By measuring the electrical properties of thin semiconductor films, it is possible to figure out how much impurity is in them. The electrical characteristics of a semiconductor depend on its nature, whether it is pure or doped, crystalline or amorphous [116].

Ohm's law states that the current I (in amps) in a sample is precisely proportional to the potential difference V (in Volts) between two places on this sample [117]:

$$\mathbf{R = V/I} \qquad \textbf{(2-6)}$$

Where:

R= represents the sample resistance measured in Ohms.

Resistance to the passage of electric current is a quality that can also be referred to as electrical resistivity, particular electrical resistance, or volume resistivity. A low resistivity suggests a substance that easily permits electric charge to travel. The Greek letter $\rho_{el.}$ $(rho)_{el}$ is widely used to denote resistivity. The Ohm multiplied by metre (Ω·m) is the (SI) unit system of electrical resistivity, however alternative units such as (Ω·cm) are occasionally used [115].

Assume that a piece of material with a length l (m) and a cross-section area an is conducting current (m^2). The electrical resistivity ρ can be defined as [117]:

$$\boldsymbol{\rho = R\,A\,/\,l} \qquad \textbf{(2-7)}$$

Specifically, electrical conductivity, also known as specific conductance, evaluates a substance's ability to convey an electric current. It is often denoted by the Greek letter σ (sigma), although (kappa) (particularly in

electrical engineering) and γ (gamma) are also occasionally employed. Its (SI) unit refers to Siemens per metre (S/m) [115].

Where conductivity σ represents the inverse of the resistivity ρ [117]:

$$\boldsymbol{\sigma = 1/\rho} \qquad \textbf{(2-8)}$$

R_e is the reflectance, which is calculated by employing equation [118]:

$$\mathbf{R = 1-T-A} \qquad \textbf{(2-9)}$$

The wave's exponential fall as it moves through a material is proportional to the extinction coefficient, which is described as [109]:

$$\mathbf{k = \frac{\alpha\lambda}{4\pi}} \qquad \textbf{(2-10)}$$

Where (k) represents the extinction coefficient and (λ) represents the wavelength of the incident radiation

Based on equations (2-9) and (2-10) the interdigitated electrode geometry was utilised to estimate the resistances (2-10**)** [117]:

$$\boldsymbol{\sigma = L/RTWN_r} \qquad \textbf{(2-11)}$$

Where:

T= represents the film thickness.

L= reprsents the gap between fingers.

W= reprsents the overlap distance between the electrodes.

N_r = represents the number of fingers of interdigitated electrodes (n=10-15).

R= reresents the films resistance.

The temperature dependence electrical conductivity of the materials can be analyzed by the Arrhenius equation [119]:

$$\boldsymbol{\sigma = \sigma_\circ \exp\left[\frac{E_a}{K_B T}\right]} \qquad \textbf{(2-12)}$$

Where:

$\sigma_\circ$ = represents constan.

E_a = represents the activation energy.

K_B = represents Boltzmann constant equal 1.38×10^{-23} J/K.

T = temperature in Kelvin.

Using the previous equation, we can get the activation energy equation:

$$\mathbf{E_a = \frac{T * ln\sigma}{1000} * K_B * 1000 \left(\frac{J}{K}\right)} \qquad \textbf{(2-13)}$$

2.6: Electrodes Deposition

Technique has been around for a very long time. It is a process of coating a thin layer of one metal on top of a different metal to modify its surface properties, by donating electrons to the ions in a solution. This bottom-up fabrication technique is versatile and can be applied to a wide range of potential applications. Electrodeposition is gaining popularity in recent years due to its capability in fabricating one-dimensional nanostructures such as nanorods, naowires and nanotubes [120] .

Electrode is the type of electronic conductor, usually metals partly immersed in an electrolytic solution, and imparts or receives electrons from the medium in a storage battery, solid, gas, or vacuum. Electrodes are used commonly in electrochemical cells, semiconductors like diodes, and different types of medical devices. In the electrolysis of electrochemical cells, the electrical energy from the external sources is used to perform a chemical change or redox reaction [120].

Different Types of Electrodes

- Metal-metal ion electrode.
- Metal-insoluble salt electrode.
- Metal-amalgam electrode.
- Gas-ion electrode.
- Redox electrode.

2.7: Sensing Properties

A chemical sensor is defined as a device that receives physical and chemical signals and converts them into electrical signals .As a result of the chemical reaction that occurs between the sensitizer and the dissolved gas [121]. Oxides of semiconductor materials in the manufacture of chemical sensors due to their high sensitivity and its low cost. Sensors are used to detect the presence of unwanted gases in the atmosphere. This includes the leakage of some hazardous gases in the reactors, as well as being used in laboratories that require high purity and in various other places [122].

The principle of the sensor's work is based on the electron exchange between a surface semiconductors and gas molecules. There is a weak interaction between the gas molecules and the surface of the semiconductor by Vander Waals forces, which is known as physical adsorption, where the shape of the adsorbed part does not change. In the case of a strong interaction between surface atoms and gas molecules, it is called chemical adsorption type of adsorption chemical bonds are formed between gas molecules and surface atoms, and adsorption increases with the presence of surface defects. Solid-state gas sensors, are the most promising avenues again for promotion of new gas sensors that may be used for a wide variety of applications in the area of gas sensing. A number of advantages of solid-state gas sensors have piqued the interest of both the industrial and scientific communities. These advantages include their small size, high sensitivity, and the ability to detect very low concentrations at the level of ppm (particles per million) or even ppb (particles per billion) of a wide range of gaseous chemical compounds. Solid-state gas sensors are being developed for a variety of applications [122].

In our daily lives, we come into contact with many dangerous and flammable gases. Some of these gases contribute to air pollution and hurt our health. On account of the need to detect these gases properly, gas sensors have received a great deal of research attention due to their benefits, which

include their low cost, small construction, extended lifespan, and straightforward circuitry [123, 124]. Additionally, metal oxide semiconductor (MOS) gas sensors, which are resistive in nature, have grown in popularity in the gas sensors field [125].

Gas sensor performance is measured by responsiveness, operating temperature, detection limit, response/recovery time, and selectivity [126]. Response is determined using R_a and R_g, where R_a is air resistance and R_g is gas resistance. Response cannot be directly tested. The technique of computation is different since the resistance change trend depends on the kind of semiconductor and targeted gas. In contrast to the p-type semiconductor, the n-type semiconductor's conductivity rises when it comes into contact with a reducing gas. As a result, the response for an n-type semiconductor is R_g/R_a in an oxidising gas and R_a/R_g in a reducing gas; however, the situation is the reverse for a p-type semiconductor, as shown in Table (2.1). Response reflects variable sensitive materials and gas sensing sensitivity of sensors. Selectivity reveals if gas sensors are capable of recognising a particular gas[127].

In general, the temperature at which sensors are most responsive increases initially and then declines as the temperature rises. In addition to these features, other indices are set up to show how well sensors can detect gases. The detection limit defines the application field for gas sensors, which is the lowest gas concentration they can detect. Response time is the period between introducing the intended gas and when resistance stabilises. On the other hand, recovery time is the time between removing the targeted gas and when air resistance stabilises. These considerations influence the usage of gas sensors [127].

Table (2.1): Gas sensors responses in various environments [127].

Sensitive Material Types	Aimed Gas Type	Response (S)
n-type	oxidizing	R_g/R_a
	reducing	R_a/R_g
p-type	oxidizing	R_a/R_g
	reducing	R_g/R_a

Many of these indices are connected with sensitive materials, which are crucial to gas sensors. As a result, a variety of methods have been investigated for a long time to overcome the shortcomings of gas sensors, such as their sluggish reaction, lack of selectivity, high working temperature, and long response/recovery time. Nanomaterial, which has at least one dimension in the nanoscale (1-100 nm), has been discovered to be a superior choice for gas sensing than standard materials. Specifically, this is because its unique characteristics (for example, optical, electrical, thermal and magnetic characteristics) are the result of various interactions between subatomic particles, including those caused by quantum confinement, by surface interactions, and by effects like the macroscopic quantum confinement effect [128].

Nanostructure and morphology, which describe how the main units (electrons, ions, atoms, molecules, etc.) that creates nanomaterials are put together and arranged, work well for gas sensing characteristics. An organised nanostructure and morphology was revealed to have further effects on materials and increase their gas sensing characteristics as research advanced, as did the inclusion of other elements through doping or decoration. These findings will be detailed in the next sections [128].

Industrial activities, transportation, and energy generation are the main human-caused pollution causes [129]. Carbon dioxide (CO_2), methane (CH_4),

and ozone (O_3) are only a few of the gases that are released into the atmosphere. Above extremely low exposure levels, these chemicals can be harmful to human health. Some of these dangerous species are nitrogen dioxide (NO_2) and ammonia (NH_3). To control dangerous levels of contaminants, it is important to keep an eye on harmful gases in the field. When people's health is at risk, gas sensors can make it harder for cars to access city centres to protect the public's health [130].

Chemoresistive sensors are widely used due to their sensitivity, cheap cost, repeatability, and ease of use [131]. Other methods, such as gas chromatography, electrochemistry, and optical sensors, have certain disadvantages due to their higher cost, need for skilled staff, and continued difficulty in miniaturising and exporting measuring equipment outside of the laboratory [132]. Chemoresistive sensors may be converted to in-field readings with little power usage [133], especially at room temperature. This can result in a reduction in the complexity of the circuitry that drives the sensor. However, selectivity is still a problem, particularly with reference to metal oxides, and there is no clear solution to this problem [134]. Arrays of sensors have been utilised in certain solutions to address this issue, but in most cases, doing so is more expensive and complicates sensor design and data processing [135].

Until meantime, zinc oxide as semiconducting oxide is well known as potential resistance based gas sensor. However, Higher operating temperature becomes the drawback of its widespread applications in the area of real time gas detection, particularly, in combustible and volatile gas environment. In this contest, global research efforts were keen to reduce the temperature that the sensor device working on and the literature [106] has comprehensively reviewed the room temperature gas sensing properties of ZnO. Much more attention is predominantly waged to the effective approaches that produce room temperature gas detection of ZnO based gas sensors, mostly including; doping with other materials, morphology enhancements and light initiations.

Finally, some perceptions for future enquiry on room temperature gas detection resources are deliberated as well [107].

2.7.1 Gas Sensor Parameters

2.7.1.1 Sensitivity

Sensitivity (S) can be defined as R_{Air}/R_{Gas} for reducing gases or R_g/R_a for oxidizing gases, where R_a stands for the resistance of gas sensors in the reference gas (usually the air) and R_g stands for the resistance in the reference gas containing target gases. Both R_{Air} and R_{Gas} have a relationship with the surface reaction (s) taking place [136]. The sensitivity of a sensor is a measure of the lowest concentration of an analytic gas that can be detected. The sensitivity can be calculated with respect to the mean base line response of the sensor relative to its response to a particular analytic gas concentration [137]. The following equation shows the normalized sensitivity of the sensor operating under a fixed set of physical operating conditions[137]:

$$\mathbf{R_a / R_g = G_g / G_a} \qquad \textbf{(2-14)}$$

Where:

R_a: is the film's resistance in the air.

R_g: is the film's resistance in the presence of a gas.

G_a: is the film's electrical conductivity in the air.

G_g: In the presence of a gas, is the electrical conductance of the film.

Another approach to calculating the sensitivity (S) by using equations (2-15) and (2-16) for reducing and oxidizing gases and vapors, respectively [138] :

$$\mathbf{(S) = \Delta R / R_a = | (R_a - R_g) / R_a | \times 100\%} \qquad \textbf{(2-15)}$$

$$\mathbf{(S) = \Delta R / R_g = | (R_g - R_a) / R_g | \times 100\%} \qquad \textbf{(2-16)}$$

Although it can be calculated from the current as in the relation [138]:

$$\mathbf{S = (I_g - I_a) / I_a \times 100\%} \qquad \textbf{(2-17)}$$

Where: I_a is the sample current measured in the natural environment and I_g is the sample current recorded in the test gas.

2.7.1.2 Response Time

The response time (τ_{res}) is defined, as reported previously in the literature, as the time interval over which the resistance of the sensor material attains a fixed percentage (usually 90 %) of the final value when the sensor is exposed to the full-scale concentration of the gas. In applications such as detecting flammable or combustible gases to prevent fires, a short reaction time is very important [139].

2.7.1.3 Recovery Time

The time required to recover to within 10% of the original baseline when the flow of reducing or oxidizing gas is withdrawn is defined as the time required to recover to within 10% of the original baseline when the flow of reducing or oxidizing gas is withdrawn when the target gas is switched off. Figure (2.2) shows how this is determined from sensor data by graphing conductance as a function of time and recovery time to be ready for the next detection [140].

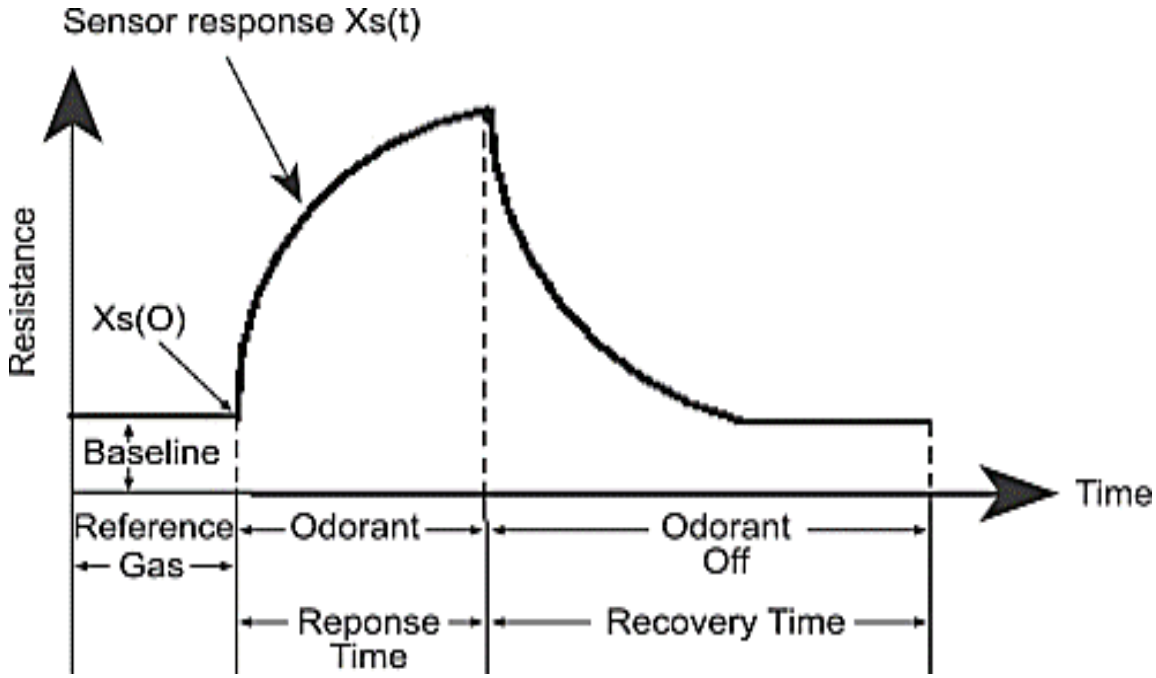

Figure (2.2): Response and Recovery Time for gas sensor [140].

2.7.2: Types of Sensors

There are many types of sensors as follow [141]:

1-Acoustic sensors are used to calculate the polarization and amplitude wave. phases, and wave velocity.

2-Thermal sensors are used to measure temperature and heat flow and specific heat.

3-Electrical and Magnetic sensors are uses to detect magnetic fields, current, magnetic moment, charge potential, conductivity, magnetic flux, magnetic permeability, capacitance, inductance, and resistance.

4-Optical sensors are used in night vision systems and machines imaging, and can be used to measure certain optical properties.

5-Mechanical sensors are used to measure speed, acceleration, strength, momentum, stress, torque, pressure, roughness, stiffness, viscosity, and composition of materials.

6-Biological and Chemical sensors are uses in chemical characterization and in biological disease diagnostic systems.

2.8: NO_2 gas

Nitrogen dioxide (NO_2) is a gas types that plays an important role in certain industrial, farming, and healthcare sectors. However, there are still significant challenges for NO_2 sensing [142]. It is a gas reddish-brown non-combustible toxic has a strong odor suffocating and usually uses the symbol NO_x to denote the oxides of nitrogen (NO_2, NO). The two referred to them in air pollution because they toxic and take part in photochemical reactions that occur in the air that led to the formation of fog, and emit this oxide to the atmosphere by natural sources, and despite the fact that the total amount gases NO_x emitted to atmospheric air about 1/6 the amount of CO gas emitted to the air, but the disadvantages of NO_x gases amounting to 22 times the

harmful effects of gas CO. NO_2 gas is more toxic because it turns mediated moisture to nitric acid, which inhaled lead to significant damage to the lungs and respiratory system, as well as break down oxides of nitrogen in the presence of oxygen and light to result in the ozone gas to be and this gas severe damage to the respiratory system .Therefore, it has become necessary to manufacture a gas sensor to detect the proportion of this gas in the environment [143]. Nitrogen dioxide is prepared by reacting copper with concentrated nitric acid. As in the following equation [142]:

$4HNO3\ (aq) + Cu\ (s) \rightarrow Cu\ (NO3)2\ (aq) + 2NO2\ (g) + 2H2O\ (aq)$ (2-18)

The detection of toxic gases has attracted great attention owing to the harmful effects these gases have on health . Poisonous gases, including nitrogen dioxide (NO_2) is prone to not only causing respiratory diseases and neurological disorders, but is also responsible for air pollution and are detrimental to the environment . NO_2, is considered one of the most harmful gases to human health and the environment. It is formed as a result of multiple sources in both daily life and chemical industry, such as vehicle exhaust and fossil fuel combustion . Low concentrations of NO_2, at levels greater than 1 ppm, can cause serious damage to the human respiration system and lung tissue, and increase the risk of emphysema and bronchitis. Furthermore, NO_2 is not only a component of acid rain, but also participates in ozone formation, which may lead to the formation of micro-particles in the air . In these regards, the detection of harmful NO_2 gas has emerged as one of the most important aspects of sensing techniques and research. The variety of response range is caused by two factors together, the increased specific surface area and the reduced oxygen containing groups [142].

3.1: Materials and Preparations

This chapter is employed to represent the methodologies used in this work during the measurements as well as the materials that utilized to prepare solutions and thin films. Figure(3.2) shows Work Scheme of the experimental procedure for the main steps that followed in this work.

3.1.1: Materials

All the chemical materials reagents used in this work have been purchased from commercial supplier and used as it is without any purification and presented in Table (3.1).

Table (3.1): Chemical materials reagents used in the work.

No.	Material	Structure	Supply Company	Purity
1.	Zinc Acetate Dihydrate	$Zn(CH_3COO)_2 \cdot 2H_2O$	FENGCHEN GROUP CO., LTD, China	99%
2.	2-methoxyethanol	$C_3H_8O_2$	China	99%
3.	Monoethanolamine	MEA	Sigma-Aldrich	99.9%
4.	Multi-Walled Carbon Nanotubes	MWCNTs	Sigma-Aldrich	
5.	Indium tin oxide	ITO	IMARC Group	
6.	Interdigitated Electrode	IDE	NORECS	
7.	Glass Slides		China	
8.	Deionized Water		China	
9.	Chloroform	$CHCl_3$	Sigma-Aldrich	99%
10.	Acetone	CH_3COCH_3	China	99%

3.1.1.1: Zinc Acetate Dihydrate

Zinc acetate is a salt with the formula $Zn(CH3CO_2)_2$, which commonly occurs as the dihydrate $Zn(CH3CO_2)_2 \cdot 2H2O$. Both the hydrate and the anhydrous forms are colorless solids that have been used as dietary supplements. Zinc acetates are prepared by the action of acetic acid on zinc carbonate or zinc metal [144].

3.1.1.2: 2-Methoxyethanol

2-Methoxyethanol, or methyl cellosolve, is an organic compound with formula $C_3H_8O_2$ that is used mainly as a solvent. It is a clear, colorless liquid with an ether-like odor. It is in a class of solvents known as glycol ethers which are notable for their ability to dissolve a variety of different types of chemical compounds and for their miscibility with water and other solvents. It can be formed by the nucleophilic attack of methanol on protonated ethylene oxide [145].

3.1.1.3: Ethanolamine

Ethanolamine is an organic chemical compound with the formula $HOCH_2CH_2NH_2$ or C_2H_7NO. The molecule is bifunctional, containing both a primary amine and a primary alcohol. It is a colorless, viscous liquid with an odor reminiscent of ammonia. Also, used in the coal-fired power stations for absorbing post-combustion CO_2 emissions. The solvent is readily available, its cost is low, and its absorption rate is fast [146].

3.1.1.4: Multi-Walled Carbon Nanotubes (MWCNTs).

Multi-walled carbon nanotubes (MWCNTs) are a special form of carbon nanotubes in which multiple single-walled carbon nanotubes are nested inside one another. Although MWCNTs are still classed as a 1-dimenional form of carbon, the unique properties that are seen within single-walled and double-walled carbon nanotubes are not as prominent. The reason for this is the higher probability of defects occurring . These disadvantages are offset by

the increased dispersability of MWCNTs, and the reduced cost in synthesis and purification of these materials [72].

3.1.2: Preparation

3.1.2.1: Sol-Gel Method

In this work, ZnO thin films were prepared by sol-gel method. Zinc acetatedehydrate, 2-methoxyethanol and monoethanolamine (MEA) have been used as starting, precursor and catalyst materials. 21.9 g of zinc acetate dehydrate was first dissolved in a mixture of (133ml) of 2-methoxyethanol and (6.03ml) of MEA solution at room temperature. The molar ratio of MEA to zincacetate was maintained at 1.0 and the concentration of zinc acetate was 0.75 M. The solution was stirred at 60 ^{o}C for 2 h to yield a clear and homogeneous solution, which served as the precursor solution. The color was turned to dark yellow indicating very fine colloidal nanoparticles was attained [147]. The mixture was aged at room temperature for (24) h and remain unchanged as indication of successful ZnO nanoparticles formation. Same process was repeated with the addition of 14 mg multi walled carbon nanotubes with the Zinc acetatedehydrate, 2-methoxyethanol and (MEA).

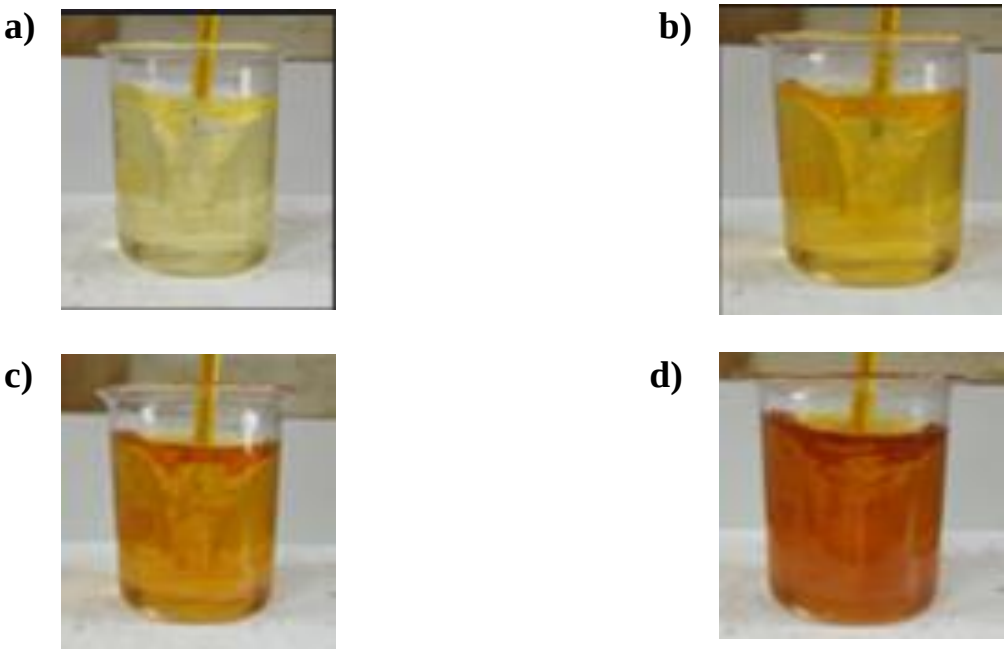

Figure (3.1): The color change of ZnO during: (a) 25 min. (b) 50 min. (c) 70 min. (d) 90 min.

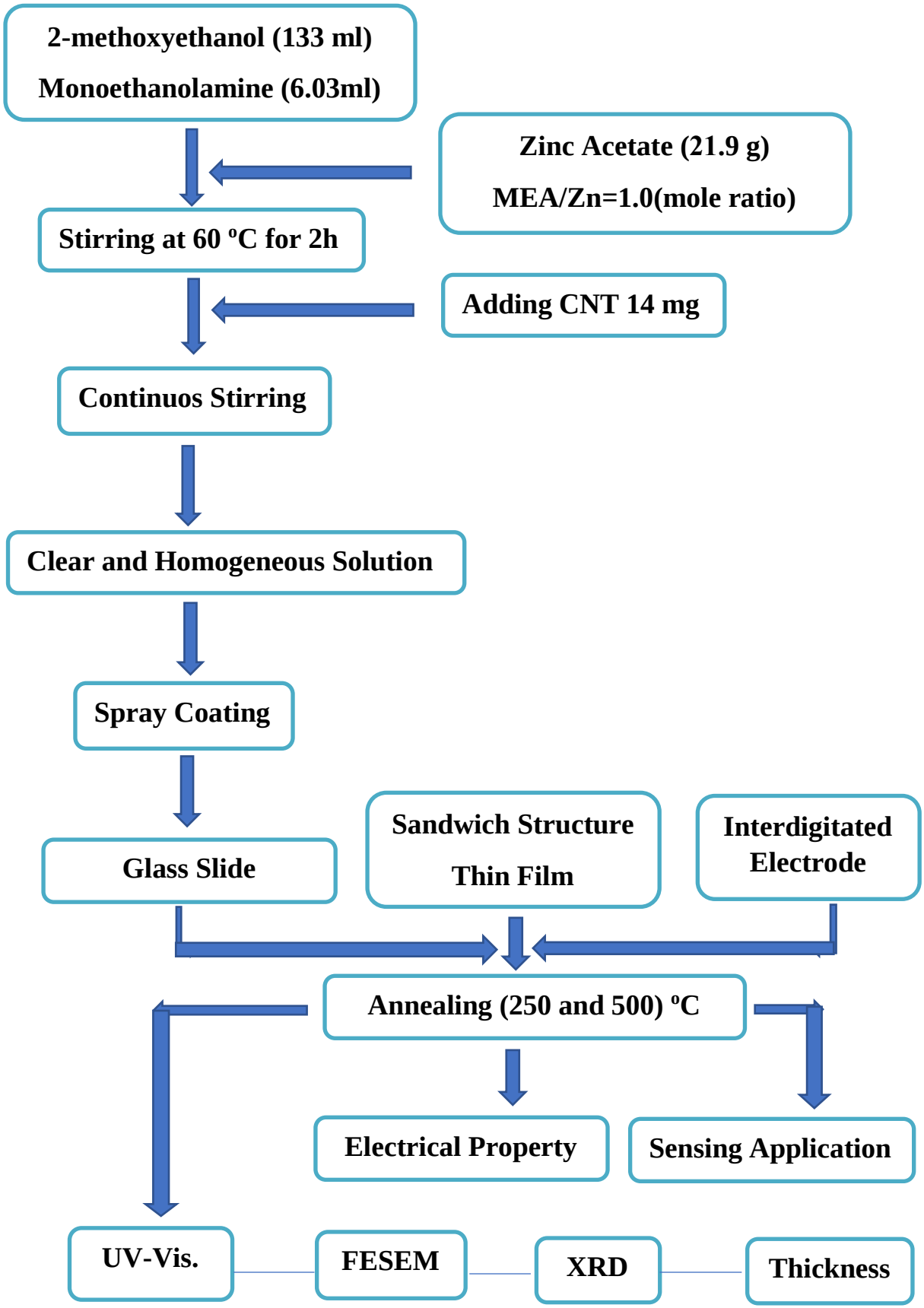

Figure (3.2): Work Scheme of the experimental procedure for the main steps that followed in this work.

3.1.2.2: Spray Pyrolysis Coating

Spray Pyrolysis Coating All the substrates are cleaned thoroughly with acetone using ultrasonic path. The ZnO thin films were deposited on glass substrate, and interdigitated electrodes using spray coating, before starting the spraying process, it is very important to choose the substrate place, substrate temperature, spraying distance, spraying flow rate and spraying time to obtain a homogeneous film within the spraying area. The solution is sprayed onto glass substrate which for optical and structural characterizations, and the ITO substrates were further made as sandwich structure devices by thermal evaporating aluminum top electrodes for performing electrical investigations and sensor measurements. vertical height (18) cm between the spray device and the bases after the temperature reaches (80)^{o}C and with a spray time (1) min to each spray to another to keep the thermal stability of the glass substrate. The process was repeated (5 and 10) sprinkle to obtain the required thickness. After the completion of the spraying process the glass substrate are left for (2) min to cool down.

Chemical techniques for the preparation of thin films consist of several simple devices (electric heater, self-control device for spraying process, temperature sensor, digital voltage reader with temperature, temperature controller, nitrogen gas cylinder, electro-mechanical valve to control and control the gas flow, gas pressure regulator).

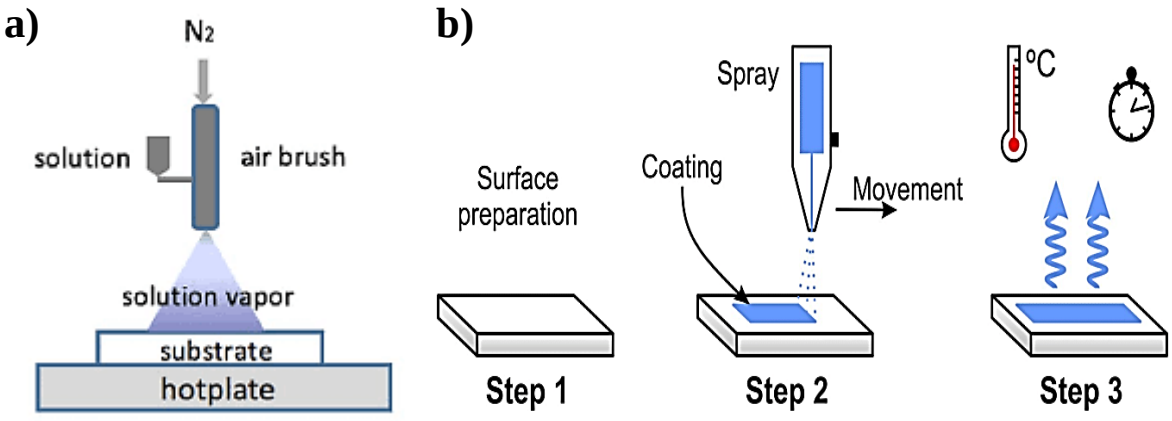

Figure (3.3): Chemical Spray Pyrolysis System.

3.1.2.3: Annealing

Annealing is a heat treatment process that changes the physical and sometimes also the chemical properties of a material to increase ductility and reduce the hardness to make it more workable.

The annealing process requires the material above its recrystallization temperature for a set amount of time before cooling. The cooling rate depends upon the types of metals being annealed.

After being Films deposited by spray coating, they were annealed at (250 and 500) ^{o}C at a programmable furnace. In the samples heated at (250)^{o}C where the furnace temperature was raised to (30)°C by (12) min and it was (150)^{o}C by (10) and it remained stable at (150)°C for (10) min and by (30) min it was raised to (250)°C and it remained stable at (250)°C by (15) min and it was cooled to (100)°C and then it was cooled to room temperature.

The samples heated at (500)^{o}C where the furnace temperature was raised to (30)°C by (22) min and it was (250)^{o}C by (10) and it remained stable at (250) °C by (25) min it was raised to (500)°C by (20) min and it remained stable at (500)°C by (25) min and it was cooled to (250) °C by (10) and then it was cooled to room temperature. Figures (3.4) and (3.5) represent the programmed segments of heating for clarity.

* Note: In Figure (3.6) the samples on the right side of each (a, b and c) represent the thin films that heated at (500)^{o}C respectively, while the ones on the left side represent the thin films that heated at (250)^{o}C

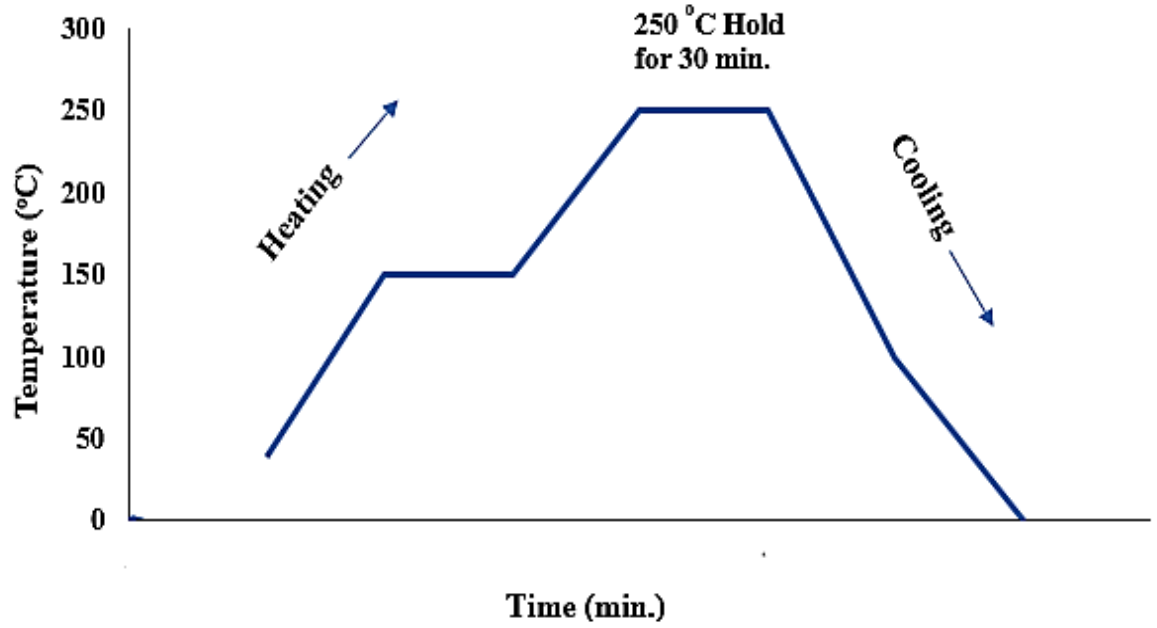

Figure (3.4): Heating and cooling according to the output of the program of the samples heated at (250) °C.

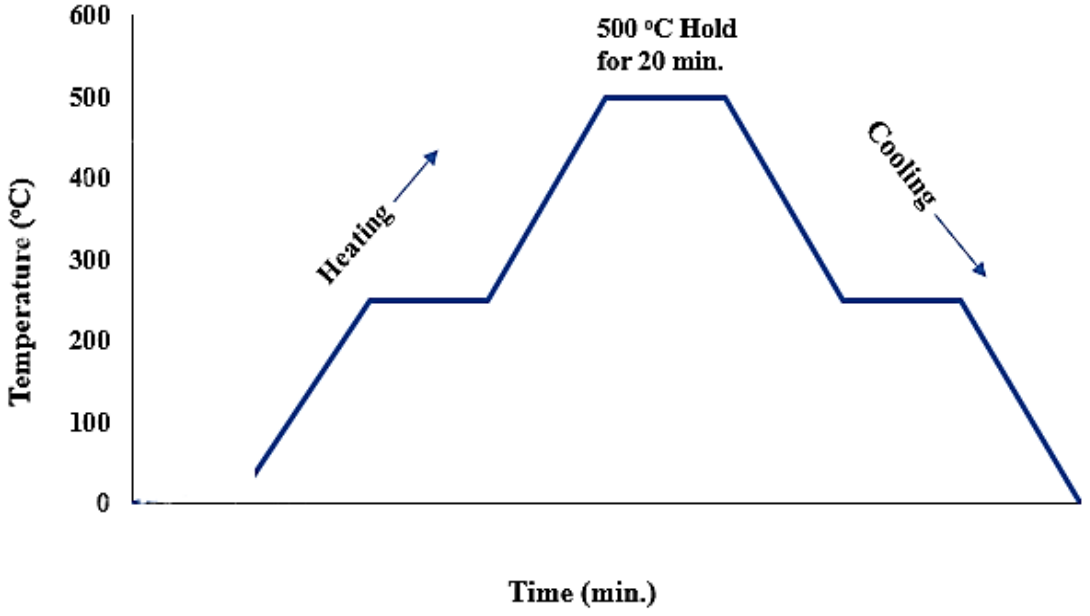

Figure (3.5): Heating and cooling according to the output of the program of the samples heated at (500) °C.

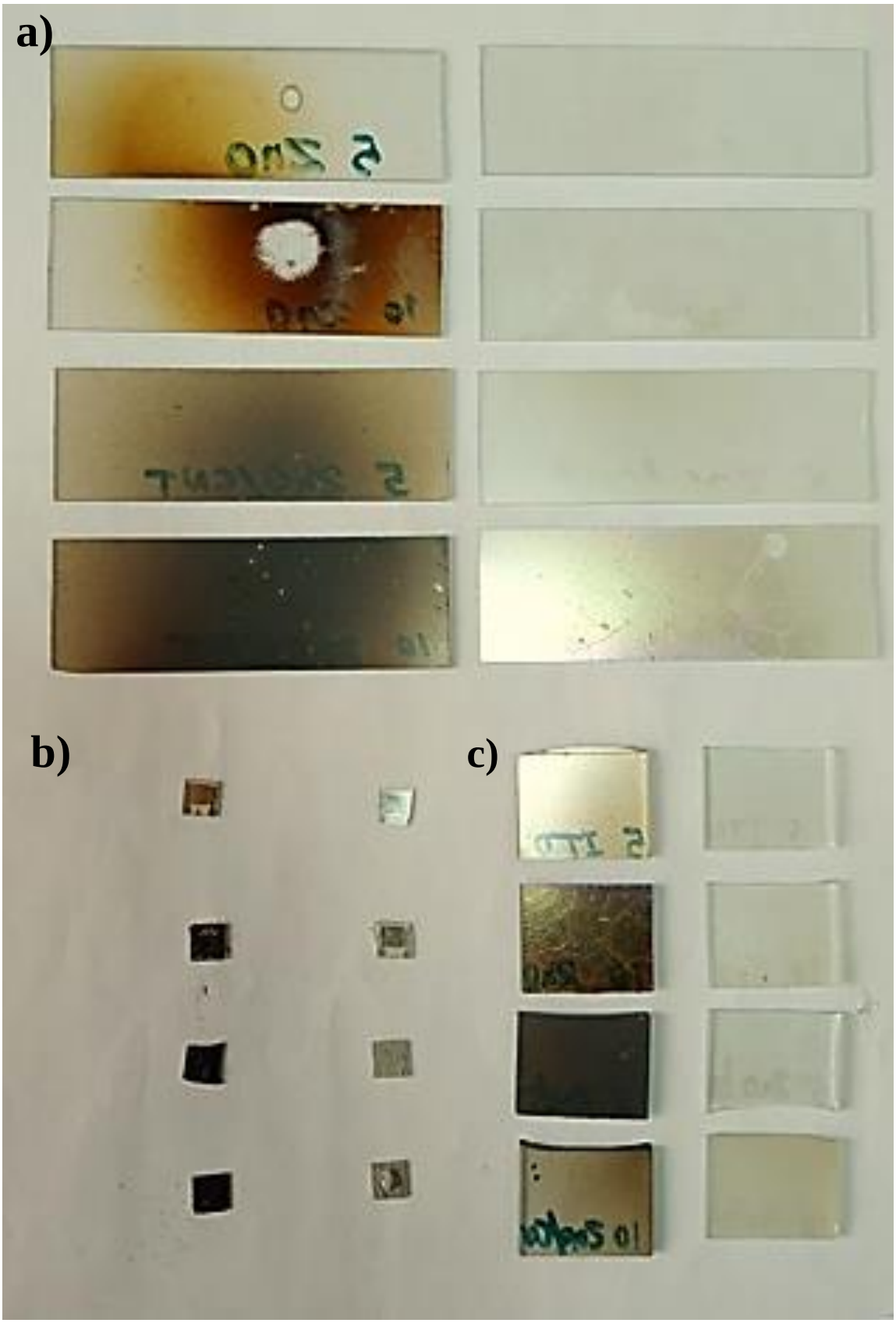

Figure (3.6): The samples of ZnO and ZnO/CNT thin films at sprayed (5 and 10) sprinkles heated at (250 and 500)^{o}C for : (a) glass substrates. b) Interdigitated electrodes. c) ITO substrates.

3.1.2.4: Electrodes Deposition

Two types of device configurations were studied in the current work; sandwich film structure and planar structure using Intedigitated Electrodes. For sandwich structures (Figure 3.7a), Indium Tin Oxide (ITO) coated glass substrates were used. ITO substrates were washed in Acetone, rinsed with water and then left to dry in a desiccator. Active layers have been deposited from diluted solutions onto the ITO substrates using spray-coating method. Top electrodes were evaporated through shadow mask under vacuum with pressure of about $2x10^{-5}$ mbar using vacuum thermal deposition. The rate of film deposition was controlled by a film thickness monitor at the rate 0.1 $nm.s^{-1}$, and the obtained thickness was 40 nm. In such kind of devices, to calculate conductivity from I-V curves, the cross section area (A) will be the device active area as determined by the overlap area between the active layer and the top electrode and l is the film thickness which can be determined utilizing spectroscopic ellipsometry.

In the planar structure (Figure 3.7b), the interdigitated electrode geometry is used to determine the conductivity from equation (2-11)

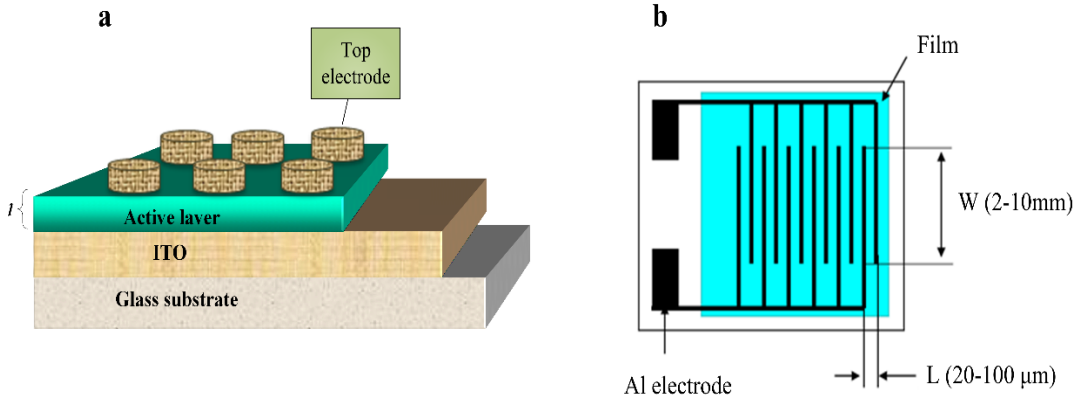

Figure (3.7): Schematic illustration of devices structure used in this study, (a) sandwich structure and (b) interdigitated electrodes

3.1.2.5: Thermal evaporation

Vacuum deposition via thermal evaporation includes two simple processes; evaporation and condensation. It brings to mind the familiar process by which liquid water appears on the lid of a boiling pan but, the situation and heat source are quite different.

Evaporation process occurs in vacuum, where gases other than the source material are almost completely removed before the evaporation begins. Therefore, particles can travel straight to the deposition target avoiding collision with the background vapor. Hot objects inside the evaporation chamber, such as heating filaments, creates an unwanted vapors that limit the quality of the vacuum. Generally, other unwanted gases collide with the evaporated material may react with them. For example, if aluminium is deposited in the presence of oxygen, it will form aluminium oxide. They also reduce the amount of vapor that reaches the substrate, which makes the thickness difficult to control [148].

Edwards E306A Thermal Evaporator has been used to evaporate a metal film onto a substrate. The metal source to be evaporated, typically gold and aluminium, is placed in a suitable filament or crucible, in which a large current is passed. The metal melts, and evaporates onto the target substrate above the source, producing a film. The thickness of the metal film is monitored in-situ using a quartz crystal thickness monitor (Model Edward FTM5) Even though the turret can accommodate up to four different materials, and changed via manual rotation, the most common practice was to evaporate single material during one pump-down cycle.

The major components of the Edwards E306A Thermal Evaporator are :

- A diffusion pump supported by a rotary pumping system.
- Chamber.
- An electrical system, which incorporates the Edwards E306A Thermal Evaporator Controller.

3.1.2.6: Substrates

All substrates have been washed thoroughly using Acetone followed by thorough rinsing with deionized water and then left to dry in a desiccator

3.1.2.6.1: Intedigitated Electrodes (IDE)

First, The substrate washed with Acetone, rinsed with deionised water and left to dry in a desiccator. We deposited gold on glass directly, Thin layer ~ 1 nm in thickness of gold was deposited on top of the glass after that we deposited the thin film were deposited from diluted solutions on it by spray-coating method, and we measured it directly, that is, it measures the surface conductivity, as well as its hybrids with MWCNTs to allow more interaction of electrons with the film surface in the case of FESEM study.

3.1.2.6.2: Sandwitch Structure

The substrates were used for electrical property studies. First, the substrate was cut using diamond cutter, washed with Acetone, rinsed with deionised water and left to dry in a desiccator. The bottom electrode is ITO, after that we deposited the thin film on it. Thin films were deposited from diluted solutions onto the glass substrates by spray-coating method, after that we deposited aluminum electrodes. This structure called the sandwitch structure, and measures the conductivity in depth across the film.

Indium-doped tin oxide (ITO)-coated glass substrates are used as conductive bottom electrodes in electrical measurements in the case of sandwich device structure.

3.2: Characterisations

UV-Visible Absorption Spectroscopy is used to study the optical properties and energy gaps calculations. Fourier Transform Infrared technique has been employed to investigate the chemical functional groups of the prepared samples. X-Ray Diffraction has been utilized to reveal the structure and grain size calculations. Morphology of the prepared samples

was explored using scanning electron microscopy technique. Keithly semiconductor characterization system has been utilized to investigate the electrical properties. Homemade instrument was used to carry out the sensor measurements.

3.2.1: UV-Visible Absorption spectrophotometer

This technique works on the basis of the measurement of interaction of electromagnetic radiations (EMR) with matter at particular wavelength [149].

UV-Visible absorption spectra have been recorded on Shimadzu (1800) UV-Visible spectrophotometer. A spectrophotometer is designed around three fundamental parts: the source, the monochromator, which constitute the optical section and the detection system Figure (3.8). These components are typically integrated in a unique framework to make spectrometers.

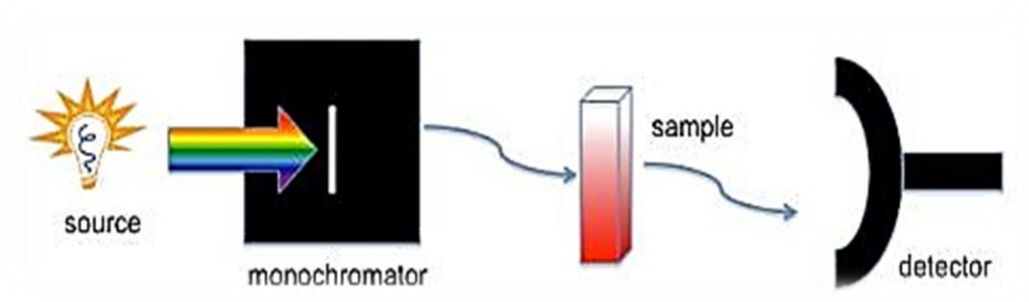

Figure (3.8): Illustration of a single beam UV-vis instrument [150].

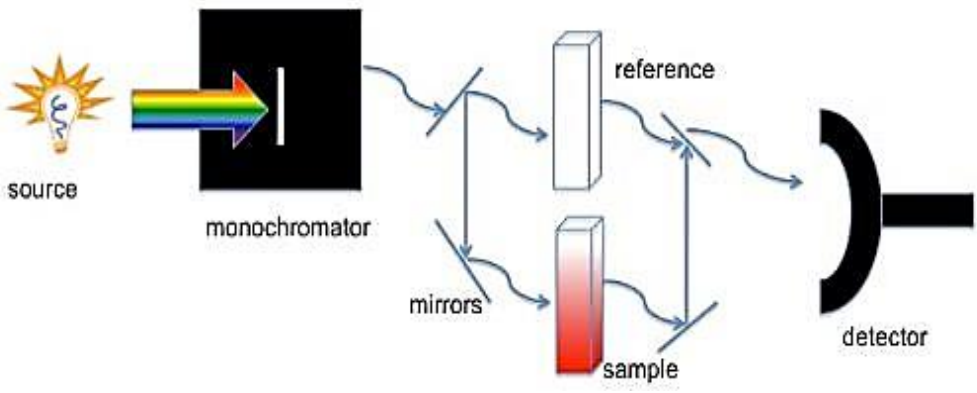

Figure (3.9): Illustration of a double beam UV-vis instrument [150].

A double-beam UV-IR 1800 Shimadzu spectrophotometer was used to measure the absorption of SnS thin films in the range (400-1000) nm. The background correction is taken for each scan. The transmittance and reflectance data can be used to calculate absorption coefficients of the films at a different wavelength, which have been used to determine the energy gap E_g. As shown in Figure (3.10). At University of Babylon/ College of Science/ Department of Physics.

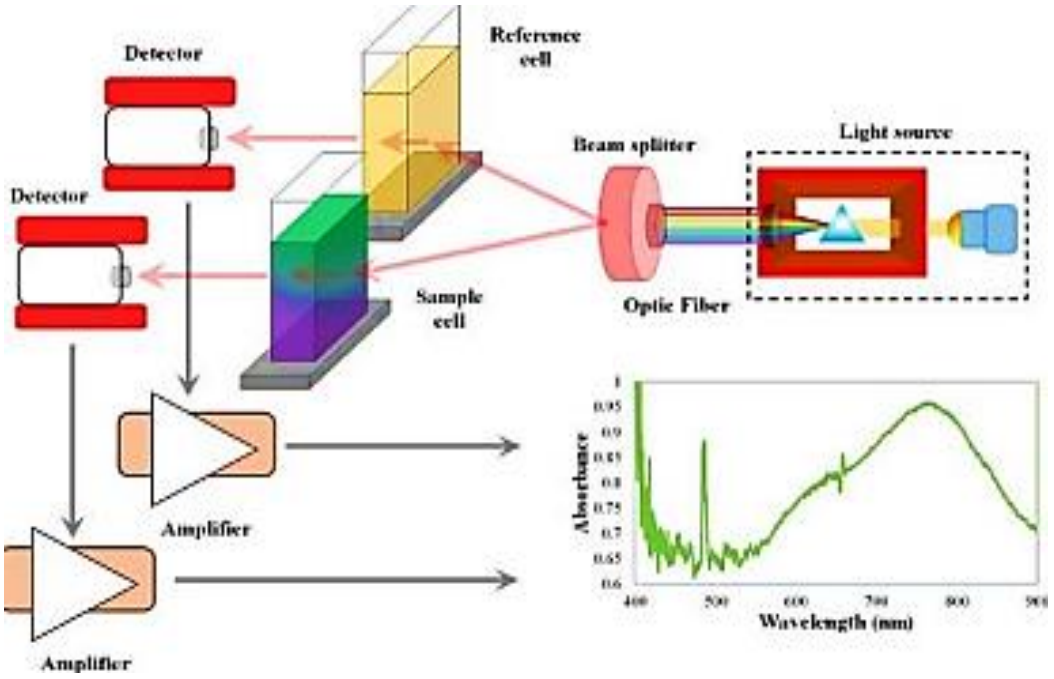

Figure (3.10): Schematic of UV spectrophotometer [138].

3.2.2: DC Electrical Characterization

The Model (2400) Kiethely Semiconductor Characterization System (2400) has been used for the DC electrical characterization of ZnO thin films utilizing interdigitated electrodes device configurations and electric oven type (Memmert Lab Oven UFB 400,400W).

The system is specified to work at the (1 pA- 1 A) current range with the maximum voltage of (21- 210) V, and (200 mV- 200 V) voltage range with the maximum current of (10.5- 105) mA.

This system can automatically perform (I-V) measurements of semiconductor devices and test structures, using up to eight Source-Measure Units (SMUs). A variety of supported external components enhance the capabilities of this machine. In Thin Films Laboratory/ University of Babylon/College of Science/ Department of Physics.

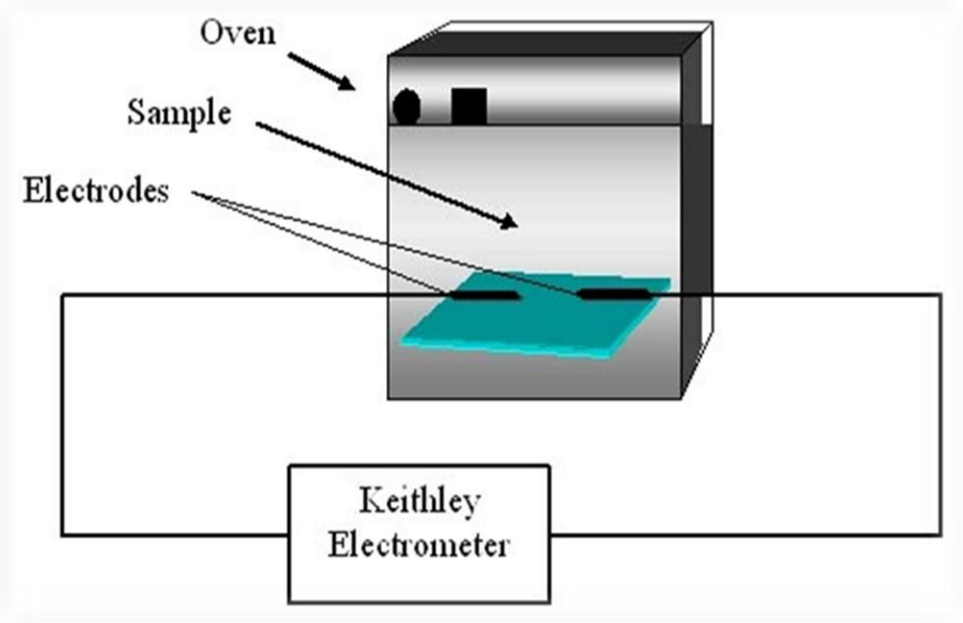

Figure (3.11): Schematic of the Circuit for measuring D.C conductivity.

3.2.3: X-Ray Diffraction

XRD is a common technique that determine a sample's composition or crystalline structure. For larger crystals such as macromolecules and inorganic compounds, it can be used to determine the structure of atoms within the sample. If the crystal size is too small, it can determine sample composition, crystallinity, and phase purity. This technique sends x-ray beams through it. X-ray beams are chosen because their wavelength is similar to the spacing between atoms in the sample, so the angle of diffraction will be affected by the spacing of the atoms in the molecule, as opposed to using much larger wavelengths, which would be unaltered by the spacing between atoms. The x-rays then pass through the sample, “bouncing” off of the atoms

in the structure, and changing the direction of the beam at some different angle, theta, from the original beam. This is the angle of diffraction.

X- Ray Diffraction (XRD) is one of the widely used experimental techniques for determining crystal structure and lattice parameters [151]. X-ray are electromagnetic radiations of the same nature as light but of much larger energy and smaller wavelength. The X-rays used in crystallography have a wavelength of about (1) Å which is comparable to atomic dimensions [152]. The relationship describing the angle at which a beam of X-rays of a particular wavelength diffracts from a crystalline surface was discovered by William H. Bragg and W. Lawrence Bragg and is known as Bragg's law [153]:

$$\boldsymbol{2d(hkl)sin\theta = m\lambda} \qquad \textbf{(3-1)}$$

Where (λ) is wavelength of the X-ray (1.5406) Å, (θ) is Bragg diffraction angle of the XRD peak in degree (scattering angle), (m) is integer representing the order of the diffraction peak, and ($d(hkl)$) is inter-plane distance of (i.e atoms or ions or molecules). The crystallite size of the deposits is estimated from the full width at half maximum (FWHM) of the most intense diffraction line by Debye Scherrer's formula as follows [154]:

$$\boldsymbol{D_S = 0.94\ \lambda / \beta cos\ \theta} \qquad \textbf{(3-2)}$$

Where, (D_S) is crystallite size, and (β) is (FWHM) in radians.

The structural and morphological properties of ZnO thin films have been measured by sending the samples abroad (Islamic Republic of Iran, University of Tehran, Iran). X-ray diffraction (XRD) analysis shown in Figure (3.12) is used to determine the crystal structure of thin films. The source of radiation is Cu (k) with wavelength (=1.54060), current (30) mA, and voltage (40) kV in the (X-ray) diffractometer type (PW1730 Philips) made in (USA). The films were deposited on glass slides for the carrying out these measurements.

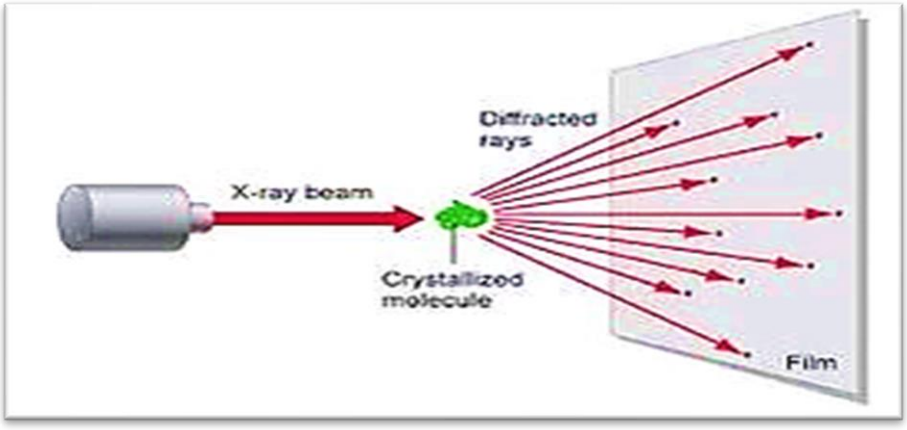

Figure (3.12): Schematic of X-ray diffract meter (XRD) [155].

3.2.4: Field Emission Scanning Electron Microscopy (FESEM)

A field emission scanning electron microscopy (FESEM) is a type of microscope which uses a focused beam of electrons to scan a surface of a sample to create a high resolution image. SEM produces images that can show information on a material's surface composition and topography [156].

Accelerated electrons in an FESEM carry significant amounts of kinetic energy, and this energy is dissipated as a variety of signals produced by electron-sample interactions when the incident electrons are decelerated in the solid sample. These signals include secondary electrons Secondary electrons and backscattered electrons are commonly used for imaging samples: secondary electrons are most valuable for showing morphology and topography on samples and backscattered electrons are most valuable for illustrating contrasts in composition in multiphase samples[156].

The morphological properties of ZnO thin films have been measured by sending the samples abroad (Islamic Republic of Iran, University of Tehran, Iran). Field emission scanning electron microscope shown in Figure (3.13) was used in this research. The FESEM type (Mira3) is Made in the Czech Republic. The films were deposited on glass slides for the carrying out these measurements.

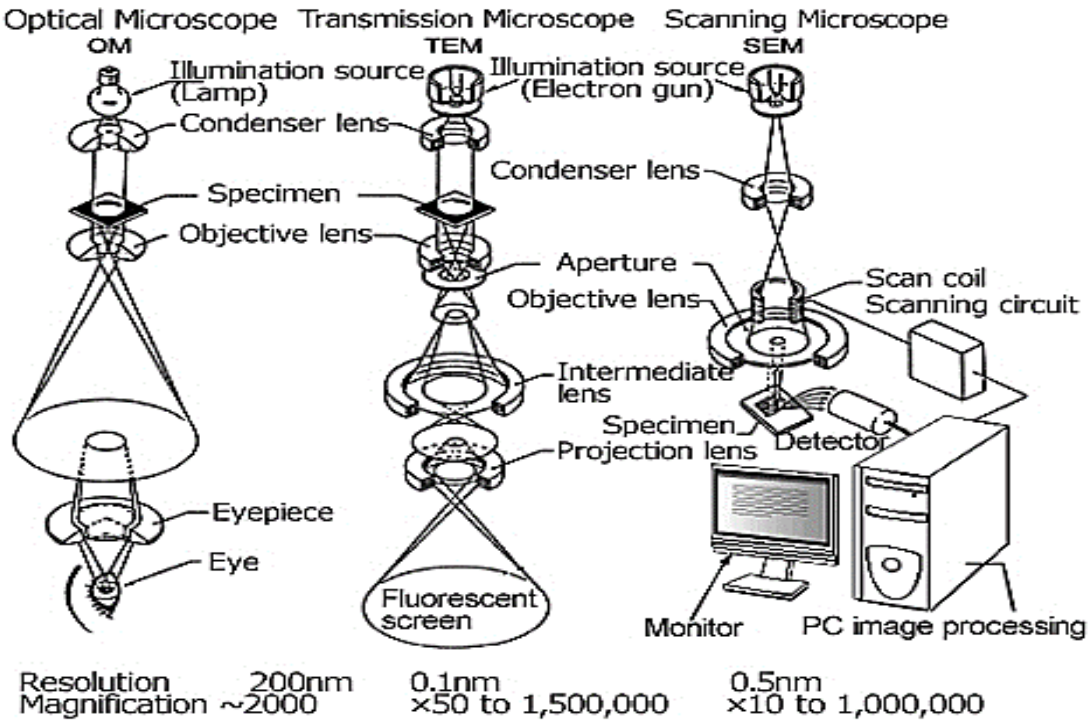

Figure (3.13): Field emission scanning electron microscopy (FESEM) instrumentation [157].

3.2.5: Fourier Transform Infrared (FTIR)

FTIR stands for Fourier transform infrared, the preferred method of infrared spectroscopy. When IR radiation is passed through a sample, some radiation is absorbed by the sample and some passes through (is transmitted). The resulting signal at the detector is a spectrum representing a molecular 'fingerprint' of the sample. The usefulness of infrared spectroscopy arises because different chemical structures (molecules) produce different spectral fingerprints that's mean, is a technique which is used to obtain infrared spectrum of absorption, emission, and photoconductivity of solid, liquid, and gas [158].

In FTIR analyses, Infrared light from the light source passes through a Michelson interferometer along the optical path. The Michelson interferometer comprises a beam splitter, moving mirror, and fixed mirror. The light beam split into two by the beam splitter is reflected from the moving mirror and fixed mirror, before being recombined by the beam

splitter. As the moving mirror makes reciprocating movements, the optical path difference to the fixed mirror changes, such that the phase difference changes with time. The light beams are recombined in the Michelson interferometer to produce interference light. The intensity of the interference light is recorded in an interferogram, with the optical path difference recorded along the horizontal axis [159].

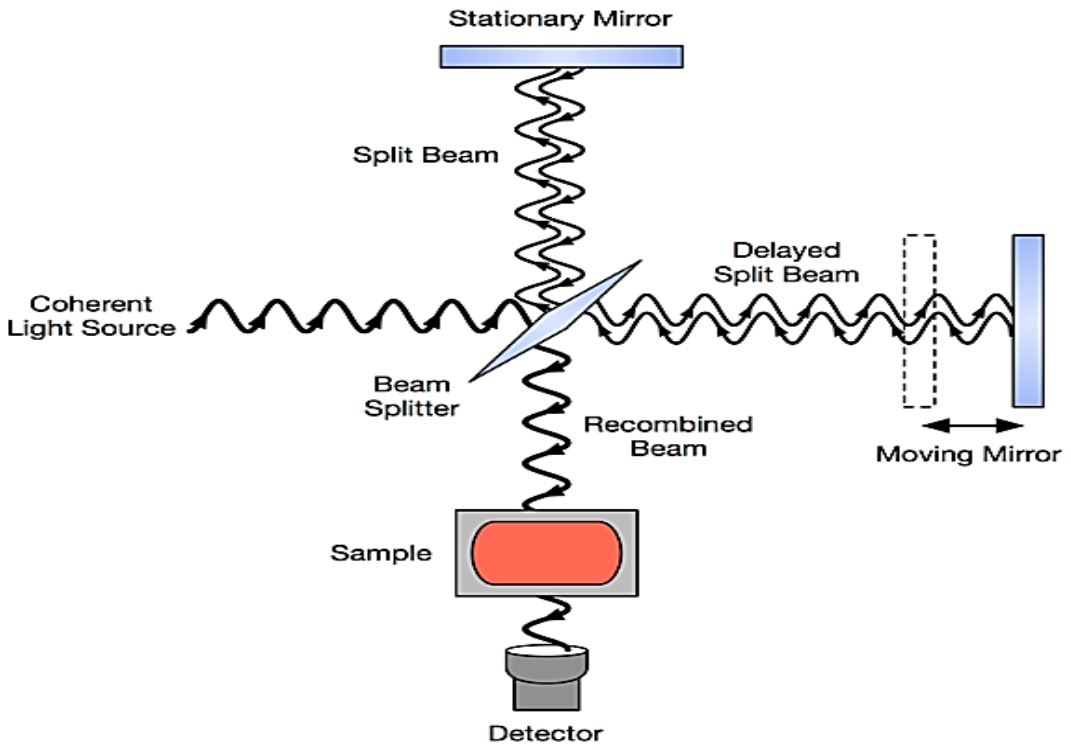

Figure (3.14): Schematic diagram of a Michelson interferometer, configured for FTIR [160].

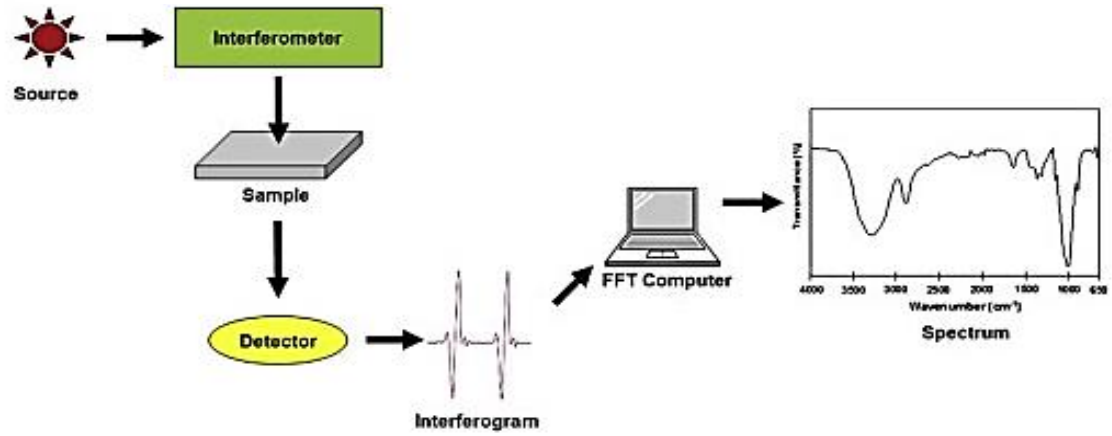

Figure (3.15): FTIR processing.

3.2.6: Sensing System

A schematic cross-sectional view of the gas sensor testing system, test chamber, and photos of the mounted sensor and test chamber are illustrated schematically in Figure (3.16). The unit consists of a vacuum-tight stainless steel cylindrical test chamber of diameter (26 cm) and of height (10 cm) with the bottom base made removable. The effective volume of the chamber is (5306.6 cm^3); it has an inlet for allowing the test gas to flow in and an air admittance valve to allow atmospheric air after evacuation. Another third port is provided for vacuum gauge connection. A multi-pin feed through at the base of the chamber allows the electrical connections to be established to the heater assembly as well as to the sensor electrodes via spring-loaded pins

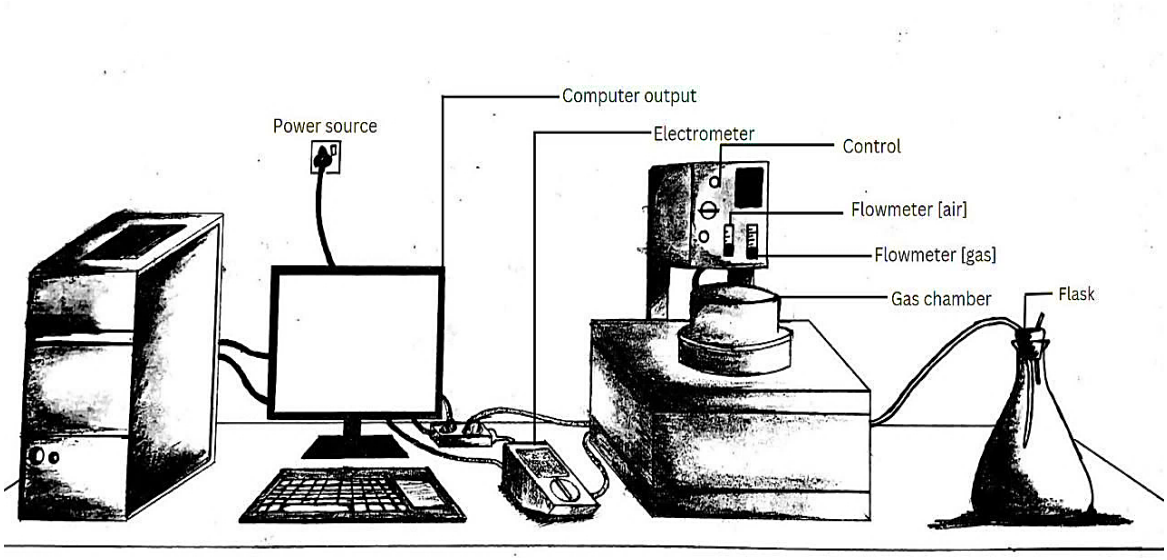

Figure (3.16): Diagram of electrical circuit of gas sensing measurements.

The heater assembly consists of a hot plate and a k - type thermocouple inside the chamber to control the operating temperature of the sensor. The thermocouple senses the temperature at the surface of the film exposed to the analyte gas. PC-interfaced digital multimeter of type (UNI-T UT81B), and laptop PC, is used to register the variation of the sensor conductance (reciprocal of resistance) exposed to predetermined air - gases ratio. The chamber can be evacuated using a rotary pump to a rough vacuum. A gas mixing manifold is incorporated to control the mixing ratios of the test and

carrier gases before being injected into the test chamber. This test is carried out in the thin films Laboratory of University of Babylon/ College of Science/ Department of Physics.

3.2.6.1: Sensor Testing Procedure

The operation of the test setup is illustrated in the following points:

1. The test chamber is opened and the sensor placed on the heater. The necessary electrical connections between the pin feed through and the sensor spring loaded pins and the thermocouple are made. Doing so, the test chamber is closed.

2. Then, the rotary pump is switched on to evacuate the test chamber. Setting the sensor desired operating temperature is done using temperature controller.

3. After that, using the needle valves the flow rate of the carrier and test gases flow meters is adjusted.

4. Next, the gas of known concentration in chamber is allowed to flow to the test chamber by opening the valve.

5. Measurement of the resistance variation of the sensor for the known concentration of test gas ratio is observed by the PC - interfaced digital multimeter of type (UNI-UT81B).

6. At the first time the digital multimeter record the biasing current of air flow, after that switch-on the testing gas, and after several second the current has low variation, then switch-off the test gas to record the recovery time.

7. The above measurements are repeated for the other required temperatures or concentrations of the test gas.

4.1: Introduction

This chapter is employed to represent all the outcome of the current study including structural, optical and electrical properties of the ZnO and ZnO/CNT thin films, which are prepared by sol-gel method and deposited using spray coating as well as the effect of annealing temperature.

4.2: Sol-Gel and Spray Coating

Sol-Gel technique is simple method and recently, has attracted much attention due to their potential in the applications of metal oxides nanoparticle synthesis [161]. The most effects factors on thin films prepared by spray coating is the substrate temperature which set to be (80) ^{o}C. Another parameters such as the spray time is also crucial and is set to be (1) min . The vertical height between the spray device and the bases was (18) cm. According to these parameters high homogeneity was obtained.

4.3: Fourier Transform Infrared (FTIR)

Figure (4.1) shows the FTIR spectra of the ZnO and ZnO/CNT hybrid materials. The inset to the figure 1 represents the sigma aldrich FTIR of ZnO. As obviously can be seen that, there is a high similarity between the prepared ZnO spectrum and the sigma's one indicated excellent purity for the ZnO nanoparticles synthesized in this study. The spectra obtained have clearly shown the Zn-O absorption peak near 546 cm^{-1}. The absorption bands at 3450 and 2923 cm^{-1} are attributed to O-H vibration stretching from Zn-O-H sorts and C-H stretching vibration correspondingly [162]. The free O-H stretching bond at 3450 cm^{-1} arises due to reaction of ZnO nanoparticles and hydroxide group. It is worth mentioning that the color of solution in a mixture of 2-methoxyethanol and monoethenolamine is orange where as that of solution of alcohol is transparent. The peak at 715 cm^{-1} which appeared only in the spectrum of the hybrid material, is may be attributed to the carbon-carbon

stretching of carbon nanotubes [162]. This peak indicated the successful decorating of ZnO nanoparticles onto sidewall of carbon nanotubes.

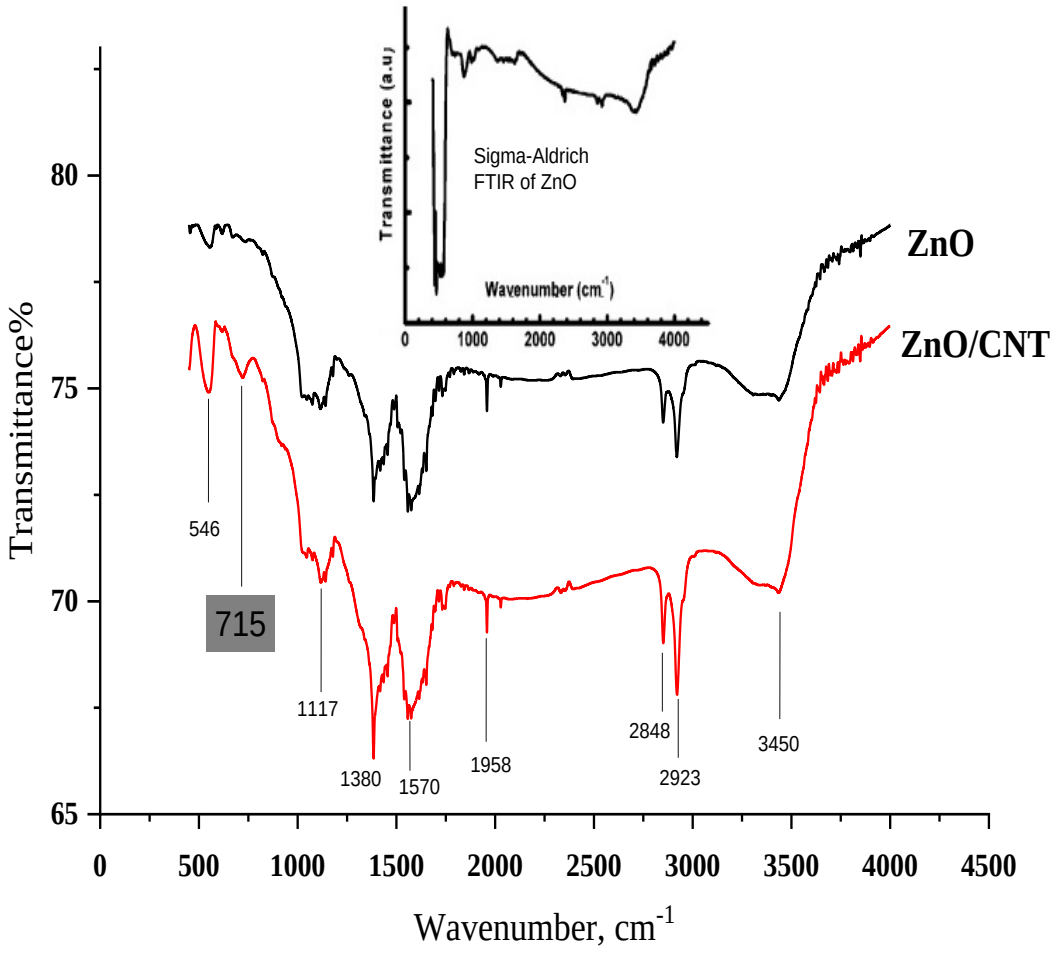

Figure (4.1): The FTIR spectra of ZnO and ZnO/CNT heated at (500)ºC prepared by sol-gel method. The inset is sigma Aldrich spectrum of ZnO.

4.4: Field Emission Scanning Electron Microscopy (FESEM)

Scanning electron microscopy technique has been used to study the topography of the samples prepared in this work. At low magnification images, samples annealed at 250º C, surface has examined a cracked surface while those annealed at 500º C show quite homogeneous surface indicating higher temperature is needed for the ZnO thin films to be achieved adequately. These images are presented in Figure (4.2) for the clarity.

In addition irregular thin films have been produced when heated at 250^{o} C while spherical-type morphology was shown by samples treated at 500^{o} C for half an hour. Figure (4.2) represents the uniform arrangement of ZnO grains with nano scale down to ~ 22nm. Zinc oxide usually tends to form nano-sphere structure [163], rod-like structure [164], or nano-flower structure [165] depending on preparation method, coating and heat treatment.

Figure (4.4) shows the SEM images of the samples containing CNT have shown clear tubes decorated by ZnO nanoparticles confirming the successful anchoring of the ZnO onto side-wall of the carbon nanotubes. This foundation was also reported elsewhere [166]

a) **b)**

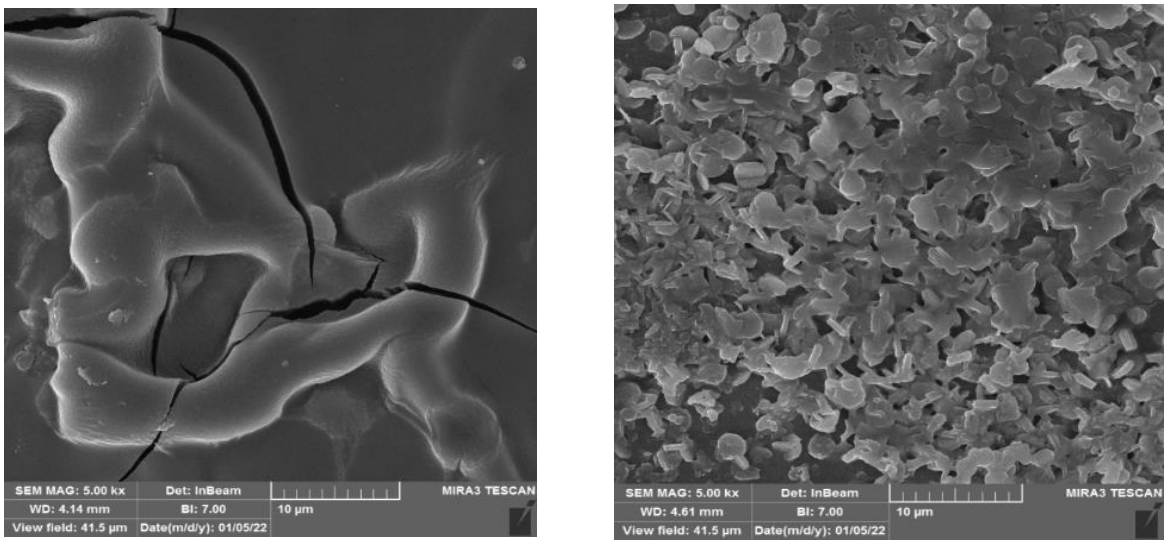

Figure (4.2): SEM images at 5kx (10 µm) magnification of sprayed ZnO thin films prepared by sol-gel (a) annealed at 250^{o} C and (b) annealed at 500^{o} C.

a) **b)**

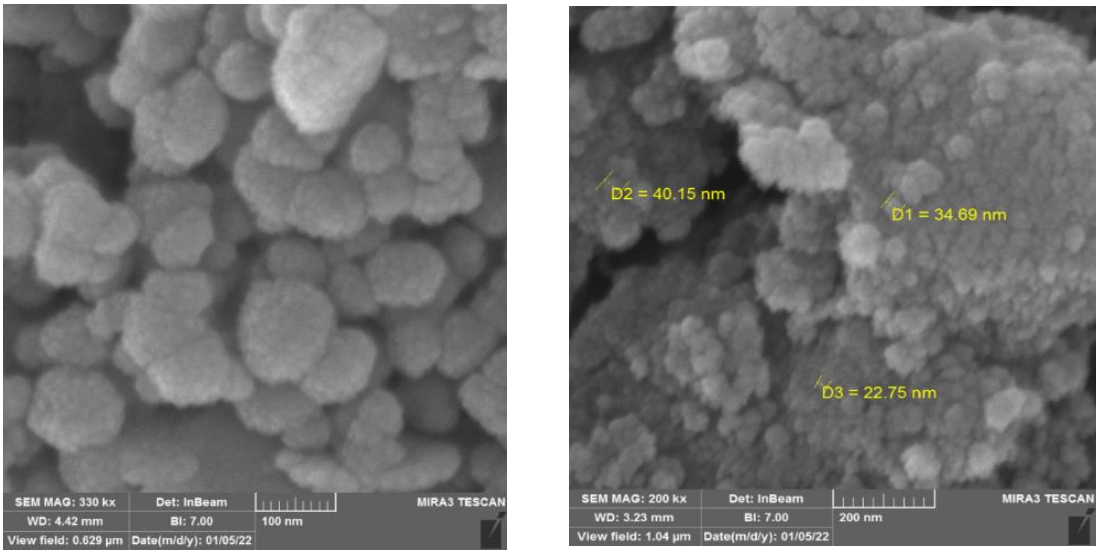

(c)

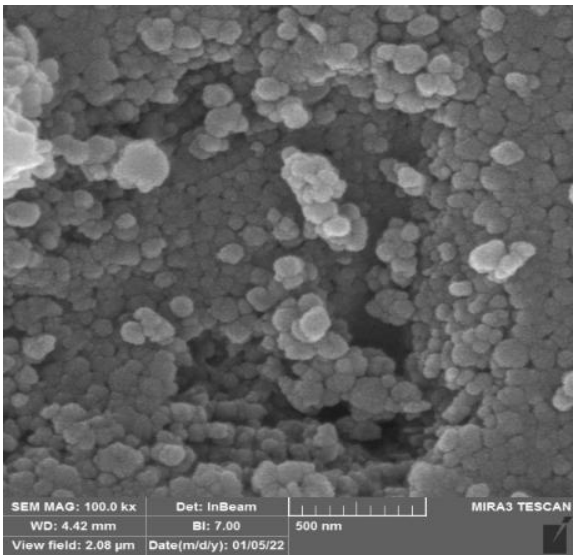

Figure (4.3): The spherical like structure of ZnO at different magnifications (a) 330 kx (100nm), (b) 200kx (200nm) shows the grain size of the nanoparticles, (c)100 kx (500nm).

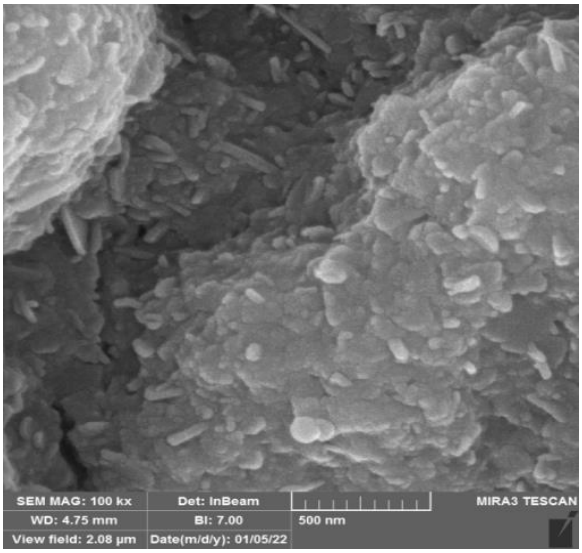

Figure (4.4): SEM image of the sample containing MWCNTs.

4.5: X-Ray Diffraction (XRD)

XRD pattern of ZnO and ZnO/CNT hybrid thin films at sprayed (5 and 10) sprinkles and annealed at different temperatures (250 and 500)ºC are shown in Figures (4.5) and (4.6). In the as deposited samples and annealed to (250)ºC, the XRD curves of ZnO show no clear indication of crystallinity which indicates their amorphous nature and increase with addition CNT. This broadening of peaks can be ascribed to the scattering of the particles at low temperature [167].

The annealing at (500)ºC Figures (4.6) and (4.7) affected the crystallinity of the samples clearly and showed the presence of many peaks in the XRD pattern and enhanced the crystal quality of the film. The presence of prominent diffraction peaks reveals the polycrystalline nature of the films. The patterns in Figure (4.6) show that all the thin films of pure ZnO thin films at the (5) sprinkle and annealed at temperatures (500ºC) have a peak located at (36º) corresponds to (101) plane, in addition to another shallow to another peaks located at (43.2 º and 62.6º) which corresponds to direction

{(102) and (103)} respectively. While the patterns show that all the thin films of ZnO/CNT thin films at the (5) sprinkle and annealed at temperatures (500^{o}C) have a peak located at (31.4^{o}) corresponds to (104) plane, in addition to another peaks located at (34^{o} , 36^{o} , 47.2 ^{o} , 56.2 ^{o} , and 62.6^{o} , 67.6^{o}) which corresponds to (104), (110), (202), (116), (211) and (208) respectively. The diffraction lines are consistent with the values reported in the database of ZnO (JCPDS card no PDF 079-0208) and ZnO/CNT (JCPDS card no PDF 001-1036).

It can be concluded that all the films deposited in these experimental conditions show high and intense diffraction peak . The presence of prominent peaks shows that the films are polycrystalline with the hexagonal structure as reported previously [167].

From Table (4.1) the crystallite size calculated by Debye Scherrer formula. The crystallite size, full width half maxima (FWHM) of the diffraction peaks values are listed in the table.

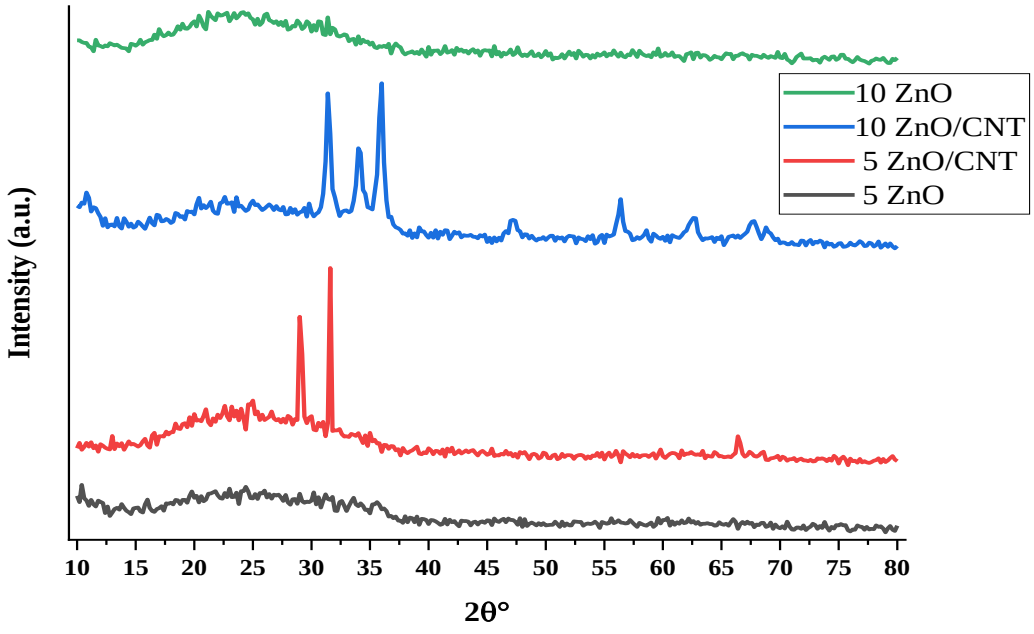

Figure (4.5): XRD pattern of ZnO and ZnO/CNT thin films at the (5) sprinkle and annealed at temperatures (250)^{o}C .

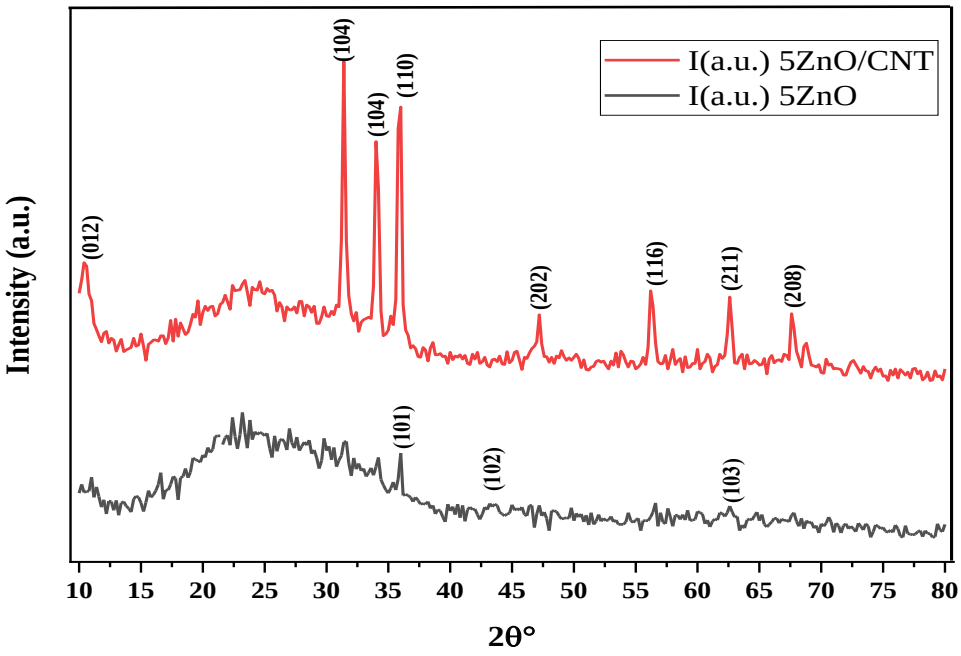

Figure (4.6) XRD pattern of ZnO and ZnO/CNT thin films at the (5) sprinkle and annealed at temperatures (500)^{o}C .

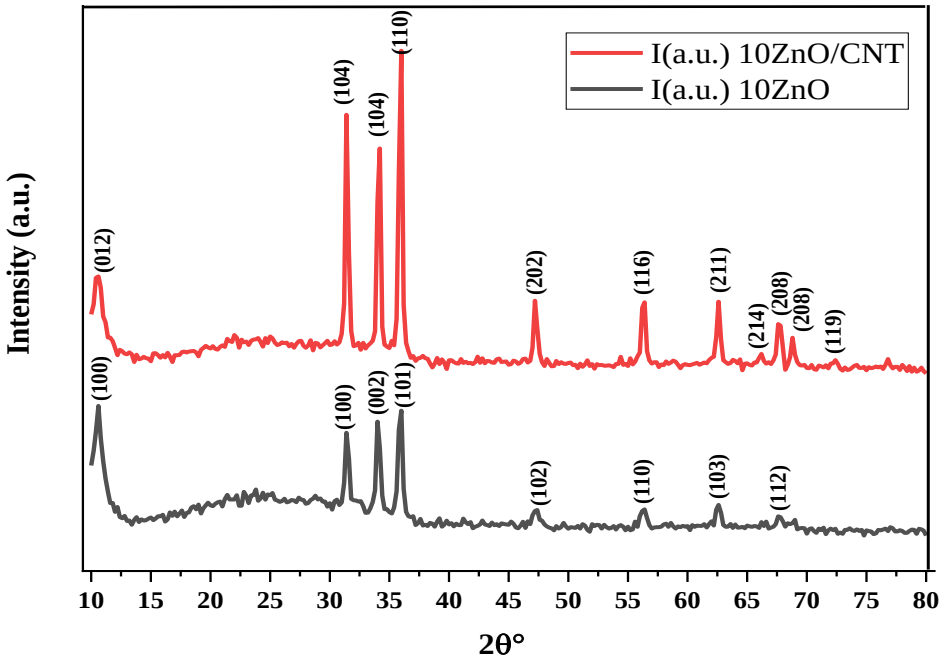

Figure (4.7): XRD pattern of ZnO and ZnO/CNT thin films at the (10) sprinkle and annealed at temperatures (500)^{o}C .

Table (4.1): XRD data results of ZnO and ZnO/CNT thin films as deposited 5 Sprinkles and annealed at (500) °C.

No.	Substrate 5 Sprinkles at (500)°C	2θ (degree)	d (Å)	(hkl)	FWHM (degree)	Crystallite size (nm)
1	ZnO	35.851	2.504	(101)	0.590	14.3
		43.566	2.077	(102)	0.984	8.8
		62.793	1.487	(103)	0.960	11.9
2	ZnO/CNT	10.566	8.372	(012)	0.590	13.7
		31.421	2.847	(104)	0.394	21.4
		34.068	2.631	(104)	0.590	14.3
		35.919	2.500	(110)	0.590	14.3
		47.128	1.928	(202)	0.590	14.9
		56.331	1.633	(116)	0.590	15.5
		62.588	1.484	(211)	0.393	24.1
		67.747	1.382	(208)	0.720	13.4

Table (4.2): XRD data results of ZnO and ZnO/CNT thin films as deposited 10 Sprinkles and annealed at (500) °C.

No.	Substrate 10 Sprinkles at (500)°C	2θ (degree)	d (Å)	(hkl)	FWHM (degree)	Crystallite size (nm)
1	ZnO	10.618	8.331	(100)	0.787	10.2
		31.442	2.845	(100)	0.590	14.2
		34.054	2.632	(002)	0.590	14.3
		35.906	2.501	(101)	0.590	14.3
		47.350	1.919	(102)	0.590	14.9
		56.359	1.632	(110)	0.590	15.5
		62.611	1.483	(103)	0.590	16.0
		67.654	1.383	(112)	0.720	13.4
2	ZnO/CNT	10.599	8.346	(012)	0.787	10.2
		31.430	2.846	(104)	0.590	14.2
		34.114	2.628	(104)	0.590	14.3
		35.944	2.498	(110)	0.590	14.4
		47.279	1.922	(202)	0.590	14.9
		56.296	1.634	(116)	0.590	15.5
		62.588	1.484	(211)	0.590	16.0
		66.051	1.414	(214)	0.590	16.3
		67.670	1.384	(208)	0.590	16.4
		68.849	1.363	(208)	0.590	16.5
		72.364	1.304	(119)	0.720	13.8

4.6: UV-Visible Absorption Spectra

The size of nanoparticles plays significant role in varying all characteristics of materials. Therefore, size developments of semiconductors' particles became essential to investigate the material properties [168]. One of the most important equipment to examine the optical properties of nano-sized materials is the UV-Visible absorption spectroscopy. Figure (4.8) shows the absorbance spectra of the ZnO and ZnO/CNT hybrid thin films at different spraying sprinkles; (5 and 10) and annealed at different temperatures; (250) ^{o}C, and (500) ^{o}C in the wavelength of (300-1000) nm. It was found that the absorption of all samples appeared in the UV range 300 nm. This phenomenon is arising from the intrinsic electron transition between highher occupied moleccular orbital (HOMO) and lower unoccupied moleccular orbital (LUMO). Another exitonic bands were found at about 380 nm due to the nano size particles. This edge is very clear in the samples annealed at 500 ^{o}C (Figure (4.8) b and c) suggesting the successful formation of ZnO nanoparticles at this range of annealing temperature [169].

The loading of CNT to the samples results in red shift in the absorption spectra indicating the successful anchoring of nano-size ZnO onto the cross wall of carbon nanotubes. In addition, effective utilization of the created electron-hole pairs via carbon nanotube modification took place.

Another finding that should be given attention is the shape of the spectra. By looking to the spectra of ZnO/CNT which heated at 250 ^{o}C, it can clearly be seen that the curve is likely to be similar to the spectra of original CNT which is feature less as reported previously [170]. However, at 500 ^{o}C, the spectra of ZnO/CNT showed the same characteristics of ZnO spectra suggesting successful decorating of nanoparticles onto the CNTs.

The values optical band gap (E_g) were derived supposing direct transition from the edge of the HOMO and LUMO bands as there have been linear regions in all curves. The plot of $(\alpha h\upsilon)^2$ as a function of the energy of

incident light (*hυ*) was exhibited in Figure (4.9). Tauc equation were utilized to obtain the optical band gap from the intercept of the extrapolated linear portion of the arc with the x-axis and recorded in Table (4.3). There is a variation of the band gap energy of ZnO and ZnO/CNT where the optical band gap (E_g) of the samples which contains CNT decreases giving intense evidence of CNT presence which narrow the band gaps of ZnO, allowing better absorption [171].

The direct band gap of the ZnO films was decreases as the annealing temperatures increases, this is expected to take place because of the deviation in lattice weaknesses and strain. The crushed lattice is likely to deliver a wide band gap due to the bigger repulsion between the oxygen 2p and the zinc 4s bands [172]. On the other hand, the band gap values of ZnO thin films decreases with the increasing of number of sprays. In addition, the energy gap could be decreased with the increasing of the crystallinity and the grain size factors.

Table (4.3): The optical energy gap calculated from Tauc plot.

Specimen	Energy gap (ev)
ZnO, 5 sprays, 250 ºC annealed	3.28
ZnO/CNT, 5 sprays, 250 ºC annealed	3.12
ZnO, 10 sprays, 250 ºC annealed	3.26
ZnO/CNT, 10 sprays, 250 ºC annealed	2.91
ZnO, 5 sprays, 500 ºC annealed	3.25
ZnO/CNT, 5 sprays, 500 ºC annealed	3.20
ZnO, 10 sprays, 500 ºC annealed	3.19
ZnO/CNT, 10 sprays, 500 ºC annealed	2.63

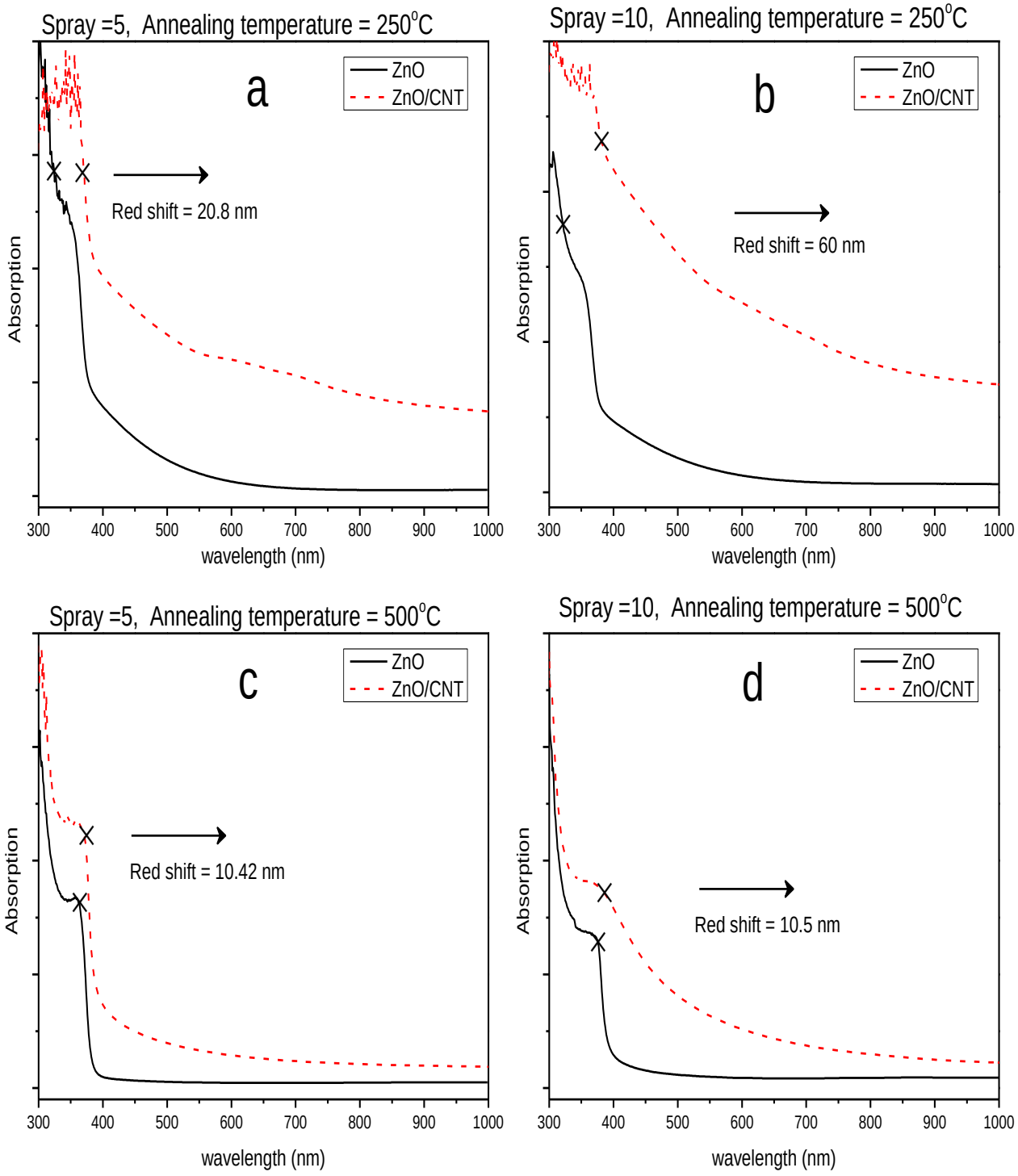

Figure (4.8): UV-Visible absorbance spectra of ZnO and ZnO/CNT hybrid thin films annealed at different annealing temperature and deposited onto glass substrates using spray pyrolysis procedure.

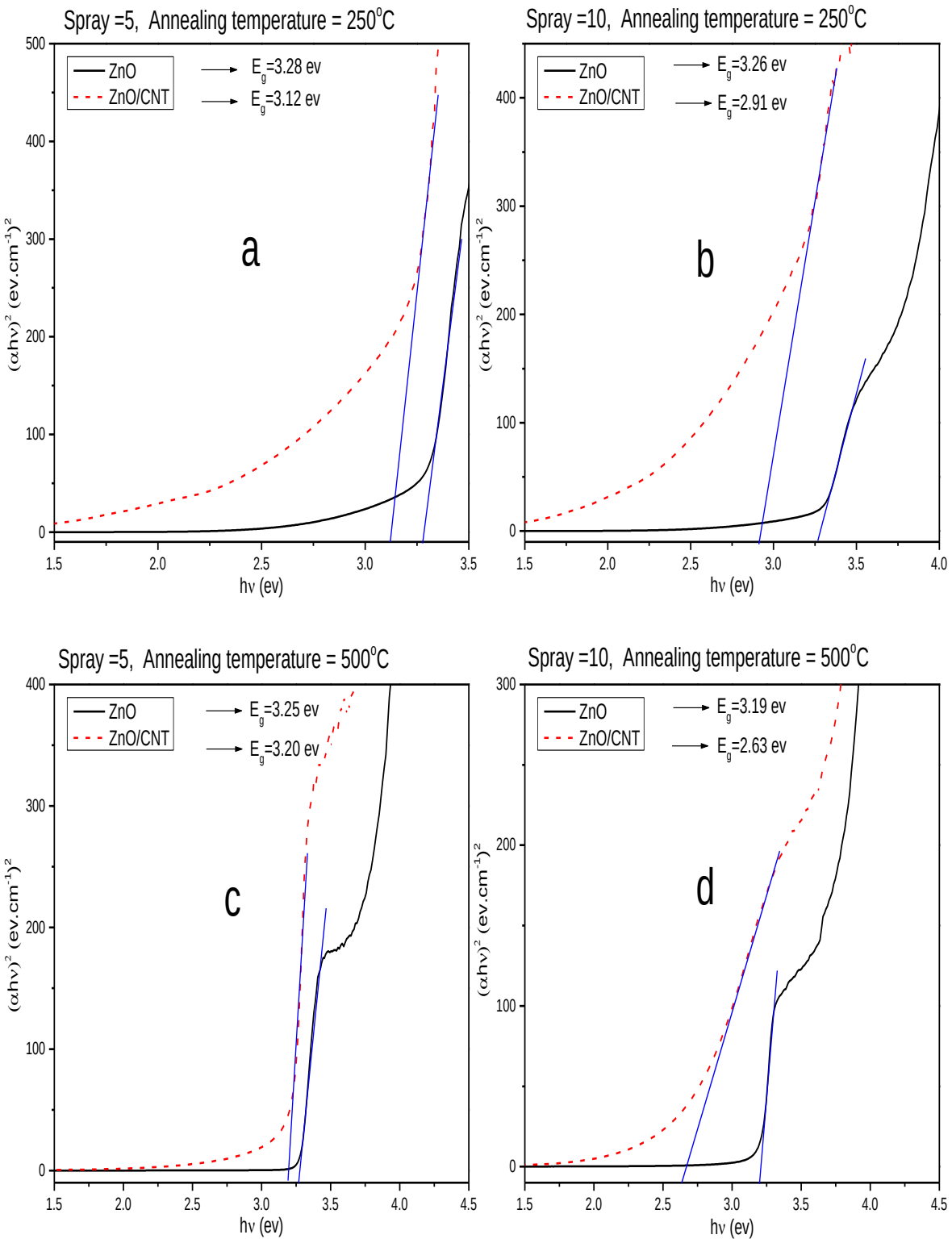

Figure (4.9): $(\alpha h\upsilon)^2$ versus photon energy of ZnO thin films at the (5 and 10) sprinkle and annealed at temperatures; (250°C) and (500°C) for ZnO and ZnO/CNT.

4.7: I-V Characteristics

Figures (4.10) (a,b,c, and d) shows the current vs voltage of the ZnO and ZnO/CNT hybrid thin films at sprayed (5 and 10) sprinkles heated at (250)°C. It was found that the zinc oxide was not achieved in Figures (4.10) (a and b) so its conductivity is low, while the conductivity in the zinc oxide carbon nanotube is very high at (500)°C. The reason is due to conductivity of carbon nanotube, where the conductivity increased with the time while the resistance decreased as shown in Figures (4.10) (c and d).

Fitting	Slope	R=1/slope (Ω)	Thickness (cm)	σ ($\Omega^{-1}cm^{-1}$)
ZnO	1.53214E-7	6.52684E+6	8.7E-6	7.0443E-6
ZnO/CNT	1.45222E-4	6.88599E+3	9.1E-6	0.00638

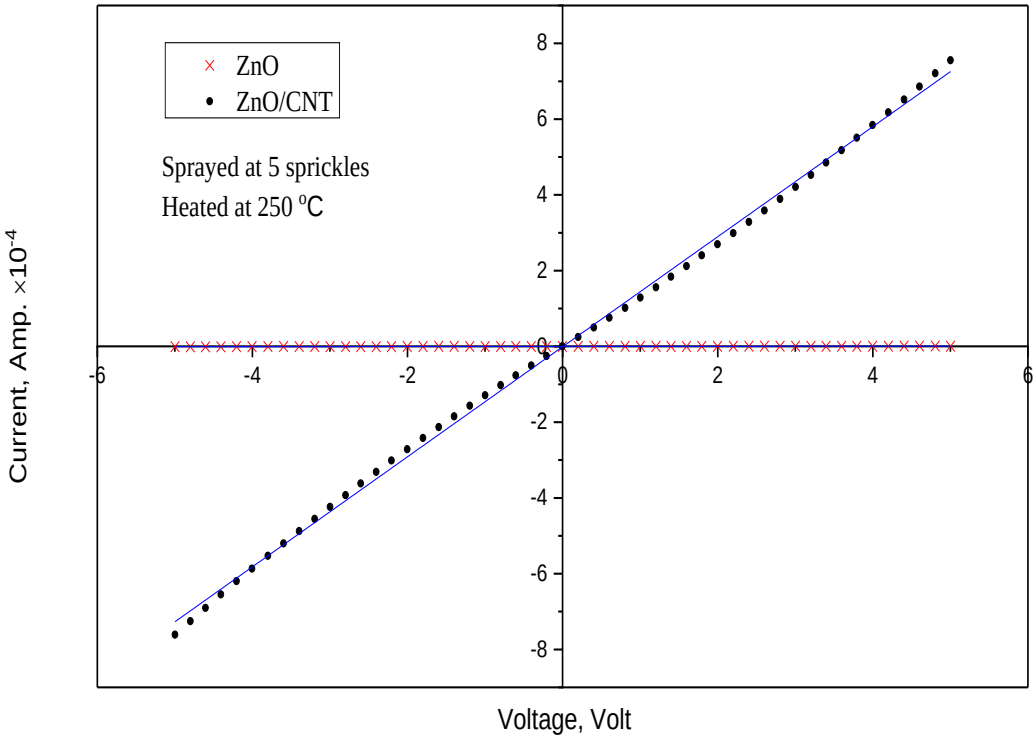

Figure (4.10)(a): The current vs voltage of the ZnO and ZnO/CNT hybrid thin films at sprayed (5) sprinkles heated at (250)°C.

Fitting	Slope	R=1/slope (Ω)	Thickness (cm)	σ ($\Omega^{-1}cm^{-1}$)
ZnO	2.08162E-8	4.80396E+7	9.5E-6	8.7647E-7
ZnO/CNT	8.31463E-5	1.2027E+4	1.02E-5	0.00326

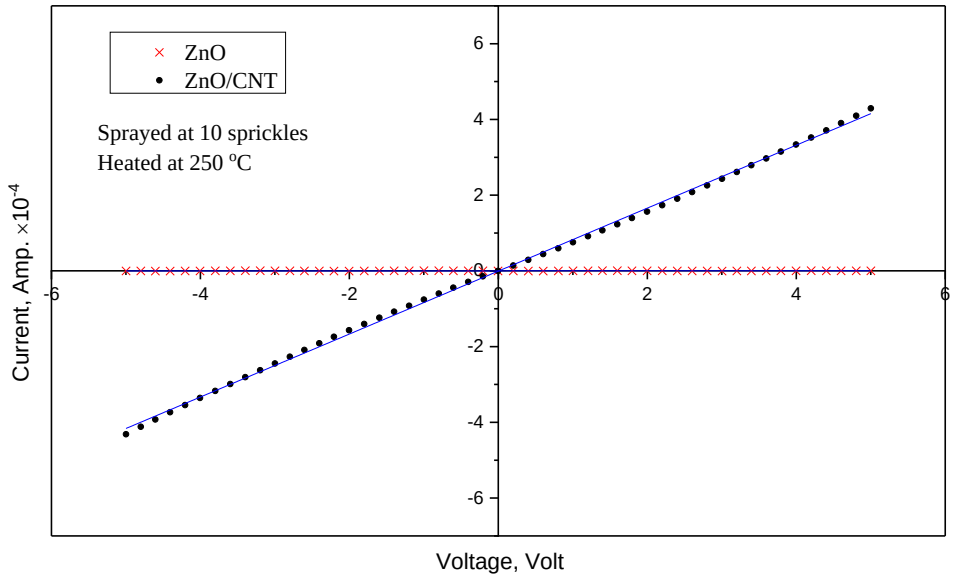

Figure (4.10)(b): The current vs voltage of the ZnO and ZnO/CNT hybrid thin films at sprayed (10) sprinkles heated at (250)°C.

Fitting	Slope	R=1/slope (Ω)	Thickness (cm)	σ ($\Omega^{-1}cm^{-1}$)
ZnO	1.48019E-6	6.75589E+5	8.6E-6	6.88461E-5
ZnO/CNT	3.33122E-6	3.0019E+5	9.4E-6	1.41754E-4

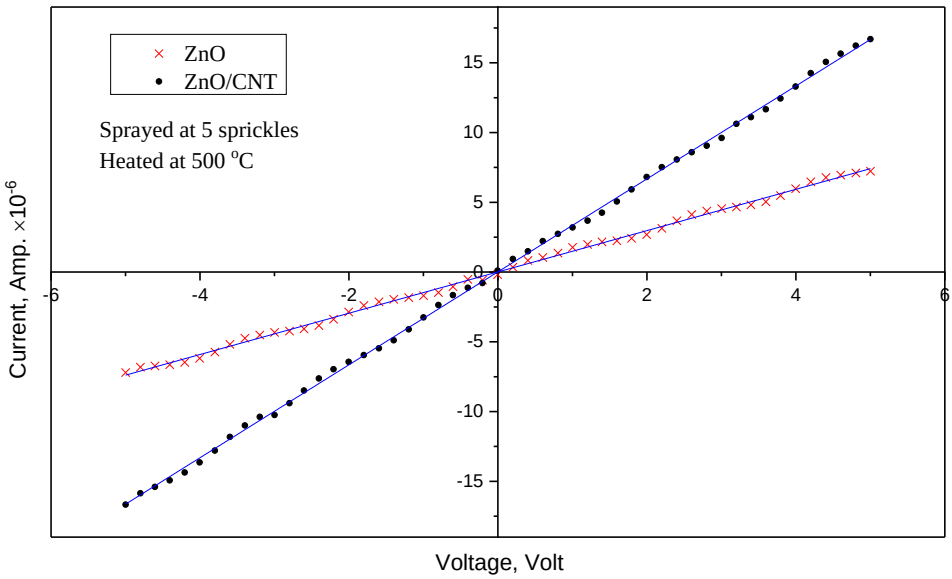

Figure (4.10)(c): The current vs voltage of the ZnO and ZnO/CNT hybrid thin films at sprayed (5) sprinkles heated at (500)°C.

Fitting	Slope	R=1/slope (Ω)	Thickness (cm)	σ ($\Omega^{-1}cm^{-1}$)
ZnO	5.1459E-7	1.9433E+6	9.8E-6	2.10037E-5
ZnO/CNT	1.275E-6	7.84314E+5	1.09E-5	4.6789E-5

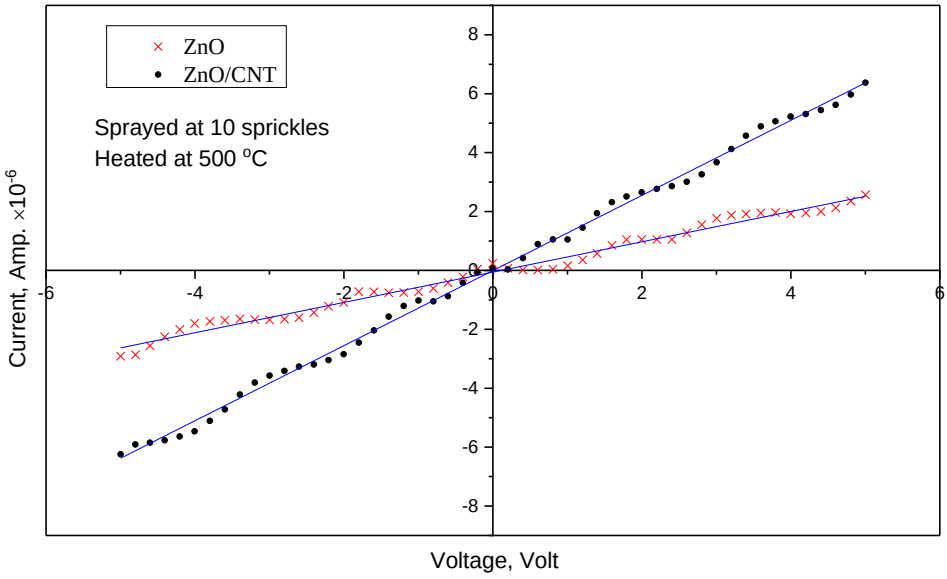

Figure (4.10)(d): The current vs voltage of the ZnO and ZnO/CNT hybrid thin films at sprayed (10) sprinkles heated at (500)^{o}C.

4.8: Thermal Dependence Conductivity

Semiconducting material is an element, which has resistivity between conducting and insulating materials. Semiconductors are insulator at 0 Kelvin, nonetheless, they can be conductors by increasing temperature to the edge that improved to rise in conducting electron compactness [173].

When temperature is higher, the cloud of electrons gain more energy to overlap the energy break to the conduction region from the ground state, consequently, more electrons can vigor easily to the conduction levels and thus resistance get lower with temperature. However, due to temperature rise, in conductors the atoms vibrate giving a resistance to the free electrons [174].

When the temperature is increased, some of the covalent bonds in the semiconductor breakdown as a result of thermal energy provided. This breakdown causes those electrons to be free which are involved in the

creation of these bonds. These free electrons organize a small electric current when voltage is applied through the material. As a sequence, some of the ground electrons obtain plenty energy to arrive the conduction area and therefore become free electrons. Under the influence of electric voltage, these electrons would create electric current.

The conduction of an intrinsic semiconductor is directly dependent of the number of hole electron pairs and mobility. While temperature increases, the number of electron-hole increases, and the mobility lowers. Though, the increase in electron-hole pairs is greater than the decrease in their mobility. So, the conductivity gets higher with higher temperature. The conductivity of extrinsic semiconductors reduced with temperature raises, and that is because the number of mainstream carriers is approximately constant, while mobility is decreased [175].

Thermal dependence conductivity has been investigated for all samples that deposited on interdigitated electrodes using Keithly (2400) semiconductor characterization system for the temperature range between room temperature to (210) ^{o}C.

By looking to the samples of ZnO and ZnO/CNT which are heated at (250) ^{o}C, it can clearly be seen that it did not give any clear results and no obvious semiconducting performance was exhibited, The reason for this is that zinc oxide was not achieved, meaning that it did not work as a semiconductor even in the presence of carbon nanotubes. However, samples annealed at 500 ^{o}C have shown typical behavior of zinc oxide semiconductor.

In the lateral structure, the interrdigitated electrode is used to define the conductivity built on the Eq.(2-11) [175]:

$$\boldsymbol{\sigma = L/RTWNr}$$

Where T is the thickness of the film, L is the distance between fingers, W is the overlaping between the electrodes, Nr is the number of the fingers of interdigitated electrodes and (R) is the films resistance.

When the temperature increases the conductivity increases because of the increase in the number of electrons that are able to reach the conduction band.

The plots of σ vs. 1000/T of ZnO thin film annealed at (500) ^{o}C is revealed in Figure ((4.11) a and b). The dependency of conductivity upon temperature exhibits three altered regions I, II and III. The regions I and III correspond to difference in the conduction mechanism. The conductivity rises with increasing temperature, as the temperature is increased, more of the charge carriers overwhelmed the activation energy barrier and contribute in the conductivity. Region II shows opposite behavior as the conductivity decreases with the temperature goes higher. This finding is suggested to be due to the electron recombination as will discussed further below .

The conductivity of zinc oxide thin films could be investigated by the well-known Eq. (2-12)[176]:

$$\boldsymbol{\sigma=\sigma_{\circ}exp[Ea/K_BT]}$$

where (σ_o) is the pre-exponential factor, (Ea) is the activation energy for electrical conductivity corresponding to the energy difference between donor level and conduction level, (K_B) is Boltzmann constant equal (1.38×10^{-23}) J/K and (T) temperature in Kelvin.

E_I and E_{III} activation energies for I and III regions were stimulated from the linear area of Figure (4.11(a)), respectively. The calculated E_I and E_{III} values were 0.1046eV and 1.6042eV, respectively. The amount of the activation energy E_I = 0.1046eV calculated from the conduction statistics is tiny in comparison with optical energy gap. These finding could be

interpreted by the fact that the activation energy is the energy that required for conduction from one location to another, whereas, the optical energy gap corresponds to other transitions. These energies at dissimilar temperature regions (I and III) specify the existence of 2 donor planes. These planes are the "shallow" and "deep" donor levels in the energy band gap of the semiconducting ZnO. The value of 0.1046eV is to the "shallow donor level", while the value of 1.6042eV corresponds to the "deep donor level". Therefore, it is estimated that in region III, the electronic conductance of the ZnO is thermally motivated (activated) from the "deep donor level" to the conduction region.

The region II is a transition region, The linier behavior at high temperature in E_{II} of the curve indicate the activation type of conduction is dominating but the curve deviate at low temperature. Hopping mechanism dominated on the second half of the curve where the electrons have no sufficient energy to jump directly, however, hopping from ground level to temporary level and then to conduction band [177]. In which more charges should be ionized from the "shallow donor level" and so, the carriers are depleted and consequently, the conductivity reduces with the increase of temperature up to activation of charges in "deep donor level" start. In addition, Lee et al. [178] stated that the electrical conductivity for nano-phase ZnO having particle size of 60 nm is in the range 2×10^{-6} to 2×10^{-4} S/cm at 450-600 ^{o}C. The higher value of conductivity of ZnO nanostructured film studied could be clarified as the conductivity of the ZnO film is credited to the "trapping" of electrons in the grain boundaries.

The films are an n-type semiconductor due to the occurrence of intrinsic defects such as oxygen vacancies and Zn interstitials [179]. By comparing models of pure ZnO with models that contain carbon nanotubes ZnO/CNT, which have been represented in Figure (4.12), it can clearly be seen that the transition region is almost very small, and the deviation is not sharp. CNT

can create more trapping levels which at the same time these levels work as donor levels leading to electron transfer more easily and that interpret the smallest activation energy shown in the samples having CNT. All the activation energies are concise in Table (4.4).

Table(4.4). Activation energies calculated from figures (4.11 and 4.12)

Samples heated At (500)^{o}C	Activation energy (eV)		
	Ea_1	Ea_2	Ea_3
ZnO (5 sprays)	0.104629325	-0.02196973	1.60423015
ZnO (10 sprays)	0.19085176	-0.37555468	1.230456929
ZnO/CNT (5 sprays)	0.001390669	-0.01617058	0.578869513
ZnO/CNT (10 sprays)	0.06691746	-0.0738568	0.75825254

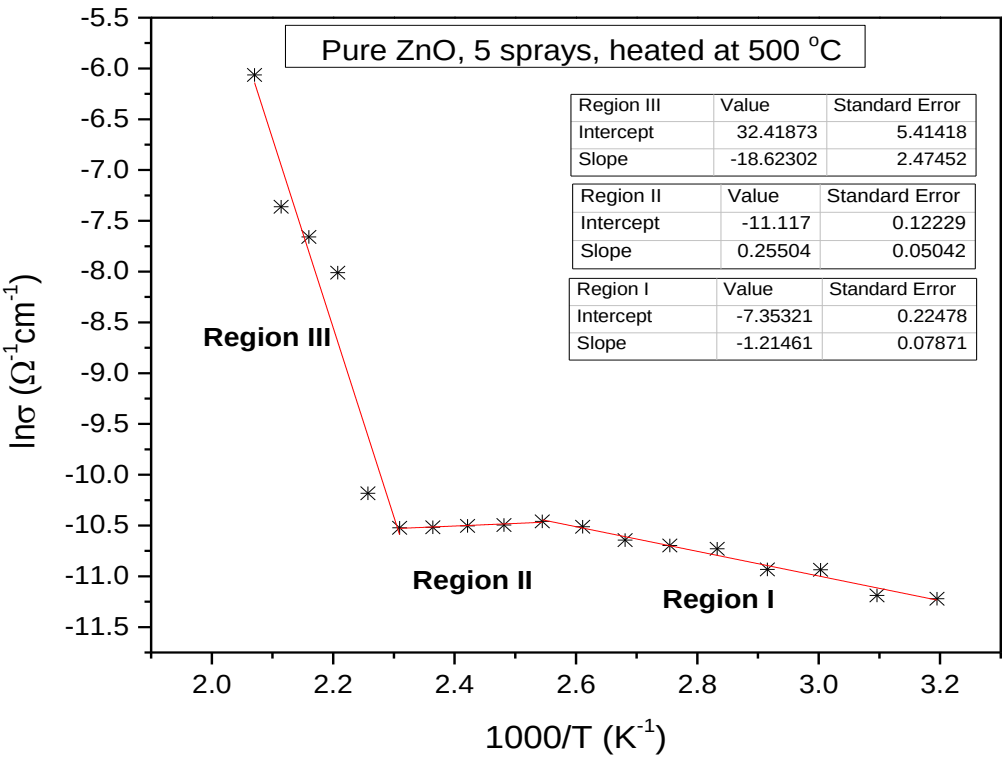

Figure (4.11) (a): Arrhenius Plot of ln σ vs. 1000/T of pure ZnO, 5 sprays nanostructured thin film at 500 °C annealing temperature.

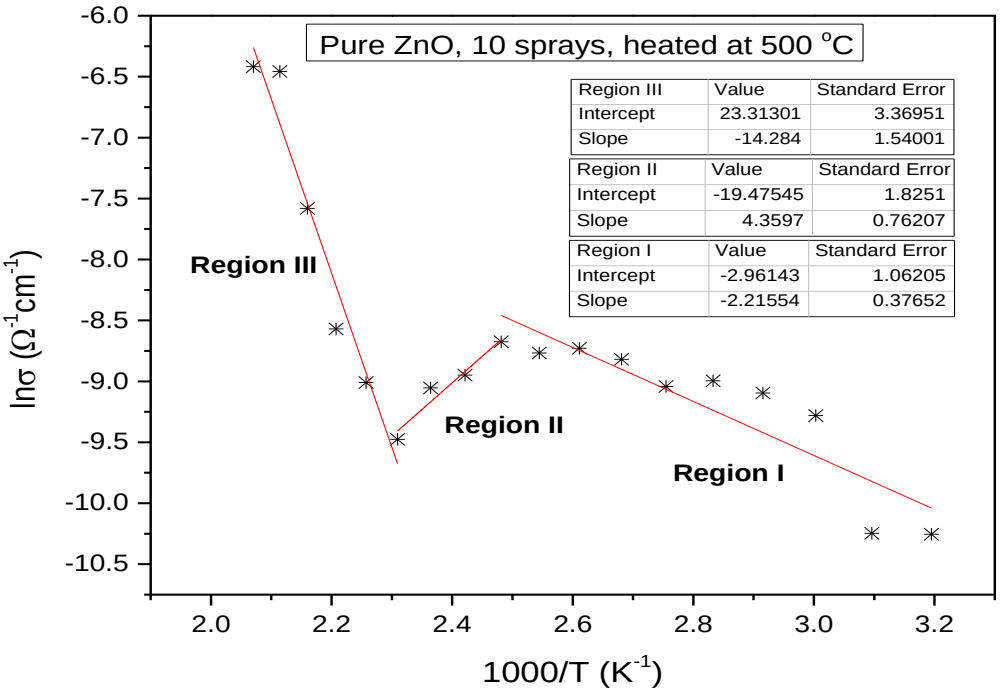

Figure (4.11) (b): Arrhenius Plot of ln σ vs. 1000/T of pure ZnO, 10 sprays nanostructured thin film at 500 °C annealing temperature.

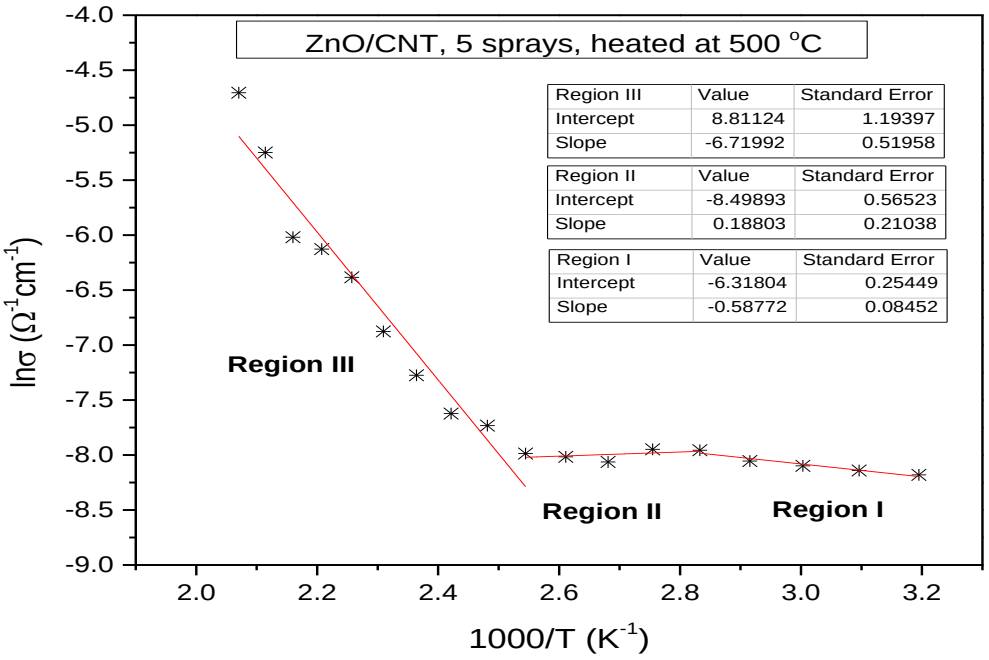

Figure (4.12) (a): Arrhenius Plot of ln σ vs. 1000/T of ZnO/CNT, 5 sprays nano-structured thin film at 500 °C annealing temperature.

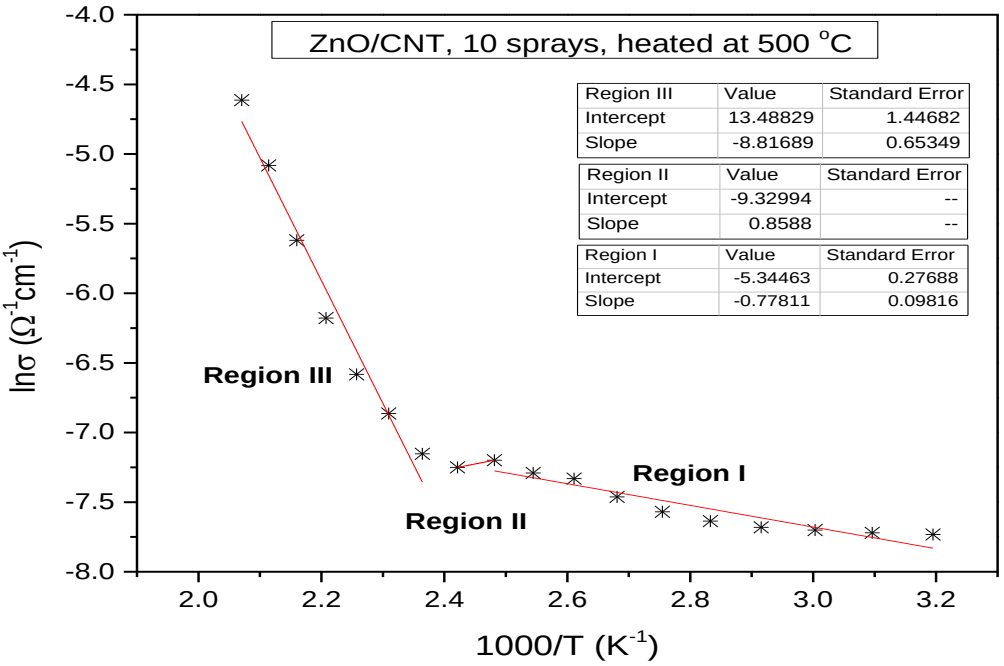

Figure (4.12) (b): Arrhenius Plot of ln σ vs. 1000/T of ZnO/CNT, 10 sprays nanostructured thin film at 500 °C annealing temperature.

4.9: Gas sensing

Samples were exposed to NO_2 at the concentration of 100 ppm using homemade resistive sensing system at room temperature. Gas sensors with very high responding to odorants, at the same time working at room temperature are considered as more attractive devices because of their low power consumption and long lasting stability [180]. The sensitivity (S) of the sensor is calculated for reducing and oxidizing gases and vapors, the electrical resistance of the thin films was measured in the air, and the presence of gas NO_2 at different temperatures. A known amount of target gas is introduced after the ohmic resistance of the sensor material is stabilized. The recovery characteristics (when the target gas is with drawn) are also monitored as a function of time. From Figures below we can note that the sensitivity of all films increases with an increasing substrate temperature of films. Because the sensitivity depends on grain size and grain boundary. The distance between the grains was small and includes the interaction between oxygen absorbed and gases that occurs when any grain boundary will increase interaction and increase sensitivity.

Figures (4.13) to (4.17) show The time dependency of the response upon exposure to 100 ppm For selected gases for the ZnO and ZnO/CNT films.

Figure (4.13) (a and b) shows the response vs. time of ZnO and hybrid films towards NO_2. It is obviously seen that ZnO are not reversible as the resistance has not come to the initial value after the gas being disposed from the sample surface. Whereas, the hybrid film have shown quite interesting performance due gas interaction which make them promising candidate for sensing applications. It is expected that the presence of CNT in the composite film inhibits the diffusion of gas molecules inside the film and most interaction takes place on the surface of the film [181].

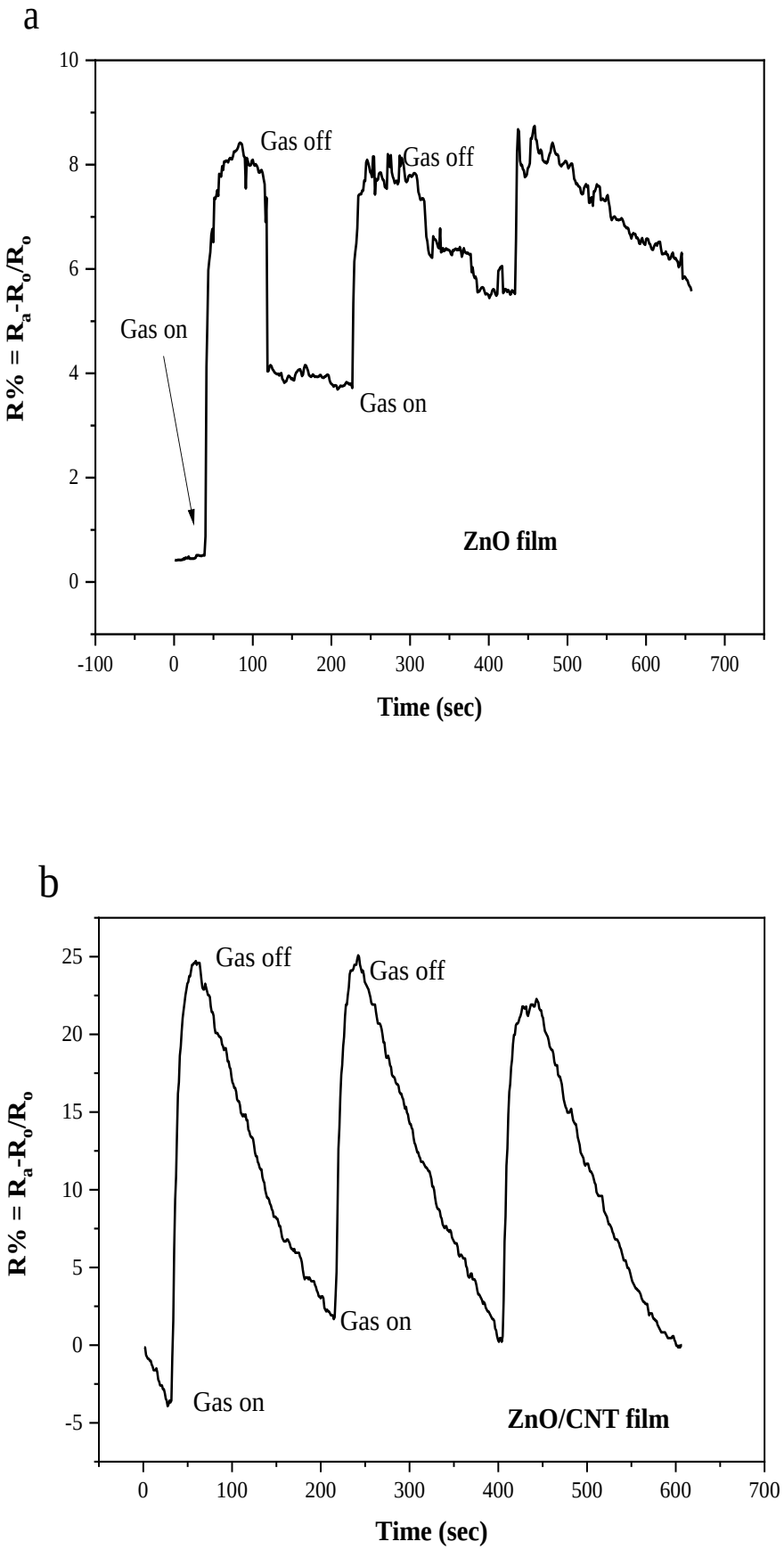

Figure (4.13) (a and b) : The time dependency of the response upon exposure to 100 ppm NO_2 gas for the ZnO and ZnO/CNT thin films.

Figure (4.14) illustrates that ZnO sensor heated at a temperature 500ºC has a response time for dimethylformamide, but it have not a recovery time, while ZnO/CNT sensor heated at the same temperature has a response time and recovery time.

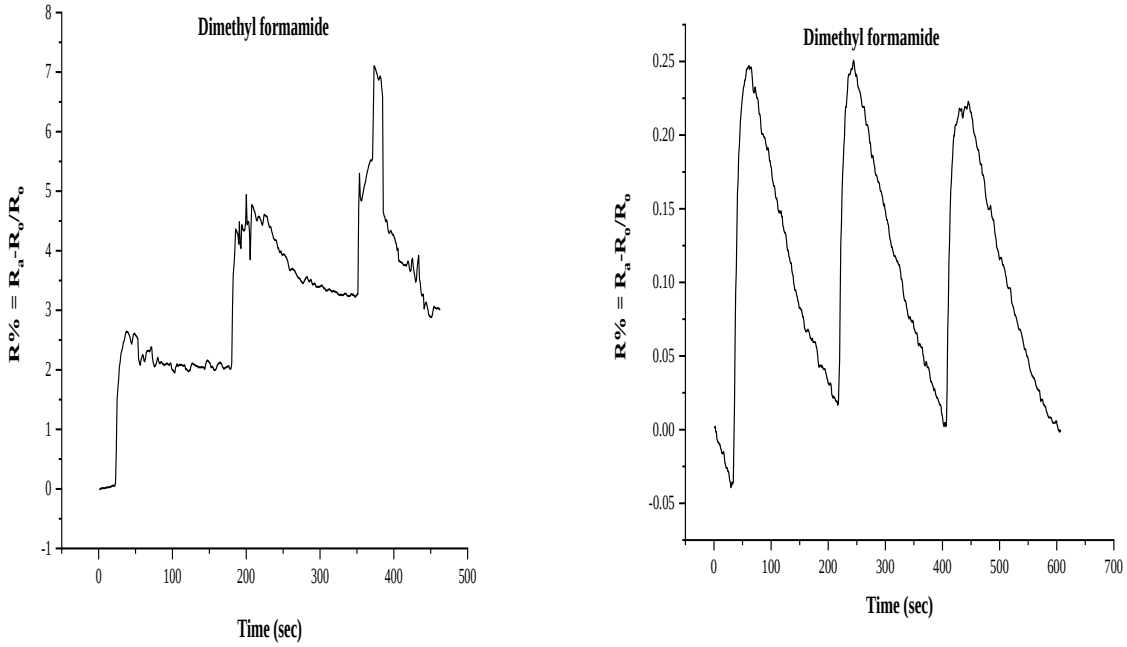

Figure (4.14): The time dependency of the response upon exposure to 100 ppm Dimethyl formamide gas for the ZnO and ZnO/CNT thin films.

Figure (4.15) has a response time and a recovery time for Acetone gas which means that the sensitivity of films increases with an increasing substrate temperature of films because it depends on grain size and grain boundary but it doesn't have response time to NH_3 gas When we were in the laboratory.

We note that the ZnO sensor which heated under a temperature of 500ºC has a response and recovery time for Ethanol gas because resistance increases in presence of contaminant, but it decreases in presence of it for ZnO/CNT sensor as shown in Figure (4.16):

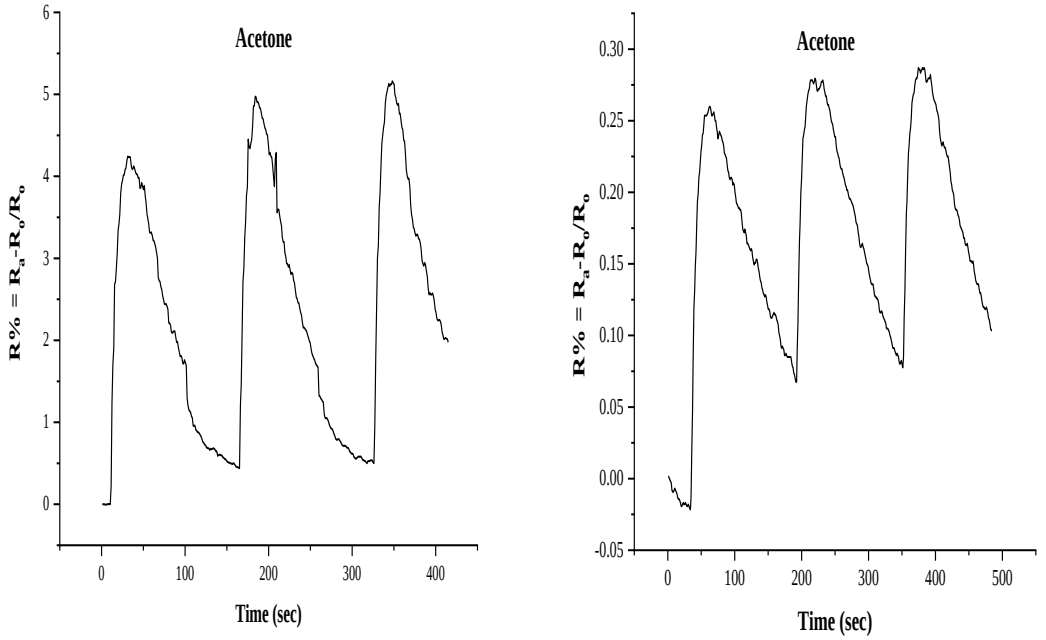

Figure (4.15): The time dependency of the response upon exposure to 100 ppm Acetone gas for the ZnO and ZnO/CNT thin films.

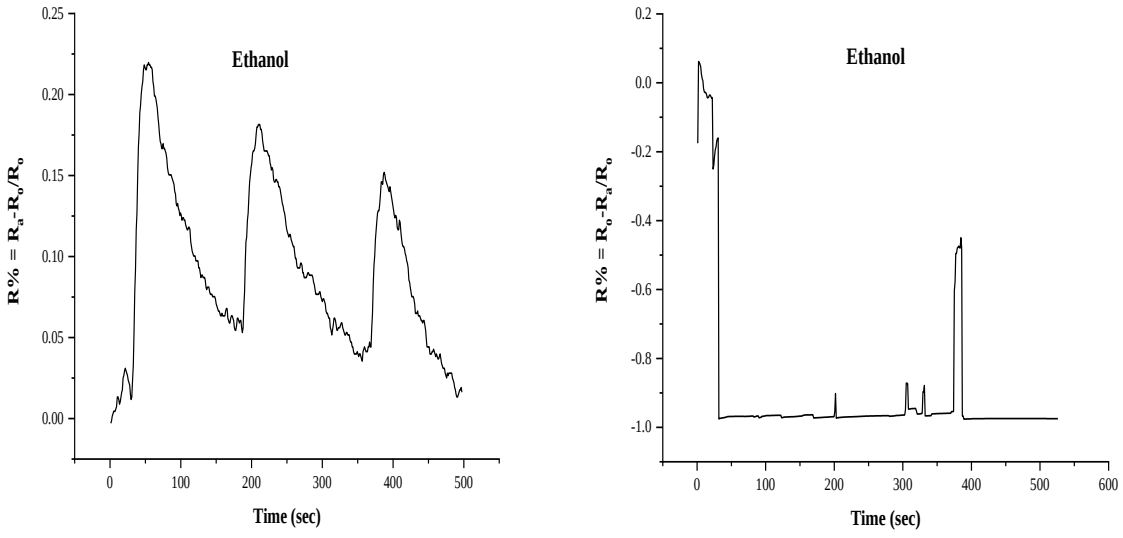

Figure (4.16): The time dependency of the response upon exposure to 100 ppm Ethanol gas for the ZnO and ZnO/CNT thin films.

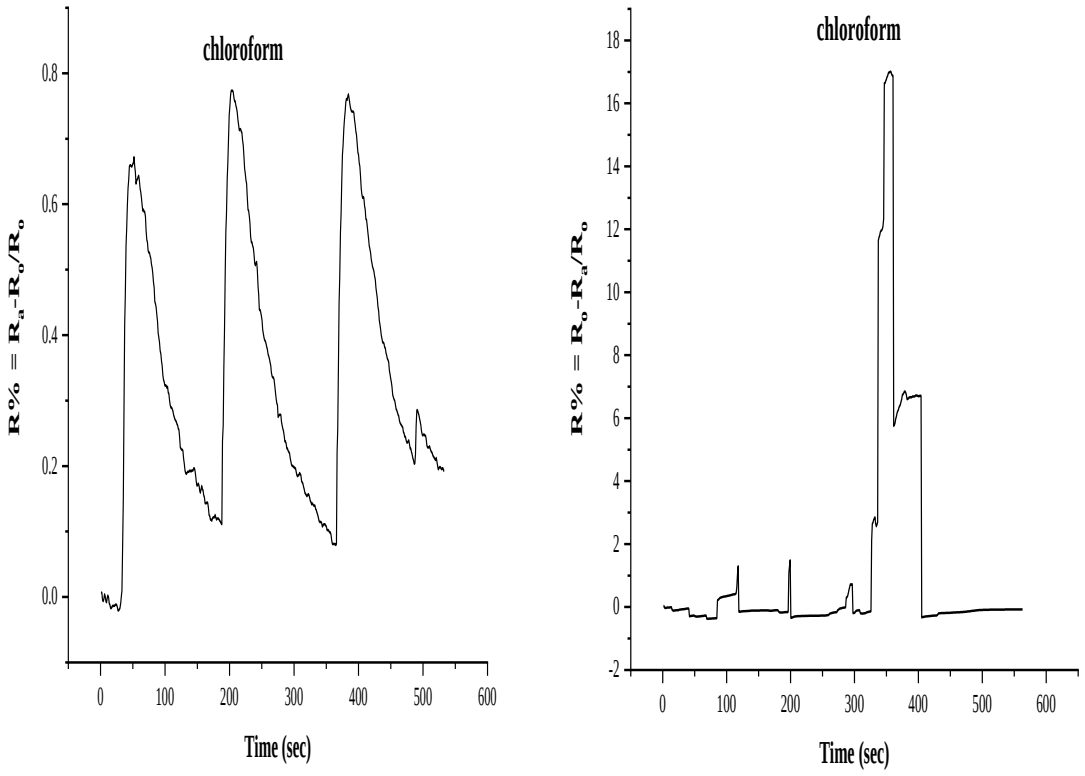

Figure (4.17): The time dependency of the response upon exposure to 100 ppm Chloroform gas for ZnO and ZnO/CNT thin films.

The relation between response time and recovery time shown in Figure (4.18), Where we observed the value of response time and recovery time depends on gas concentration and the temperature at which the sensor operates.

The response and recovery times have been calculated as 90% of the maximum response after gas on and 90% of the returning to initial state after gas off and found to be 10 and 150 second respectively as shown in Figure (4.18).

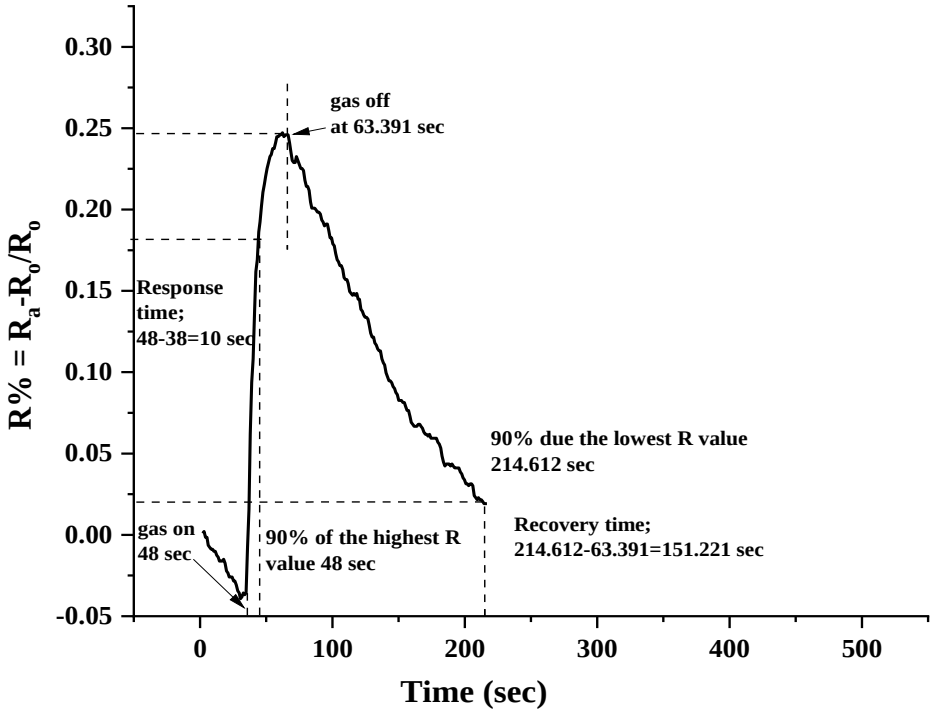

Figure (4.18): Response and Recovery time of ZnO/CNT thin film for NO_2 at 500 ^oC.

5.1: Conclusions

- The color of the synthesized solutions was orange indicating very fine size nano particles were achieved.
- UV-Visible absorption spectroscopy have revealed that the energy gaps of all prepared samples were affected dramatically with the temperature of annealing (500)^{o}C and the existence of carbon nanotubes.
- The temperature dependence conductivity and Arrhenius plots have shown that the samples have three regions of conduction mechanisms typical of zinc oxide.
- The adding of CNT generate more trapping levels which at the same time these levels work as donor levels leading to electron transfer more easily and that interpret the smallest activation energy shown in the samples having CNT.
- NO_2 gas interaction with the synthesized devices has been studied and the results show that the existence of carbon nanotubes reduces the chemical interaction and so complete recovery achieved after purging the samples with fresh air.

5.2: Future Works

A further investigation can be suggested to develop this work as follows:

- Applying the synthesis devices as solar cell by adding silicon dioxide as a deplesion region.
- Applying the prepared nano particles as antibacterial for some hazardous bacteria.
- Synthesis of zinc oxide thin films according to another method, studying the same properties dealt with this research and comparing the results, as well as Preparation of zinc oxide thin films with different value of thickness by increasing the number of sprays, as well as using different substrates and different deposition technique.

References

[1] S. Barthwalab and N. B. Singhc, *"ZnO-CNT Nanocomposite:A Device as Electrochemical Senso"*, Materials Today: Proceedings, vol. 4, No. 4, Pp.5552-5560, (2017).

[2] Z. L. Wang, *" Nanostructures of zinc oxide"*, Materials Today: Proceedings, vol. 7, No. 26, Pp. 26-33, (2004).

[3] C. M. Lieber, *"One-dimensional nanostructures: Chemistry, physics & applications"*, Solid State Communications, vol. 107, No. 11, Pp. 607-616, (1998).

[4] Q. Zhang, Y. Zhao, Z. Jia, Z. Qin, L. Chu, J. Yang, J. Zhang, W. Huang and X. Li, *"High stable, transparent and conductive ZnO/Ag/ZnO nanofilm electrodes on rigid/flexible substrates"*, Energies, vol. 9, No. 6, (2016).

[5] H. Huang, G. Fang, X. Mo, H. Long, L. Yuan, B. Dong, X. Meng and Zhao, *" ZnO-based fairly pure ultraviolet light-emitting diodes with a low operation voltage"*, IEEE Electron Device Letters, vol. 30, No. 10, (2009).

[6] Z. Q. Zheng, J. D. Yao, B. Wang and G. W. Yang, *"Light-controlling, flexible and transparent ethanol gas sensor based on ZnO nanoparticles for wearable devices"*, Journal of Scientific Reports, vol. 5, No. 11070, (2015).

[7] Ü. Özgüra, Ya. I. Alivov, C. Liu, A. Tekeb, M. A. Reshchikov, S. Doğanc, V. Avrutin, S-J. Cho, and H. Morkoçd, *"A comprehensive review of ZnO materials and devices"*, Applied Physics, vol. 98, No. 4, (2005).

[8] X. Li, R. Shen, B. Zhang, X. Dong, B. Chen , H. Zhong, L. Cheng, J. Sun and G. Du, *"Nitrogen doped ZnO thin films prepared by photo-assisted metal-organic chemical vapor deposition"*, Nanoscience and Nanotechnology, vol. 11, No. 11, Pp. 9741-9744, (2011).

[9] N.M Roshchina, P.S. Smertenko, V.G. Stepanov, L.V. Zavyalova and O.S. Lytvyn, *"Some properties of thin film structures on the base of ZnO obtained by MOCVD method"*, Solid State Phenomena, vol. 200, (2013).

References

[10] D.G. Ayana, V. Prusakova, C. Collini, M.V. Nardi, R. Tatti, M. Bortolotti, L. Lorenzelli, A. Chiappini, A. Chiasera, M. Ferrari, L. Lunelli, and Sandra Dirè, *" Sol–gel synthesis and characterization of undoped and Al-doped ZnO thin films for memristive application"*, AIP Advances ,vol. 6, No. 11, (2016).

[11] S. Dutta, S. Chattopadhyay, A. Sarkar, M. Chakrabarti D. Sanyal and D. Jana, *"Role of defects in tailoring structural, electrical and optical properties of ZnO"*, Journal of Progress in Materials Science, vol. 54, No. 1, Pp.89-136, (2009).

[12] G. Abdelouahab, B. Said, B. Boubaker, and C. Foued, *"Preparation of transparent conducting ZnO:Al films on glass substrates by ultrasonic spray technique"*, Semiconductors, vol. 34, No. 7, (2013).

[13] Y. Caglar, S. Ilican, M. Caglar, and F. Yakuphanoglu, *"Influence of Mn incorporation on the structural and optical properties of sol gel derived ZnO film"*, Sol-Gel Science and Technology, vol. 53, No.2, Pp. 372-377, (2010).

[14] C. Tsay, K. Fan, S. Chen, and C. Tsai, *"Preparation and characterization of ZnO transparent semiconductor thin films by sol–gel method"*, Alloys and Compounds, vol. 495, No. 1, Pp. 126-130, (2010).

[15] A. krueger, *"Carbon Materials and Nanotechnology*", WILY-VCH Verlag GmbH and Co.KGaA, germany, (2010).

[16] C. Carter and M. Norton, *"Ceramic materials; Science and Engineering*", First Edition, New York: Springer, (2013).

[17] G. Yi, C. Wang, and W. Park, *"ZnO nanorods: synthesis, characterization and applications"*, Semiconductor Science and Technology, vol. 20, No. 4, p. 22, (2005).

References

[18] S. K. Patra, "A novel chemical approach to fabricate ZnO nanostructures", M.Sc. Thesis, Indian Institute of Technology Kharagpur Kharagpur, India, (2013).

[19] S. J. Pearton, D.P. Norton, K. Ip, Y.W. Heo, and T. Steiner, *"Recent progress in processing and properties of ZnO*", Progress in Materials Science, vol. 50, No. 3, (2005).

[20] M. H. Shinen, "*Preparation of Nano-thin films of ZnO by Sol – Gel method and applications of solar cells Hetrojunction*", Journal of Natural Sciences Research, vol. 4, No.1, (2014).

[21] Jin Xu, "*Luminescence in ZnO*", M.Sc. Thesis Virginia Commonwealth University Richmond, Virginia, (2004).

[22] R. K. Thareja and Sh. Shukla, " *Synthesis and characterization of zinc oxide nanoparticles by laser ablation of zinc in liquid*", Journal: Applied Surface Science, vol. 253, No. 22, (2007).

[23] Han Ho Choi, "*Synthesis and characterization of tailoered zinc oxide nanostructures and their engineered nanocomposites*", PhD Thesis, Florida State University, (2004).

[24] L. Liao, J. C. Li, D. F. Wang, C. Liu, C. S. Liu, Q. Fu, and L. X. Fan, "*Field emission property improvement of ZnO nanowires coated with amorphous carbon and carbon nitride films*", Nanotechnology, vol.16, No. 6, (2005).

[25] Y. Xia, P. Yang, Y. Sun, Y. Wu, B. Mayers, B. Gates, Y. Yin, F. Kim, and H. Yan, "*One-Dimensional Nanostructures: Synthesis, Characterization, and Applications*", Advanced Materials, vol. 15, No. 5, (2003).

[26] J. E. Nause, "*Fluorescent substrate offers route to phosphor-free LEDs*", Comp. Semicond, (2005).

References

[27] H. Hartnagel, A. L. Dawar, A. K. Jain, and C. Jagadish, "*Semiconducting transparent thin films*", Institute of Physics Publishing, Bristol and Philadelphia, (1995).

[28] D. C. Look, "*Materials Science and Engineering: B; Recent advances in ZnO materials and devices",* vol. 80, No. 3, pp. 383-387,(2001).

[29] R. Mimouni, O. Kamoun, A. Yumak, A. Mhamdi, K. Boubaker, P. Petkova and M. Amlouk, *"Effect of Mn content on structural, optical, opto-thermal and electrical properties of ZnO: Mn sprayed thin films compounds",* Journal of Alloys and Compounds, vol. 645, pp.100-111, (2015).

[30] D. Zhang, Y. He and C. W. Wang, *"Structure and optical properties of nanostructure zinc oxide films with different growth temperatures",* Optics & Laser Technology, vol. 42, No. 4, pp. 556-560, *(*2010).

[31] N. Karousis, N. Tagmatarchis and D. Tasis, *"Current progress on the chemical modification of carbon nanotubes"*, Chemical Reviews, vol. 110, No. 9, Pp. 5366-5397, (2010).

[32] L. Nasdala, A. Kempe, and R. Rolfes, *"Are finite elements appropriate for use in molecular dynamic simulations?",* Composites Science and Technology**,** vol. 72, pp.989-1000, (2012).

[33] D. Lashmore, B. White and M. Schauer, J. Mann, *"Synthesis and electronic properties SWCNT sheets*", Materials Research Society Symposium Proceedings, vol. 1081, Pp.107-112, (2008).

[34] E. A. Laird, F. Kuemmeth, G. A. Steele, K. Grove-Rasmussen, J. Nygård, K. Flensberg and L. P. Kouwenhoven, "Quantum Transport in Carbon Nanotubes", Reviews of Modern Physics, vol. 87, No. 3, Pp.703-764, (2015).

References

[35] X. Lu and Z. Chen, *"Curved Pi-Conjugation, Aromaticity, and the Related Chemistry of Small Fullerenes (<C_{60}) and Single-Walled Carbon Nanotubes"*, Chemical Reviews, vol. 105, No.10, Pp. 3643-3696, (2005).

[36] S. Hong, and S. Myung, "Nanotube Electronics: A flexible approach to mobility", Nature Nanotechnology, vol. 2, No. 4, Pp. 207-208 (2007).

[37] Vasylenko, J. Wynn, P. V. C. Medeiros , A.J. Morris, J. Sloan and D. Quigley, *"Encapsulated nanowires: Boosting electronic transport in carbon nanotubes"*, Physical Review B, vol. 95, No. 12, (2017).

[38] R. Zhang, Y. Zhang, Q. Zhang, H. Xie, W. Qian and F. Wei, "Growth of Half-Meter Long Carbon Nanotubes Based on Schulz–Flory Distribution", ACS Nano, vol. 7, No. 7, Pp. 6156-6161, (2013).

[39] W. Xueshen, L. Qunqing , X. Jing, J. Zhong , W. Jinyong, L. Yan, J. Kaili and F. Shoushan, *"Fabrication of Ultralong and Electrically Uniform Single-Walled Carbon Nanotubes on Clean Substrates"*, *Nano Letters*, vol. 9, No. 9, Pp. 3137-3141, (2009).

[40] S. Barthwal and N. B. Singh, *"ZnO-CNT Nanocomposite:A Device as Electrochemical Sensor"*, Materials Today: Proceedings, vol.4, No. 4, Pp. 5552-5560, (2017).

[41] S. Krishnamoorthy and A. A. Iliadis, Solid State Electron., volume 52, p.1710, (2008)

[42] H. Tang, M. Yan, H. Zhang, S. Li, X. Ma, M. Wang, and D. Yang, Sens. Actuators B., vol. 114, p.910, (2006).

[43] M. K. Gupta, N. Sinha, B. K. Singh, N. Singh, K. Kumar, and B. Kumar, Mater. Lett., vol. 63, p.1910, (2009)

[44] C. D. Natale, R. Paolesse, E. Martinelli, and R. Capuano, Anal. Chim. Acta, vol. 824, No.1, (2014).

[45] S. Salehi, E. Nikan, A. A. Khodadadi, and Y. Mortazavi, Sensors and Actuators B: Chemical, vol. 205, p.261, (2014).

References

[46] X. Pan, and X. Zhao, J. Chen, A. Bermak, and Z. Fan, "*A fast-response/recovery ZnO hierarchical nanostructure based gas sensor with ultra-high room-temperature output response*", Sensors and Actuators B: Chemical, vol. 206, Pp.764-771, (2015).

[47] N. Sinha, J. Ma, Yeow and T. W. John, "Carbon Nanotube-Based Sensors", Nanoscience and Nanotechnology, vol. 6, No.3, pp. 573-590, (2006)

[48] X. Liu, J. Sun, and X. Zhang, "Sensors and Actuators B: Chemical", vol.211, p.220, (2015).

[49] A. Bakin, A. Behrends, A. Waag, H. J. Lugauer, A. Laubsch, and K. Streubel, Proceedings of the IEEE, vol.e 98, No. 1281, (2010).

[50] A. D. Corso, M. Posternak, R. Resta, and A. Baldereschi, "*Ab initio study of piezoelectricity and spontaneous polarization in ZnO*", Physical Review B., vol. 50, No. 15, (1994).

[51] M. E. Roberts, M. C. LeMieux, and Z. Bao, " *Sorted and Aligned Single-Walled Carbon Nanotube Networks for Transistor-Based Aqueous Chemical* Sensors", The Journal of Physical Chemistry ABC; ACS Nano, vol. 3, No. 10, Pp.3287-3293, (2009).

[52] S. Daniel, T. P. Rao, K. S. Rao, S. U. Rani, G. R. K. Naidu, H. Y.Lee, and T. Kawai, "*A review of DNA functionalized/grafted carbon nanotubes and their characterization*", Sensors and Actuators B: Chemical, vol. 122, No.2, Pp.672-682, (2007).

[53] Z. Mahdavifar, N. Abbasi, and E. Shakerzadeh, Molecular Liquids, volume 204, Pp. 1-270, (2015).

[54] X. Wang, Q. Li, J. Xie, Z. Jin, J. Wang, Y. Li, K. Jiang, and S. Fan,Nano Lett., volume 9, 3137, (2009).

[55] M. F. Yu, O. Lourie, M. J. Dyer, K. Moloni, T. F. Kelly, and R. S.Ruoff, Science,volume 287, p.637, (2000).

[56] N. V. Hieu, N. P. Duc, T. Trung, M. A. Tuan, and N. D. Chien, "Sensors and Actuators B: Chemical", volume 144, p.450, (2010).

[57] C. Y. Wang and S. Adhikari, "Phys. Lett. A", volume 375, 2171, (2011).

[58] M. Tak, V. Gupta, and M. Tomar, Journal of Materials Chemistry B, volume 1, 6392, (2013).

References

[59] Y. Zhang, X. Sun, L. Pan, H. Li, Z. Sun, C. Sun, and B. K. Tay, *"Solid State Ionics*", vol. 180, 1525, (2009).

[60] J. Y. Jung, H. J. Song, Y. J. Kang, D. H. Oh, H. Jung, Y. S. Cho, and D. J. Kim, Materials Research", vol. 18, p.529, (2008)

[61] K. Moszak, A. Szczurek, B. Babiarczuk, B. Borak and J. Krzak, *"ZnO sol-gel oxide coatings as materials for UV optical filters"*, Advanced Materials Letters, (2017).

[62] S. Sanjeev and D. Kekuda, *"Effect of Annealing Temperature on the Structural and Optical Properties of Zinc Oxide (ZnO) Thin Films Prepared by Spin Coating Process"*, Journal: IOP Conference Series: Materials Science and Engineering, vol. 73, No. 1, (2015).

[63] D. D. Mulmi, A. Dhakal and B. R. Shah, *"Effect of Annealing on Optical Properties of Zinc Oxide Thin Films Prepared by Homemade Spin Coater"*, Nepal Journal of Science and Technology, vol. 15, No.2, (2014).

[64] A. Ghosh, N.G. Deshpande, Y.G. Gudage, R.A. Joshi, A.A. Sagade, D.M. Phase, and Ramphal Sharma, *"Effect of annealing on structural and optical properties of zinc oxide thin film deposited by successive ionic layer adsorption and reaction technique"*, Journal of Alloys and Compounds, vol. 469, No. 1-2, (2009).

[65] E. F. Keskenler, G. Turgut, M. F. Keskenler, *"Characterization of ZnO thin films grown by sol-gel spin coating technique regarding precursor solution"*, Turkish Journal of Materials, vol.2, No. 1, (2017).

[66] A. J. Ghazai, E. A. Salman, and H. Zahraa, *"Synthesis and characterization of ZnO thin films using Spin Coating technique"*, JOURNAL OF THI-QAR SCIENCE, vol. 5, No. 4, (2016).

[67] Sh. M. Ambalagi, H. K. Inamadar, and B. Sannakki, *"Mechanism of DC Conductivity Measurement of Zinc Oxide Doped Polyaniline Nanocomposites"*, Materials Today, vol. 3, No. 10, (2016).

[68] Y. Natsume, and H. Sakata, *"Zinc oxide films prepared by sol-gel spin-coating"*, Journal of Thin Solid Films, vol. 372, No. 1-2, (2000).

[69] S. Iijima, *"Helical microtubules of graphitic carbon"*, Nature, vol. 354, Pp.56-58, (1991)

References

[70] S. Iijima, *"T. Ichihashi, Single-shell carbon nanotubes of 1-nm diameter"*, Nature, vol. 363, Pp.603-605, (1993).

[71] N. Nakashima, *"Soluble carbon nanotubes: Fundamentals and applications"*, Inter. J. Nanosci., vol. 4, Pp.119-137, (2005).

[72] N. Nakashima and T. Fujigaya, *"Fundamentals and applications of soluble carbon nanotubes"*, Chem. Lett., vol. 36, Pp.692-697, (2007).

[73] R.H. Baughman, A.A. Zakhidov and W.A. De Heer, *"Carbon nanotubes - The route toward applications"*, Science, vol.297, Pp.787-792, (2002).

[74] W. Wang, K.A.S. Fernando, Y. Lin and M.J. Meziani, *"Metallic single-walled carbon nanotubes for conductive nanocomposites"*, J. Am. Chem. Soc., vol.130, Pp.1415-1419, (2008).

[75] P.L. McEuen, M.S. Fuhrer and H. Park, *"Single-walled carbon nanotube electronics"*, IEEE Transactions on Nanotechnology, vol. 1, Pp.78-84, (2002).

[76] C.V. Nguyen, Q. Ye and M. Meyyappan, *"Carbon nanotube tips for scanning probe microscopy: Fabrication and high aspect ratio nanometrology"*, Measur. Sci. Tech., vol. 16, Pp.2138-2146, (2005).

[77] N.M. Gabor, Z. Zhong, K. Bosnick, J. Park and P.L. McEuen, *"Extremely efficient multiple electron-hole pair generation in carbon nanotube photodiodes"*, Science., vol. 325, Pp.1367-1371, (2009).

[78] A.L. Ndiaye, C. Varenne, P. Bonnet, E. Petit, et al. Elaboration of single wall carbon nanotubes-based gas sensors: Evaluating the bundling effect on the sensor performance, Thin Solid Films. Vol.520, 4465-4469, (2012).

[79] M.D. Shirsat, T. Sarkar, J. Kakoullis Jr., N.V. Myung, B. Konnanath, A. Spanias, A. Mulchandani, Porphyrin-functionalized single-walled carbon nanotube chemiresistive sensor arrays for VOCs, Journal of Physical Chemistry C., vol. 116, Pp.3845-3850, (2012).

[80] S.C. Lim, D.S. Lee, H.K. Choi, I.H. Lee, Y.H. Lee, Field emission of carbon-nanotube point electron source, Diamond and Related Materials., vol. 18, Pp.1435-1439, (2009).

[81] P.J. Boul, K. Turner, J. Li, M.X. Pulikkathara, R.C. Dwivedi, E.D. Sosa, Y. Lu, O.V. Kuznetsov, P. Moloney, R. Wilkins, M.J. O'Rourke, *"Single*

References

wall carbon nanotube response to proton radiation", Physical Chemistry C., vol. 113, Pp.14467-14473, (2009).

[82] A.P. Terzyk, A. Pacholczyk, M. Wiśniewski, P.A. Gauden, "*Enhanced adsorption of paracetamol on closed carbon nanotubes by formation of nanoaggregates: Carbon nanotubes as potential materials in hot-melt drug deposition-experiment and simulation*", Colloid Interface Science, vol. 376, Pp. 209-216, (2012).

[83] N.M. Bandaru, N.H. Voelcker, Glycoconjugate-functionalized carbon nanotubes in biomedicine, Journal of Materials Chemistry, vol. 22, Pp.8748-8758, (2012).

[84] L. Henrard, E. Hernández, et al. Van der Waals interaction in nanotube bundles: Consequences on vibrational modes, Physical Review B - Cond. Mat. Mater. Physics, vol. 60, Pp. 8521-8524, (1999).

[85] N.I. Alekseev, N.A. Charykov, "*The characteristic size of carbon nanotube bundles*", Physical Chemistry A., vol. 83, Pp.1176-1181, (2009).

[86] S. Chiashi, Y. Murakami, Y. Miyauchi, S. Maruyama, Cold wall CVD generation of single-walled carbon nanotubes and in situ Raman scattering measurements of the growth stage, Chemical Physics Letters., Pp.386, 89-94, (2004).

[87] E.P. Dillon, C.A. Crouse, A.R. Barron, Synthesis, characterization, and carbon dioxide adsorption of covalently attached polyethyleneimine-functionalized single-wall carbon nanotubes, ACS Nano., vol. 2, Pp.156-164, (2008).

[88] S. Chen, W. Shen, G. Wu, D. Chen, M. Jiang, *"A new approach to the functionalization of single-walled carbon nanotubes with both alkyl and carboxyl groups"*, Chem. Phys. Lett., vol. 402, Pp. 312-317, (2005).

[89] S. Barthwal and N. B. Singhc ,"*ZnO-CNT Nanocomposite:A Device as Electrochemical Sensor*", Materials Today: Proceedings, vol.4, No. 4, Pp. 5552-5560, (2017).

[90] B. Alemour, M. H. Yaacob, H. N. Lim and M. R. Hassan, "*Review of Electrical Properties of Graphene Conductive Composites*", International Journal of Nanoelectronics & Materials, vol. 11, No. 4, Pp.371-398, (2018).

References

[91] L.-M. Cursaru, S. N. Valsan ,M.-E. Puscasu, I. A. Tudor, N. Z. Ivan, B. S. Vasile and R. M. Piticescu, "*Study of ZnO-CNT Nanocomposites in High-Pressure Conditions*", Journals of Materials, vol. 14, No. 18, (2021).

[92] F. S. Alamro, A. M. Mostafa, H. A. Ahmed and A. Toghan, "*Zinc oxide/carbon nanotubes nanocomposite: Synthesis, characterization and catalytic reduction of 4-nitrophenol via laser assistant method* ", Surfaces and Interfaces, vol. 26, (2021).

[93] M. Basit, M. Abbas, N. Ahmad, S. Javed and N. A. Shah, "*Synthesis of ZnO/CNT Nanocomposites for Ultraviolet Sensors*", frontiers in material, (2022).

[94] L. Znaidi, Materials Science and Engineering: B, **174**, 18–30, (2010).

[95] A, K.Zak, R. Razali, W.H. Abd Majid and M.Darroudi, International journal of nanomedicine, vol. 6, 1399-1403 (2011).

[96] S.Talam, S.R.Karumuri and N.Gunnam, International Scholarly Research Network, vol. 1, Pp.1-6 (2012).

[97] H. Banimuslem, A. Hassan, T. Basova, I. Yushina, M. Durmuş, S. Tuncel, A.A. Esenpınar, A.G. Gürek and V. Ahsen, Key. Eng. Mat., vol.605, Pp. 461-464, (2014).

[98] Soytaş S.H., Oğuz O., Menceloğlu Y.Z. 9-Polymer Nanocomposites With Decorated Metal Oxides. In: Pielichowski K., Majka T.M., editors. *Polymer Composites with Functionalized Nanoparticles.* Elsevier; Amsterdam, The Netherlands: Micro and Nano Technologies, Pp. 287-323, (2019).

[99] B. K. H. Al-Maiyaly, *"Effect of Gamma Ray Irradiation on Structural and Optical Properties of ZnO Thin Films"*, Ibn Al-Haitham J. for Pure and Appl. Sci., vol. 28, No. 3, (2015).

[100] Sham E.L., Murgia V., Gottifredi J.C., Farfán-Torres E.M. V2O5-SiO2 Catalyst Prepared by the sol–gel Process in the Oxidative Dehydrogenation of n-butane. In: Delmon B., Jacobs P.A., Maggi R., Martens J.A., Grange P., Poncelet G., editors. *Studies in Surface Science and Catalysis.* vol.118,

References

Elsevier; Amsterdam, The Netherlands: Preparation of Catalysts VII, Pp. 669-678, (1998).

[101] C.M. Lampkin, “Growth characterization”, Prog. Cryst., vol. 1, No. 405, (1979).

[102] L. Eckertova, “Physics of thin films”, Plenum Press, New York, p.15, (1977).

[103] J. Pankove, “Optical processes in semiconductors”, Prentice– Hall, Inc., Englewood Cliffs, vol. 285, p. 111, (1971).

[104] A. Barranco, A. Gonzalez, and A. Palmero, “Perspectives on oblique angle deposition of thin films: from fundamentals to devices”, Journal of Progress in Materials Science, vol. 76, Pp. 59-153, (2016).

[105] K. Chopra, “Thin film device application”, Plenum Press, New York, vol.382, p.323, (1983).

[106] H. A. Banimuslem, “Organic/Carbon Nanotubes Hybrid Thin Films for Chemical Detection”, PhD Dissertation, Sheffield Hallam University, (2015).

[107] D. Newman, “Semiconductor physics and devices”, Basis Principles, Richard, University of New Mexico, vol. 435, p.211, (1992).

[108] J. Millman, “Microelectronics”, Murray–Hill, Book Company Kogakusha, volume 642, p.172, (1979).

[109] R. Elliot and A.I.Gibson, “An introduction to solid state physics and application”, Macillian Inc., vol.471, p.92, (1974).

[110] L. Kazmarski and A. Clark, “Polycrystalline and amorphouse thin films and device”, Edited by Lawrence Academic Press, New York, vol. 267, p.142, (1980).

[111] J. Taus, “Amorphous and liquid semiconductor”, Plenums Press, New York and London, vol.271, p. 99, (1974).

References

[112] O. Stenzel, "The physics of thin film optical spectra", Springer Series in Surface Sciences, vol. 978, pp. 214-220, (2015).

[113] C. Gumus, O. M. Ozkendir, H. Kavak, and Y. Ufuktepe, "Structural and optical properties of zinc oxide thin films prepared by spray pyrolysis method", J. Optoelectronics and Advanced Materials, (2006).

[114] M. Kamruzzaman, R. Dutta, and J. Podder, "Synthesis and characterization of the as-deposited Cd 1-xCo xS thin films prepared by spray pyrolysis technique", Department of Physics, Bangladesh University of Engineering and Technology, (2011).

[115] S. Saxena, "Polyvinyl Alcohol (PVA)", Chemical and Technical Assessment, First Edition , JECFA, (2004).

[116] T. Allen, S. Rutherford, S. Murray, S. Reipert, and M.Goldberg, "Field emission scanning electron microscopy and visualization of the cell interior", Cell Biology, Academic Press, vol. 115, Pp. 325-333, (2006).

[117] D. Newman, "*Semiconductor physics and devices*", Basis Principles, Richard, University of New Mexico, vol. 435, p.211, (1992).

[118] D. William, and J. Callister, *"Materials Science& Engineering. An Introduction"*, sixth Edition, John Wiley Sons Inc, (2003).

[119] G. Busch, and H. Schade, "*Lectures on Solid State Physics" International Series in Natural Philosophy*, pergamon press, Elsevier, vol. 79, (2013).

[120] N. Liu, K. Lee, and P. Schmuki, "*Reliable Metal Deposition into TiO_2 Nanotubes for Leakage-Free Interdigitated Electrode Structures and Use as a Memristive Electrode*", vol. 125, No. 47, Pp. 12607-12610, (2013).

[121] H. D. , T. W. Bfnan F. , Xhengguo Jin and Yong N., "*Microstructure, Optical and Optoelectrical Properties of Mesoporous SnO_2 Films by Hydrolysis-limited Sol–Gel Process With Different Inhibitors*" vol. 410, (1999).

References

[122] S. Bagga,"Gas Sensor-Studies on Sensor Film Deposition," wiley, P.300, (2007).

[123] Z.Li, Z. Yao, A.A. Haidry , T. Plecenik., L. Xie, L. Sun, Q. Fatima, *"Resistive-type hydrogen gas sensor based on TiO_2: A review*". International Journal of Hydrogen Energy, vol. 43, No. 45, (2018).

[124] B.C. Sertel , N.A. Sonmez , M.D. Kaya, S. Ozcelik , *"Development of MgO: TiO_2 thin films for gas sensor applications*", Ceramics International, Elsevier, vol. 45, No.3, Pp. 2917-2921, (2019).

[125] F.-L. Meng, L. Zhang, Y. Jia, J.-Y. Liu , Y.-F. Sun, T. Luo, M.-Q. Li , J.-H. Liu, X.-J. Huang , *"Electronic chip based on self-oriented carbon nanotube microelectrode array to enhance the sensitivity of indoor air pollutants capacitive detection",* Sens. Actuators B Chem. , vol. 153, Pp.103-109, (2011).

[126] M. Manjula, B. Karthikeyan and D. Sastikumar , "Sensing characteristics of nanocrystalline bismuth oxide clad-modified fiber optic gas sensor", Opt. Lasers Eng., volume 95, pp.78–82, (2017).

[127] T.-Y. Wang Y.-Y. Li, T.-T. Li , H. Yu , Y. Yang , H. Yang and X.T. Dong, "Enhanced NOx gas sensing properties of Cr_2O_3 film modified ordered porous ZnO gas sensors", Solid State Ionics., volume 326, pp.173–182, (2018).

[128] F. Laborda and E. Bolea, *"Nanomaterials Engineered Nanomaterials"* Encyclopedia of Analytical Science, Third Edition, Academic Press; Oxford, UK, Pp. 108-116, (2018).

[129] J. Hansen, M. Sato, R. Ruedy, A. Lacis and V. Oinas, *" Global warming in the Twenty-First century: An alternative scenario*", Proc. Natl. Acad. Sci. *USA* **,** vol. 97, Pp. 9875-9880, (2000).

References

[130] F.J. Ibañez and F.P:. Zamborini, "Chemiresistive Sensing with Chemically Modified Metal and Alloy Nanoparticles", Small**,** vol. 8, Pp.174-202, (2012).

[131] A. Mirzaei, S.G. Leonardi and G. Neri*, "Detection of hazardous volatile organic compounds (VOCs) by metal oxide nanostructures-based gas sensors: A review*", Ceramics International, Elsevier, vol. 42, Pp. 15119-15141, (2016).

[132] N.A. Zaidi, M.W. Tahir, M. J. Vellekoop and W. Lang, "*A Gas Chromatographic System for the Detection of Ethylene Gas Using Ambient Air as a Carrier Gas*", Sensors, vol. 17, p. 2283, (2017).

[133] F.-L. Meng, Z. Guo and X.-J. Huang, *" Graphene-Based hybrids for chemiresistive gas sensors",* TrAC Trends Anal. Chem. **,** vol. 68, Pp. 37-47, (2015).

[134] D.R. Miller, S.A. Akbar and P.A. Morris, , *"Nanoscale metal Oxide-Based heterojunctions for gas sensing: A review"*, Sens. Actuators B Chem., vol. 204, P. Scott, D. James and Z. Ali, *"Data analysis for electronic nose systems",* Microchim. Acta , vol. 156, pp. 183–207, (2006).

[136] M. G. Chung , "*Highly sensitive NO_2 gas sensor based on ozone treated graphene,"* Sensors Actuators, B Chem., vol. 166, No. 2, Pp. 172–176, (2012).

[137] D. K. Bandgar, S. T. Navale, G. D. Khuspe, S. A. Pawar, R. N. Mulik, and V. B. Patil, *"Novel route for fabrication of nanostructured α-Fe_2O_3 gas sensor,"* Mater. Sci. Semicond. Process., vol. 17, Pp. 67–73, (2014).

[138] V. N. Mishra and R. P. Agarwal, "Sensitivity, response and recovery time of SnO2 based thick-film sensor array for H2, CO, CH4 and LPG," Microelectronics J., vol. 29, No. 11, Pp. 861–874, (1998).

[139] S. R. M. Marc J. Madou, " *Chemical Sensing with Solid State Devices*," New York: Academic Press, Inc, (1989).

References

[140] J. Z. Ou , *"Physisorption-Based Charge Transfer in Two-Dimensional SnS2 for Selective and Reversible NO_2 Gas Sensing*" ACS Nano, vol. 9, No. 10, Pp. 10313–10323, (2015).

[141] Q. G. Hial, "*Improvement of ZnO and SnO_2 Hydrogen Gas Sensors*", PhD Thesis, University of Baghdad, (2011).

[142] R. P. Hamilton and M. R. Heal, *"Evaluation of method of preparation of passive diffusion tubes for measurement of ambient nitrogen dioxide*," J. Environ. Monit., vol. 6, No. 1, Pp. 12–17, (2004).

[143] R. B. Schlesinger, *"Pollution Prevention and Abatement Handbook, "* World Bank Publications, p.777, (1998).

[144] R. Wegmüller, F. Tay, C. Zeder, M. Brnić and R. F. Hurrell, *"Zinc Absorption by Young Adults from Supplemental Zinc Citrate is Comparable with That from Zinc Gluconate and Higher than from Zinc Oxide"*, The Journal of Nutrition, vol. 144, No. 2, Pp.132–136, (2014).

[145] National Institute for Occupational Safety and Health, (NIOSH) Pocket Guide to Chemical Hazards, Washington, (1997).

[146] M. Ernst, J.P. Melder, F.I. Berger, C. Koch, *"Ethanolamines and Propanolamines",* (2022).

[147] L. Znaidi, "*Sol–gel-deposited ZnO thin films: A review*", Materials Science and Engineering: B, vol. 174, No.1-3, Pp. 18-30, (2010).

[149] G.Gauglitz and J.P. Dakin, *"Spectroscopic analysis. In: John PD, Robert GWB (eds) Handbook of optoelectronic"*s, CRC Press, Boca Raton, vol. 2, Pp. 569-600, (2017).

[150] A. R. Barron, Ch.W. Duncan and P.M.V.Raja, "CHEMISTRY LibreTexts, UV-Visible Spectroscopy", (2020).

[151] Z. Khaled, "Characterization of Pure and Dopant TiO2 Thin Films for Gas Sensors Applications", PhD Thesis, Technology University, Iraq, (2010).

References

[152] P. Davidson, "Selected Topic in X-ray Scattering by LiquidCrystalline Polymers", Journal of Liquid Crystals, vol. 95, No. 0081-5993, Pp. 1-39, (1999).

[153] J. Als-Nielsen and D. McMorrow, "*Elements of modern X-ray physics"*, John Wiley and Sons, Ltd., Chichester, First Edition, (2001).

[154] C. S. Barrett and T.B. Massalski, "*Structure of metals*", Mc GrawHill, New York, (1966).

[155] R. Guinebretière, "*X-ray diffraction by polycrystalline materials*", Wiley , (2013).

[156] J. Goldstein, *"Scanning electron microscopy and x-ray microanalysis",* Kluwer Adacemic/Plenum Pulbishers, p.689, (2003).

[157] L. Reimer, *"Scanning electron microscopy : physics of image formation and microanalysis"*, Springer, p. 527, (1998).

[158] R. Sindhu and A. Pandey, "*Industrial Biorefineries & White Biotechnology*" , (2015).

[159] P. Griffiths, d. Hasseth, J. A. , "*Fourier Transform Infrared Spectrometry*", Second Edition, Wiley-Blackwell, (2007).

[160] D. Titus and S. M. Roopan, *"Fourier Transform Infrared Spectroscopy Green Synthesis; Characterization and Applications of Nanoparticles*", (2019).

[161] E. A. Meulenkamp, "Size dependence of the dissolution of ZnO nanoparticles", Journal of Physical Chemistry B, vol. 102, Issue 40, (1998).

[162] M.M. Mohamed, M.A.Ghanem, M. Khairy, E. Naguib, and N.H. Alotaibi, Applied Surface Science, vol. 487, p. 539 (2019).

[163] M. Fakhar-e-Alam, S. Rahim, M. Atif, M.H. Aziz, M.I. Malick, S.S.Z. Zaidi, R. Suleman and A. Majid, Laser Physics Letters, vol. 11, No. 025601, (2013).

[164] A.M. Nahhas, American Journal of Nanomaterials, vol. 6, 15 (2018).

References

[165] H. Chen, X. Wu and G. Shen, Nanoscale Research Letters, vol. 5, p.570 (2010).

[166] V.K. Gupta, S. Rostami, H. Karimi-Male, F. Karimi, M. Keyvanfard, and T.A. Saleh, Int. J. Electrochem. Sci., vol. 10, p. 1517 (2015).

[167] S. W. Xue, X. T. Zu, W. L. Zhou, H. X. Deng, X. Xiang, L. Zhang and H. Deng, "Effects of post-thermal annealing on the optical constants of ZnO thin film", Journal of Alloys and Compounds, (2008).

[168] A, K.Zak, R. Razali, W.H. Abd Majid and M.Darroudi, International journal of nanomedicine, vol. 6, Pp.1399-1403, (2011).

[169] S.Talam, S.R.Karumuri and N.Gunnam, International Scholarly Research Network, vol. 1, Pp.1-6, (2012).

[170] H. Banimuslem, A. Hassan, T. Basova, I. Yushina, M. Durmuş, S. Tuncel, A.A. Esenpınar, A.G. Gürek and V. Ahsen, Key. Eng. Mat., vol. 605, Pp.461- 464, (2014).

[171] M.M. Mohamed and M.A.Ghanim, M.Khairy, E.Naguib and N.H.Alotaibi , Applied surface science, vol.487, Pp.539-549, (2019).

[172] D. D. Mulmi, A. Dhakal and B. R. Shah, Nepal Journal of Science and Technology, vol. 15, Pp.111-116, (2014).

[173] S. Saxena, "Polyvinyl Alcohol (PVA)", Chemical and Technical Assessment, First Edition, JECFA, (2004).

[174] D. K. Schroder, "*Semiconductor Material and Device Characterization"*, John Wiley & Sons, New York, Pp.38-40, (1998).

[175] D. Newman, "*Semiconductor physics and devices",* Basis Principles, Richard, University of New Mexico, vol. 435, p.211 (1992).

[176] G. Busch, and H. Schade, "Lectures on Solid State Physics", pergamon press, New York, pp.357-368, (2013)

References

[177] N.T. Hung, N.D. Quang and S. Bernik, Journal of Materials Research, vol.16, Pp.2817- 2823, (2001).

[178] J. Lee, J.H. Hwang, J.J. Mashek, T.O. Mason, A.E. Miller and R.W. Siegel, Journal of Materials Research, vol. 10, Pp.2295-2300, (1995).

[179] Çetin Kılıç and A. Zunger, Phys. Rev. Letters, vol. 88, No.095501, (2002).

[180] L. Zhu and W. Zeng, Sensors and Actuators A: Physical, vol. 1, p.267, (2017).

[181] H. Banimuslem, A. Hassan, T. Basova, A. Esenpınar, S. Tuncel, M. Durmuş, A. Gürek and V. Ahsen, Sensors and Actuators B: Chemical, vol.34, p.207, (2015).